Analysis of Heterogeneities in a 20 L Bioreactor

by

Danny Kang

A thesis
presented to the University of Waterloo
in fulfillment of the
thesis requirement for the degree of
Master of Applied Science
in
Chemical Engineering

Waterloo, Ontario, Canada, 2025

© Danny Kang 2025

Author's Declaration

I hereby declare that I am the sole author of this thesis. This is a true copy of the thesis, including any required final revisions, as accepted by my examiners.

I understand that my thesis may be made electronically available to the public.

Abstract

Biological systems are utilized in various industries to produce valuable products, including biopharmaceuticals. This is done in bioreactors, which are specialized vessels that are able to precisely control key parameters, including agitation, air flow, temperature, pH, dissolved oxygen (DO), and nutrient supply. With the high demands for biopharmaceuticals caused by advancements in medicine, the need for efficient production and optimization of bioreactors has been evident. This has been especially seen during the COVID-19 pandemic, and the high costs of some products, which are inaccessible to many individuals. To optimize production, simulation models have been developed to predict effective control schemes for high growth and product yield. However, this is challenging to translate between lab-scale and industrial-scale due to the formation of gradients in industrial-scale systems, which have poor mixing. Gradients lower the efficiency of bioreactors as cells must constantly adapt to changing extracellular conditions, which cause stress and lower yields. Thus, it is necessary to validate simulation models using the gradients formed in large-scale bioreactors; however, this data is not readily available, and it is difficult to obtain such gradients in smaller-scale bioreactors.

In this work, fed-batch experiments are studied to investigate the formation of gradients in DO, k_La, pH, cell density, glucose, and acetate concentrations. This was done through the movement of sensors, turning the air on and off, and the usage of different sampling locations. The objectives of this work were first to characterize the culture with flask and batch experiments and then to use this information to carry out

the fed-batch experiments to explore the potential of measuring these gradients. Dynamic metabolic responses were observed and measured depending on the control of the glucose feeding, and consistent gradients were observed for the DO, pH, and k_La, while gradients for cell density, glucose, and acetate were not observed, which may be due to limitations in sampling times.

Finally, the metabolic responses have been modeled using modified Monod kinetics, where the modifications include self-growth inhibition, an acetate metabolic switch, and a cell density-dependent lag function. This work was done using a genetic algorithm on Python to optimize parameters, and the model was able to adapt to the different extracellular conditions presented in the fed-batch experiments.

Acknowledgements

I would like to express my gratitude first and foremost to my supervisors, Professor Marc Aucoin and Professor Hector Budman for their continuous guidance with their expertise in running bioreactors and biological modeling throughout my graduate career. They have been very supportive and knowledgeable in my inexperience working with cell culture, running bioreactors, and modeling of the metabolic kinetics in bioreactors.

Many thanks to Professor Nasser Abukhdeir as well for his contributions to my work, insights into hydrodynamics of bioreactors, and the funding that was provided for my experiments.

I would also like to thank my readers, Professor Christian Euler and Professor Valerie Ward from the Department of Chemical Engineering at the University of Waterloo for their insights and revisions to this thesis during the submission process.

Special thanks to those who have assisted me in learning to run different components of my experiments. Thanks to Aaron Yip, Jacqueline Powichrowski, and Scott Boegel for teaching me how to work with cell culture, growth media, and relevant lab equipment. Thanks to Abhishek Mishra and Bert Habicher for helping me set up and modify the bioreactor. Thanks to Mehraveh Hosseinali for providing me with the *E. coli* strain used in this work. Thanks to Professor Valerie Ward and Zahra Negahban for their expertise in running and interpreting results from the HPLC machine. Thanks to Ittisak Promma, Shuji Chang, and Martin Albury for their expertise and assisting me with developing and running simulations for the modeling work. Finally, thanks to Joshua Kunihiro for his camaraderie and advice on thesis writing and formatting. I would like to thank everyone

listed and those that may not have been mentioned here again for their intellectual contributions, advice, and discussions of my results, which were a huge help for this project.

I would like to thank the BioWorks team at the University of Waterloo for their guidance and feedback whether it be from discussions of my results or for my presentations during weekly group meetings. Their insight has been invaluable to my work with their variety of backgrounds in bio-related chemical engineering research.

A special mention to Sanofi Pasteur for providing the bioreactor equipment for the experiments.

Thanks to all my friends and church family for their support, encouragement, and prayers as they have been an invaluable presence in both my undergraduate and graduate career, especially those I have met at KCF and New Creation Reformed Presbyterian Church. I especially thank them for their help in hard times, when I was sick, and in work, life, and social balance. A special mention to Pastor Scott Wilkinson and his family for their spiritual guidance in my time at Waterloo.

Finally, I thank my family, including my parents Elijah and Jin, and my sister Clementina for their support in my student career.

Table of Contents

Author's Declaration **ii**

Abstract **iii**

Acknowledgements **v**

List of Figures **xi**

List of Tables **xvii**

List of Abbreviations **xviii**

List of Symbols **xxi**

1 Introduction **1**

1.1 Research Motivation 1

1.2 Objectives 4

2 Literature Review **7**

2.1 *E. coli* Characteristics and Significance in Biopharmaceuticals 7

2.2 *E. coli* Metabolism and Growth 11

2.3 Batch and Fed-Batch Operation 15

2.4 Bioreactor Design 19

2.5 Heterogeneities in Bioreactors 23

2.6 Metabolic and Hydrodynamic Modeling of Bioreactors 29

3 Flask and Bioreactor Experiments **34**

3.1 Overview 34

3.2 Methodology 35

3.2.1 Media Preparation for Flask Cultures 35

3.2.2 Flask Cultures 36

3.2.3 Media Preparation for Bioreactor Batch Culture 37

3.2.4 Bioreactor Batch Operation 38

3.2.5 Media Preparation for Bioreactor Fed-Batch Culture 1 39

3.2.6 Bioreactor Fed-Batch Operation 1 41

3.2.7 Media Preparation for Bioreactor Fed-Batch Culture 2 42

3.2.8 Bioreactor Fed-Batch Operation 2 43

3.3 Results and Discussion 44

3.3.1 Characterizing the *E. coli* Culture Through Flask Culture and Bioreactor Batch Operation 44

3.3.2 Bioreactor Fed-batch Operation for Potential Heterogeneity Measurement 51

3.3.3 Bioreactor Fed-batch Operation to Verify Heterogeneities 61

4 Modeling of the Fed-Batch Experiments **71**

4.1 Overview 71

4.2 Model Development for Fed-Batch Cultures 72

4.3 Results and Discussion 81

4.3.1 Modeling the First Fed-Batch Experiment 81

4.3.2 Modeling the Second Fed-Batch Experiment 86

5 Conclusions and Recommendations **92**

5.1 Conclusions 92

5.2 Recommendations 94

References **97**

APPENDICES **110**

A Supplementary Plots for Flask Culture 2 and Bioreactor Batch Operation 111

A.1 Flask Culture 2 111

A.2 Bioreactor Batch Operation 113

B Supplementary Plots and Tables for Bioreactor Fed-Batch Operation 117

B.1 Fed-Batch Experiment 1 117

B.2 Fed-Batch Experiment 2 126

List of Figures

2.1 A sample procedure of product development in *E. coli* by İncir, İ., & Kaplan, Ö. (2024). 9

2.2 An overview of glucose metabolism in *E. coli* by Wang et al. (2019). Used under the Creative Commons Attribution 4.0 International License (`http://creativecommons.org/licenses/by/4.0/`). 12

3.1 Calibration curve between optical cell density and dry cell weight density. Freeze dried cell pellet samples from the first fed-batch experiment were used to construct this plot. 45

3.2 Growth curve of *E. coli BL21 (DE3) PET-VP1* flask culture 1 at 250 rpm and 37°C. 46

3.3 Exponential phase of the growth curve to calculate the growth rate of the first flask culture. 46

3.4 Growth curve comparison between flask culture 1 and the 7.5 L batch operation at 37°C. 47

3.5 Exponential phase of the growth curve to estimate the growth rate of the 7.5 L batch culture. 48

3.6 Biomass and metabolite concentrations over time for the 7.5 L batch culture. The glucose is labeled as corrected because the measurement from the HPLC needed a correction factor of 2.48, and it was corrected based on an assumed initial glucose concentration of 3.7 g/L. 49

3.7 Growth curve comparison between the 7.5 L batch operation and the 13.5L fed-batch operation at 37°C. 52

3.8 Approximate growth rates during each growth phase as observed in the diauxic growth trend for the 13.5 L fed-batch culture. 53

3.9 Biomass and metabolite concentrations over time for the 13.5 L fed-batch culture. 54

3.10 Approximate schematic of the bioreactor including the impellers, sensor and sampling locations, reactor diameter, and approximate liquid height for the fed-batch culture. 56

3.11 DO% sensor height changes for the 13.5 L fed-batch culture at 8.98 h – 9.05 h (change 1), and 11.07 h - 11.12 h (change 2). 57

3.12 pH sensor height changes for the 13.5 L fed-batch culture at 9.37 h – 9.46 h (change 1), 11.12 h – 11.16 h (change 2), 11.26 h – 11.31 h (change 3), and 11.53 h – 11.58 h (change 4). 59

3.13 k_La measurements at different DO% sensor heights for the 13.5 L fed-batch culture at 9.09 h – 9.32 h (change 1), and 10.81 h – 11.03 h (change 2). . . 60

3.14 Growth curve comparison between the two fed-batch operations at 37°C. . 61

3.15 Approximate growth rates during each growth phase as observed in the 14 L fed-batch culture. 62

3.16 Biomass and metabolite concentrations over time for the 14 L fed-batch culture. 63

3.17 Bottom and top measurements of cell density to investigate gradient formation. 65

3.18 Bottom and top measurements of metabolite concentrations to investigate gradient formation. 66

3.19 DO% sensor height changes for the 14 L fed-batch culture at various times between 11.5 h – 19.5 h. A mean trend and 95% confidence interval are shown. 67

3.20 pH sensor height changes for the 14 L fed-batch culture between 11.33 h – 19.52 h. A mean trend and 95% confidence interval are shown. 68

3.21 k_La measurements at different DO% sensor heights for the 14 L fed-batch culture between 11.62 h – 19.36 h. A mean trend and 95% confidence interval are shown. 69

4.1 Experimental and simulated cell density for first fed-batch culture. 82

4.2 Experimental and simulated growth rate for first fed-batch culture. 83

4.3 Experimental and simulated glucose concentration for first fed-batch culture. 83

4.4 Experimental and simulated acetate concentration in first fed-batch culture. 84

4.5 Experimental and simulated DO profile in the first fed-batch culture. . . . 85

4.6 Simulated k_La for the first fed-batch culture. 85

4.7 Experimental and simulated cell density for second fed-batch culture. . . . 87

4.8 Experimental and simulated growth rate for second fed-batch culture. . . . 87

4.9 Experimental and simulated glucose concentration in second fed-batch culture. 88

4.10 Experimental and simulated acetate concentration in second fed-batch culture. 88

4.11 Experimental and simulated DO profile in the second fed-batch culture. . . 90

4.12 Simulated k_La for the second fed-batch culture. 90

A.1 Growth curve of *E. coli BL21 (DE3) PET-VP1* flask culture 2 at 250 rpm and 37°C. 112

A.2 Exponential phase of the growth curve to calculate the growth rate of the second flask culture. 112

A.3 Agitation rate in comparison to the cell density over time for the batch culture. 113

A.4 Air flow rate in comparison to the cell density over time for the batch culture. 114

A.5 DO% in comparison to the cell density over time for the batch culture. . . 114

A.6 Temperature of the batch culture over time. 115

A.7 pH in comparison to the cell density over time for the batch culture. 115

A.8 pH in comparison to the base pump output over time for the batch culture. 116

B.1 Ammonia concentration profile for the 13.5 L fed-batch culture. 118

B.2 Agitation rate in comparison to the cell density over time for the 13.5 L fed-batch culture. 118

B.3 Air flow rate in comparison to cell density over time for the 13.5 L fed-batch culture. 119

B.4 DO% in comparison to cell density over time for the 13.5 L fed-batch culture. 119

B.5 Temperature of the 13.5 L fed-batch culture over time. 120

B.6 pH in comparison to cell density over time for the 13.5 L fed-batch culture. 120

B.7 pH in comparison to the base pump output over time for the 13.5 L fed-batch culture. 121

B.8 Supplement feed pump output in comparison to the glucose concentration and cell density over time for the 13.5 L fed-batch culture. 121

B.9 Sample of air flow rate and DO% profile to show the air shut off and on to measure the $k_L a$. 124

B.10 Sample of oxygen uptake rate measurement taken from a nearly linear segment of the DO% profile when the air supply is shut off. 124

B.11 Agitation rate in comparison to the bottom cell density over time for the 14 L fed-batch culture. 126

B.12 Air flow rate in comparison to bottom cell density over time for the 14 L fed-batch culture. 127

B.13 DO% in comparison to bottom cell density over time for the 14 L fed-batch culture. 127

B.14 Temperature of the 14 L fed-batch culture over time. 128

B.15 pH in comparison to bottom cell density over time for the 14 L fed-batch culture. 128

B.16 pH in comparison to the base pump output over time for the 14 L fed-batch culture. 129

B.17 Supplement feed pump output in comparison to the glucose concentration and bottom cell density over time for the 14 L fed-batch culture. 129

B.18 Estimated glucose feeding rate for the 14 L fed-batch culture as there were uncertainties due to tubing occlusions. 134

List of Tables

4.1 Best fit model parameters and descriptions for the first and second fed-batch experiment. 81

B.1 Conditions at which the DO% sensor height changes were made and measured in the 13.5 L fed-batch culture. 122

B.2 Conditions at which the pH sensor height changes were made and measured in the 13.5 L fed-batch culture. 123

B.3 Conditions at which the k_La was measured for different DO% sensor heights for the 13.5 L fed-batch culture. 125

B.4 Conditions at which the DO% sensor height changes were made and measured in the 14 L fed-batch culture. 130

B.5 Conditions at which the pH sensor height changes were made and measured in the 14 L fed-batch culture. 132

B.6 Conditions at which the k_La was measured for different DO% sensor heights for the 14 L fed-batch culture. 133

List of Abbreviations

E. coli *Escherichia coli* 1, 3–5, 7–11, 13, 15, 26–28, 33, 34, 37, 45, 51, 67, 68, 71, 91, 92

3D three dimensional 19

ATP adenosine triphosphate 11

C:N:P:S Carbon:Nitrogen:Phosphorus:Sulfur ratio 18

CER carbon dioxide evolution rate 17, 18

CFD Computational fluid dynamics 29–32, 58

CHO Chinese hamster ovary 1, 10, 27

CM compartmental model 29, 31, 32

COVID-19 Coronavirus Disease of 2019 1, 2

DEAP Distributed Evolutionary Algorithms Python 80

DNA deoxyribonucleic acid 8

DO dissolved oxygen iii, iv, 3, 5, 16–19, 22, 28, 31, 35, 38, 39, 41, 42, 44, 50, 53–55, 57–59, 62–70, 75, 81, 84, 89, 92, 93, 95, 96, 122, 123, 130–132

ED Entner-Doudoroff 11

EMP Embden-Meyerhof-Parnas 11

HPLC high performance liquid chromatography 39, 47

HPV Human Papillomavirus 2

IgG Immunoglobulin G 10

KM50 50 mg/mL kanamycin monosulfate 36, 38, 40, 42

LB Luria Bertani 8, 13

NADH nicotinamide adenine dinucleotide 11

OD_{600} optical density at 600 nanometres 37–39, 41, 42, 44

ODEs ordinary differential equations 72, 79

OPP oxidative pentose phosphate 11

PCV pneumococcal conjugate vaccine 2

PFR plug flow reactor 28

rpm revolutions per minute 37–39, 41, 44, 122, 123, 125, 130–133

SIP sterilization in place 37, 38, 40

SLPM standard litres per minute 38, 39, 41, 122, 123, 125, 130–133

SSA stock solution A 35, 38, 40

SSB stock solution B 35, 38, 40

STR stirred tank reactor 19, 28

List of Symbols

A Acetate concentration (g/L) 73, 80

A_1 Lower asymptote in lag function 77, 78, 81

β Inflection point in lag function 78, 81

C Concentration (g/L) 75, 80

exp Exponential function with base e 77

F_1 Feeding schedule (L/h) 73

F_2 Base addition rate (L/h) 73

F_3 Volume taken out from sampling (L/h) 73

$F(t)$ Feed flow rate (L/h) 17

$g(X)$ Cell density dependent activation function for lag function 78

$g(X, S, A, C_{O_2})$ State dependent activation function for lag function 78

K_a Acetate inhibition constant on glucose growth (g/L) 73, 81

K_{a2} Monod constant on acetate (g/L) 73, 81

K_G Glucose constant for acetate switch (g/L) 73, 77, 81

k_G Growth rate coefficient (h^{-1}) 77

K_I Inhibition coefficient (g/L) 74

k_La Liquid mass transfer coefficient (h^{-1}) iii, iv, 5, 24, 25, 35, 42, 44, 54, 55, 58, 59, 64, 68–70, 72, 75, 81, 84–86, 89, 90, 92, 93, 95, 96, 125, 133

K_S Monod constant on glucose (g/L) 73, 81

K_X Self-growth inhibition constant (g/L) 76, 81

K_{X2} Biomass constant for lag function (g/L) 81

$\lambda_{\mathbf{lag}}$ Steepness of lag function curve 78

$M_s(t)$ Mass flow rate of the substrate (g/h) 17

μ Growth rate (h^{-1}) 17, 73, 80

$\mu_{\mathbf{m,acetate}}$ Maximum growth rate on acetate (h^{-1}) 73, 81

$\mu_{\mathbf{m,glucose}}$ Maximum growth rate on glucose (h^{-1}) 73, 81

m_X Cell maintenance coefficient (h^{-1}) 17, 73, 81

n_G Hill coefficient for acetate switch 77, 81

n_X Hill coefficient for self-growth inhibition 76, 81

n_{X2} Hill coefficient for biomass in lag function 81

$\mathbf{O_2}$ Oxygen 75

pH Measure of acidity or alkalinity iii, iv, 3, 5, 8, 14, 16–19, 21, 22, 28, 31, 35, 38, 39, 41, 42, 44, 50, 53–55, 57–59, 62–64, 67–69, 92, 93, 122, 123, 125, 130–133

q_A Growth associated acetate yield (g acetate/g cell) 73, 81, 89

$q_{\mathbf{O_2}}$ Specific oxygen uptake rate (g O_2/g cell/h) 75

q_S Specific substrate consumption rate (g substrate/g cell/h) 23

S Substrate concentration (g/L) 23, 73, 80

sat Saturated 75

S_0 Substrate concentration of the feed solution (g/L) 17, 73

t Time (h) 77

t_0 Time when feeding was initialized (h) 17

$\tau_{\mathbf{c}}$ Characteristic substrate consumption time (h^{-1}) 23

T_i Inflection point of Gompertz lag function 77

V Volume (L) 74

$V(t_0)$ Initial volume (L) 17

w Scaling factor in lag function 78, 81

$W(t)$ Gompertz lag function 77

X Cell density (g/L) 23, 73, 80

$X(t_0)$ Initial cell concentration (g/L) 17

$Y_{\mathbf{O}_2/X}$ Yield coefficient of oxygen on biomass (g oxygen/g cell) 81

$Y_{X/A}$ Yield coefficient on acetate (g cell/g acetate) 81

$Y_{X/S}$ Yield coefficient on glucose 17, 73, 81

Chapter 1

Introduction

1.1 Research Motivation

Fermentation processes are used in several industries including bio-pharmaceuticals, food, cosmetics, and chemicals. They are conducted in special large-scale vessels called bioreactors, which have the ability to precisely control important parameters for optimal biological growth and production. Amongst the many biological organisms that are used in bio-manufacturing, the most characterized ones include *Escherichia coli* (*E. coli*), and Chinese hamster ovary (CHO) cells. Currently, many large-scale production processes are still designed by rule of thumb or experience through trial and error, which result in suboptimal conditions for the organisms leading to lower output, more waste, and increased operating costs.

With the recent rise in demands for vaccines due to the Coronavirus Disease of 2019

(COVID-19) pandemic, and several medical advances demanding the need for biopharmaceuticals, the need for cheaper and efficient production of biopharmaceuticals has become evident. According to Global Market Insights, the biopharmaceutical market value in 2024 was $422.5 billion, and it is projected to more than double by 2034 to $921.5 billion, with similar numbers from Grand View Research [1],[2]. Some of the trends that induce the increasing demand comes from the rising number of diabetes, obesity, lysosomal storage disorders, and cancer cases, along with infectious diseases which continue to be relevant targets in the industry. New treatment options involving the use of biologics for neurological and autoimmune diseases have also been shaping the market [1]. The World Health Organization shows statistics that 16 billion vaccine doses worth US$141 billion were supplied in 2021, compared to 5.8 billion doses worth US$38 billion in 2019 [3]. This was mainly attributed to COVID-19 vaccines; however, it showed how production of biopharmaceuticals need to be efficient to meet sudden rises in demand to reduce strain on the industry. This also raised the issue of accessibility as failure to meet demands showed global shortages and higher costs. Excluding COVID-19 vaccines, 70% of all vaccines are produced by ten manufacturers, and "several of the top twenty most widely used vaccines (such as pneumococcal conjugate vaccine (PCV), Human Papillomavirus (HPV), measles, and rubella) currently rely mainly on two suppliers [3]." So, while having more manufacturers would be ideal, increasing and possibly optimizing the production capability of current manufacturers is crucial.

Consequently, bioreactor operation must be optimized to meet demand and accessibility needs. It is often very difficult to even scale up from a laboratory to industrial-scale for new biopharmaceuticals, and it is costly to run experiments to

optimize currently existing production due to the scale and time necessary. Currently, simple simulation models based on small scale experiments have been used to avoid large-scale, costly experiments to reduce costs, improve design, and overall production; however, optimizing beyond this is very limited. Optimization is difficult because bioreactors are very complex due to multiphase, multicomponent hydrodynamics, interphase mass transport, and metabolic reactions from the organism that is being used. These are affected by the overall design of the vessel, the media used, extracellular nutrient concentrations, and the controlled parameters in the bioreactor, namely, the pH, DO, temperature, agitation, gas flow rate, and feed flow rate. These parameters will all influence the cells' yield and quality of the product of interest. Another difficulty is that in smaller scale bioreactors, mixing time is very short in comparison to industrial scale bioreactors. This causes physical and biological heterogeneities to occur in large scale production, which is difficult to model using smaller bioreactors.

Therefore, model development which couples fluid flow phenomena, i.e. occurrence of multiphase regimes, interactions between components in the flow, gradients in substrate concentration, pH, DO, and other metabolites, with metabolic models for the cell has been a large area of interest so that simulation models can accurately capture large scale operation based on smaller scale experiments. However, current simulation models fall short of being able to depict this complexity very accurately. In a model developed by Pigou et al. (2014) [4], a compartmental approach to account for hydrodynamics of large-scale bioreactors and a coupled metabolic model and population balance was used to simulate an *E. coli* culture based on data from a 30,000 L bioreactor from Xu et al. (1999) [5]. It was evident that while simulation models have come a long way, there were

still many gaps to be addressed. To help address these gaps, more comprehensive data sets from bioreactor cultures are necessary to create newer and more robust models that can increase their accuracy to predict which areas in the bioreactor perform poorly due to gradients. This will allow for low-cost optimization opportunities on currently existing bioreactors such as retrofitting new sensors and feed ports to accommodate for the gradients caused by poor mixing to potentially create a more homogeneous cell culture, which will result in more efficient operation from better process control. Consequently, biopharmaceutical companies will increase profitability without the need for high capital expenditure and decrease production cost while increasing production capacity, which will increase accessibility to the product and improve Canada's biopharmaceutical industry and economy by increasing competition through world-class biopharmaceutical development and manufacturing. While it was always assumed that gradients can only be observed in bioreactors of large dimensions, we hypothesized in this work that if such gradients can be also measured in lab scale bioreactors, their effect on bio-process operations could be further studied.

1.2 Objectives

The overall goal of this work will be to obtain a comprehensive data set showing heterogeneous conditions in a 20 L pilot scale bioreactor and be able to model the data using existing simulation models. Specific objectives include the following:

1. Establishing a growth curve and growth rate for the selected *E. coli* strain at the

small scale in 50 mL flask experiments.

2. Establishing a growth curve, growth rate, glucose and acetate curves, and measuring controlled parameters in a batch operated bioreactor fermentation.

3. Modify the experimental system in order to be able to change the height of the DO sensor and the pH sensor to be able to measure heterogeneities in these parameters.

4. Assess whether the height of the sampling port could be also changed to measure heterogeneity in cell density and metabolite concentrations.

5. Using the data from the batch operated fermentation, run a fed-batch fermentation to reach a high cell density where it will be likely to be able to obtain gradients along the height of the bioreactor by changing the sensor heights. Specifically, the pH, DO, k_La, and if possible, cell density, glucose, and acetate concentrations once the culture is well-established.

6. Model the experimental data using established metabolic models and identify required modifications to improve the fitting to data.

This thesis is organized into five chapters, where Chapter 1 includes the research motivation and objectives. Chapter 2 covers the background material which covers *E. coli* characteristics and usage in biopharmaceuticals, metabolism and growth, batch and fed-batch operation, bioreactor design, heterogeneities in bioreactors, and modeling methods. Chapter 3 will discuss the results from the flask experiments, batch operation, and the two fed-batch operations of the bioreactor. These results will show the

characterization of the culture, which was used to inform the fed-batch process. Gradients observed in the fed-batch experiments will be discussed as well. Chapter 4 will discuss the development of a metabolic model, and the fitting of two fed-batch experiments. Finally, Chapter 5 will present conclusions and recommendations for future work.

Chapter 2

Literature Review

2.1 *E. coli* Characteristics and Significance in Biopharmaceuticals

E. coli is a common gram-negative bacterium that has been widely studied for over one hundred years. It is rod-shaped and facultative anaerobic, meaning that it will use oxygen if available, but otherwise can survive in anaerobic conditions [6, 7]. It is found commonly in the environment, food, and the lower guts of warm-blooded animals [6]. It can also live in feces, soil, and water for a long time due to its resilience [8]. The cells are typically 1-3 µm x 0.4-0.7 µm in size, have a cell wall, and have a peptidoglycan layer [8, 9]. The various strains are categorized into serotypes based on three antigens: 173 types of somatic or cell wall antigens (O), 103 types of capsular antigens (K), and 75 types of flagellar antigens (H) [10]. Many of these strains are known to be safe and can

be good probiotics, but pathogenic strains also exist [11]. *E. coli* is very widely used in bio-manufacturing today as a host for recombinant deoxyribonucleic acid (DNA) and protein production [12]. It is typically grown optimally at 37°C and pH of 7.0 under aerobic conditions and can double in as little as 20 minutes [7, 13]. Some common growth media include minimal media with glucose as a carbon source, ammonium salts as a nitrogen source, and trace elements, such as M9 media. Complex media such as Luria Bertani (LB) media and terrific broth are also used, and growth on solid agar plates is common in experimental studies [7, 14].

E. coli has several attractive traits which make it an excellent model organism for the study of genetics, microbiology, and biotechnology, including well-established genetics, minimal growth requirements, and high adaptability [15]. Additionally, it can serve as host for bacteriophages to grow, which allows for its use on the study of viruses. Also, asexual reproduction allows for preserving genetic modifications and repeatability of experiments [16]. *E. coli* was first found to be able to produce recombinant proteins in the 1970s when recombinant DNA technology was first introduced, and its first key usage was the production of human insulin for the treatment of diabetes [17, 18]. However, due to a lack of cell machinery, it was initially thought to not be able to produce insulin because it requires complex protein folding. However, being a heterodimer that needs oxidative protein folding, insulin was still produced [19]. Afterwards, many recombinant biopharmaceuticals such as monoclonal antibodies have been produced using a variety of hosts, including *E. coli*, yeast, fungi, insect cells, and mammalian cells [20]. Of these, *E. coli* remains to be a favorable host due to its well-established genetics, the variety of cloning techniques, and the variety of expression systems, which allow it to produce a

multitude of proteins [20].

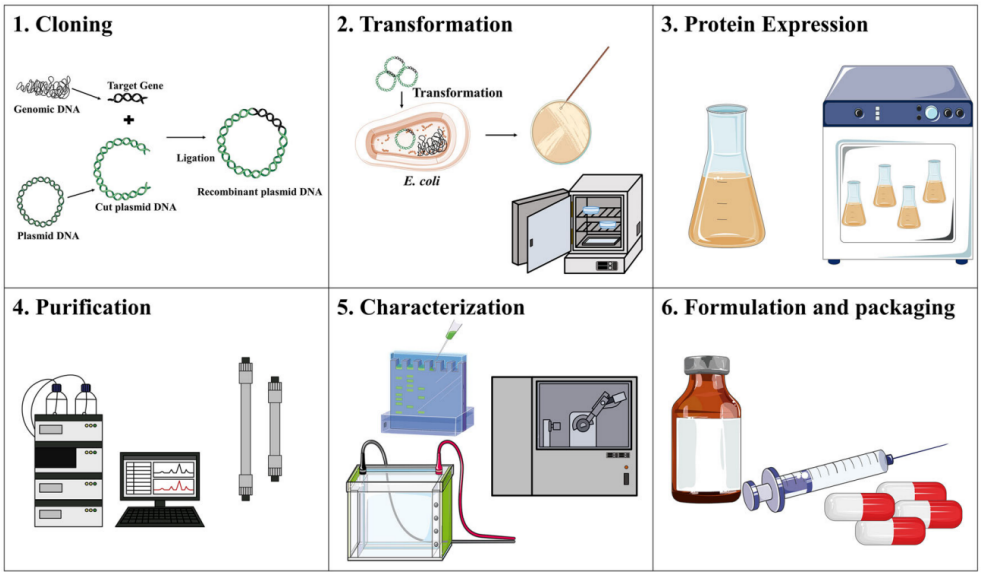


Figure 2.1: A sample procedure of product development in *E. coli* by İncir, İ., & Kaplan, Ö. (2024) [21].

E. coli also serves as a good platform for large-scale production due to its fast growth, inexpensive nutritional requirements, simplicity of scale-up, capacity of high yield, and its capability of production of high-quality pharmaceuticals [22]. Common types of biopharmaceuticals currently produced by *E. coli* include hormones, enzymes, peptides, vaccines, fusion proteins, and antibodies. Examples of these include human insulin, human urate oxidase, nesiritide, hepatitis E vaccine, romiplostim, and Ranibizumab [21]. Currently, about 30% of all therapeutic proteins are made in *E. coli*, making it very industrially significant.

As mentioned earlier, there are drawbacks to using *E. coli*. One such drawback is the usage of rare codons such as arginine codons AGG and AGA, which occur 0.14% and

0.21% of the time, respectively, which can cause translational errors [23]. To address this issue, the usage of plasmids and the replacement of rare codons with more common codons have been done and have been successful in the production of interferon-α2b [24, 25]. Another drawback is the formation of inclusion bodies caused by the aggregation of heterologous insoluble proteins, which negatively affect protein production and downstream processing [19]. Molecular chaperones have been used to prevent aggregation during protein folding, promote refolding, and promote solubilization of misfolded proteins, which reduces the occurrence of inclusion bodies [26]. Lowering the growth temperature has also been shown to reduce protein aggregation by preventing hydrophobic interactions, however, this would come at the cost of lower growth rate [27]. Other factors that may affect the formation of inclusion bodies include "medium composition, choice of expression vectors, choice of promoters, choice of expression hosts, application of fusion tags, rate of protein synthesis, inducer concentration, and duration of induction" [19]. Under fully optimized conditions, *E. coli* was able to produce fully assembled and functional active Immunoglobulin G (IgG), which shows the potential of monoclonal antibody production in *E. coli* [28]. One final drawback is the lack of cellular machinery for post-translational modifications, such as glycosylation and phosphorylation [29, 30]. This has made CHO cells more favourable to *E. coli* as they are mammalian cells with the required cellular machinery. However, progress has been made to address this issue in *E. coli* [31]. N-glycosylation is an important and common type of glycosylation, and the required machinery was able to be transferred into *E. coli* using *Campylobacter jejuni*, which enabled it to express N-glycosylated proteins [32, 33]. Some common strains of *E. coli* that are used include K-12 and BL21 (DE3). K-12 strains have

been traditionally used due to ease of plasmid propagation and cloning [34], whereas BL21 (DE3) has been increasingly used as it exhibits less protein degradation [35], faster growth [36], less acetate accumulation [37], and a T7 expression system containing an inducible promoter such as lac and ara [38].

2.2 *E. coli* Metabolism and Growth

E. coli has three native glycolytic pathways, which include the Embden-Meyerhof-Parnas (EMP) pathway, the Entner-Doudoroff (ED) pathway, and the oxidative pentose phosphate (OPP) pathway [39]. The dominant pathway is the EMP pathway, and it yields two pyruvates, two adenosine triphosphate (ATP), and two nicotinamide adenine dinucleotide (NADH) per glucose molecule [39]. The pyruvate would then enter the citric acid cycle for further metabolism as shown below in Figure 2.2.

Cell metabolism can be categorized into four groups: anabolism, oxidative catabolism, mixed-acid fermentation, and overflow metabolism [5]. Anabolism is biomass production through glucose and energy consumption. Oxidative catabolism is aerobic energy production through the oxidative pathway, which includes the EMP pathway, the citric acid cycle, and the electron transport chain [5]. Mixed-acid fermentation is anaerobic energy production through the fermentative pathway, which produces acetate, formate, D-lactate, succinate, ethanol, carbon dioxide, and hydrogen [4, 5]. Overflow metabolism is a production of acetate when there is an excess of glucose available due to saturation of the oxidative catabolism pathway [4, 5].

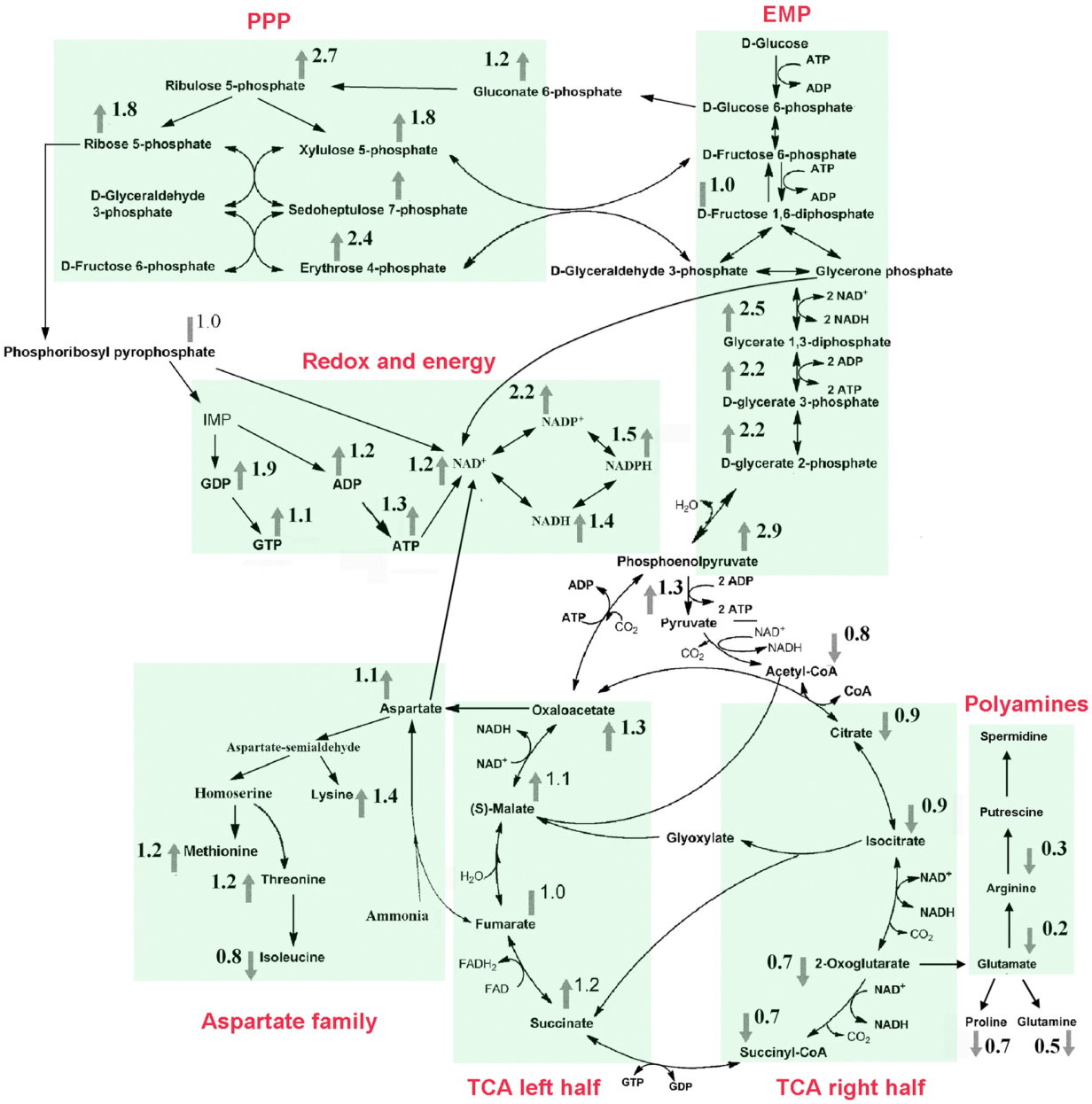


Figure 2.2: An overview of glucose metabolism in *E. coli* by Wang et al. (2019) [40]. Used under the Creative Commons Attribution 4.0 International License (`http://creativecommons.org/licenses/by/4.0/`).

Given these types of metabolism, for a high-density culture, considerations must be made, such as oxygen/nutrient requirements and acetate inhibition, so that mixed-acid fermentation and overflow metabolism is avoided [4, 41]. It has been estimated that the maximum cell density of *E. coli* is well below 250 g/L because that is the approximate density of dry cells packed in a centrifuged tube [42]. For the culture to maintain fluidity, it was found that the density should be below 220 g/L, as fluidity is lost beyond this point [43]. While the theorized maximum cell density is 200 g/L, the highest cell density reported is currently 190 g/L [37]. Regarding oxygen needs, oxygen transfer requirements are thought to not be a limitation when pure oxygen is supplied to media at 25°C. However, this is usually not practical in regular production settings because of safety concerns, cost of pure oxygen, and stress responses of *E. coli* to pure oxygen [37, 44]. For nutrients, *E. coli* requires carbon, nitrogen, phosphorus, sulfur, magnesium, potassium, iron, manganese, zinc, copper, and other growth factors [45]. Typically, the required nutrients are added to a basal broth such as LB broth or a chemically defined medium. On the other hand, higher concentrations of the main media components, sulfur, phosphorus, and trace elements must be added for higher density cultures [44]. It must be noted that most media components at a high concentration inhibit *E. coli* growth, so they must be added as they are consumed. Some reported inhibitory limits include glucose at 50 g/L, ammonium at 3 g/L, iron at 1.15 g/L, magnesium at 8.7 g/L, phosphorus at 10 g/L, and zinc at 0.038 g/L [44, 46]. It must also be made sure that precipitation does not occur due to the interaction between media components as it can affect nutrient supply, the fermentation process, and downstream processes [44]. This is one reason why some components must be sterile filtered instead of being heat sterilized,

as the heat can cause interaction between components to form precipitates. Another factor is that the osmotic pressure and conductivity of media can affect the cell membrane potential, which causes lower growth [44]. Finally, as mentioned earlier, acetate concentrations must be monitored because it inhibits growth and product formation when reaching a concentration of about 2 g/L [44]. The main cause for acetate accumulation is an excess of glucose being available, which causes rapid growth and as mentioned earlier, a saturation of the citric acid cycle and the electron transport chain [4, 47]. An additional consequence of this is that extra base must be added to the culture to control the pH as the release of acetate lowers the pH of the media [48]. This results in the accumulation of salts which creates higher osmotic pressure. To make use of the base added, ammonium hydroxide is typically used so that it can double as an extra nitrogen source [37]. The strain and medium used will affect the critical growth rate at which acetate is produced. For example, in one strain, acetate was produced when the growth rate exceeded 0.2 h^{-1} in complex media and 0.35 h^{-1} in defined media, but another strain produced when it exceeded 0.14 h^{-1} in defined media. Methods for reducing acetate production has been explored, including changing carbon sources, reducing the growth temperature (which reduces the growth rate), and through metabolic engineering [37]. This is achieved in bioreactor cultures typically by controlling the amount of substrate in the media through an efficient feeding strategy.

2.3 Batch and Fed-Batch Operation

E. coli is grown in bioreactors in different types of operation modes. Batch, fed-batch, continuous, and perfusion operating modes are used and each has advantages and disadvantages. Batch operation involves a nutrient broth with fixed initial concentrations of substrate, and the culture proceeds until substrate limitation as there are no additions of substrate during the course of the culture. Consequently, there is an accumulation of byproducts over time, and this method is used for lower cell density cultures. This mode is typically useful to characterize a culture for feeding strategies. Other advantages of this mode are that it is very simple to run and has low risk of contamination. The downsides are that the yields are very low due to the typically shorter duration, low cell density, and toxic byproduct accumulation [49]. Continuous operation is when additional substrate solution is fed while cells and culture medium are harvested. This allows for nutrient replenishment and harvesting of cells while removing byproducts. A steady state is reached by keeping the volume and growth rate constant by keeping the dilution rate equal to the growth rate. The advantage of this is that product quality can be increased through the constant growth environment, and the steady state culture can be maintained for several months to reduce downtime. The disadvantages are that it is more challenging to operate, there is a higher risk of contamination due to the continuous feeding and harvesting for extended periods of time, and there is limited traceability due to continuous harvesting rather than a batch harvest. Perfusion culture is similar to continuous culture except that cells are recycled back into the bioreactor while the culture media is harvested. This allows for byproducts to be removed and nutrients to be

replenished thus resulting in higher cell densities. Perfusion operation also leads to a higher volumetric productivity, which allows for a smaller equipment footprint as well. Similar to continuous operation, this mode is also difficult to operate, but it is slightly less prone to contamination due to shorter run durations as compared to continuous. Finally, fed-batch culture is when feed is added to the culture after a period of time in batch operation to replenish nutrients that have been consumed to increase cell density throughout the process. The feed is typically concentrated in order to lower the volume added to the culture. This mode is the most common mode of operation, and unlike batch operation, higher cell densities can be achieved due to additional substrate, which leads to longer cell cultures for higher yields. This also means that the initial substrate concentration can be lowered to improve growth and reduce byproduct formation such as acetate during the early stages of the culture compared to batch operation where higher substrate is added to try to extend the culture as long as possible. Disadvantages include higher risk of contamination due to feeding throughout the culture, and there is a lack of byproduct removal as harvesting occurs at the end of the process [49].

High cell densities are preferred to increase product generation, so fed-batch and perfusion cultures would be ideal modes of operation, where fed-batch is currently widely used due to its simplicity compared to perfusion, and it is well-established in industrial applications. There are several feeding techniques including constant feeding, increased feeding, exponential feeding, DO-stat, pH-stat, carbon dioxide evolution rate-based feeding, cell concentration-based feeding, and substrate concentration-controlled feeding [37]. Constant feeding is substrate addition at a constant rate, meaning substrate concentration will decrease as cell density increases due to higher total consumption,

resulting in reduction in the growth rate. Increased feeding involves increases of substrate feed at a gradual, linear, or stepwise rate throughout the culture, compensating for decreases in the specific growth rate [37]. Exponential feeding is similar to increased feeding, except substrate addition increases exponentially to keep the growth rate constant; it can be described by Equation 2.1, where $M_s(t)$ is the mass flow rate of the

$$M_S(t) = F(t)S_0 = \left(\frac{\mu}{Y_{X/S}} + m_X\right) X(t_0)V(t_0)\exp[\mu(t - t_0)] \tag{2.1}$$

substrate, $F(t)$ is the feed flow rate, S_0 is the substrate concentration of the feed solution, μ is the growth rate, $Y_{X/S}$ is the yield factor, m_X is the maintenance coefficient, $X(t_0)$ is the initial cell concentration, $V(t_0)$ is the initial volume, and t_0 is the time when feeding was initialized [43]. The DO-stat feeding method is when substrate is added when the DO rises due to substrate depletion. This occurs because aerobic respiration will not occur when there is no more carbon source available, which would result in an increase in DO due to lowered oxygen demand [37]. The pH-stat method is based on a similar principle, but with pH used to trigger feeding instead of oxygen. Feeding occurs when the pH rises due to depletion of the carbon source. This happens because of a release of ammonium ions from the cells when the carbon source is depleted. It must be noted that DO-stat responds more rapidly in a defined medium, whereas in semi-defined or complex media, pH-stat is more suitable due to the carbon-nitrogen substrates such as yeast extract and peptone. This is because the DO change is small with complex substrates as they get consumed after the carbon source is depleted. The carbon dioxide evolution rate (CER) based feeding is done by measuring this value to control the feeding rate. This

can be done due to the CER being approximately proportional to the consumption of the carbon source. The cell concentration can also be used to determine the feeding rate by determining the specific growth rate. Substrate concentration control-based feeding is when the substrate concentration is kept constant throughout the culture, which is similar to exponential feeding, however, a feedback control using an online glucose analyzer is done in this case. Of these methods, exponential feeding provides a useful and simple approach to feeding control. On the other hand, more sophisticated methods based on online measurement tools allow for better control of the specific growth rate due to better adaptability through feedback loops. Another strategy that may be employed is using a feeding solution that closely matches the Carbon:Nitrogen:Phosphorus:Sulfur ratio (C:N:P:S) of the target organism [37].

Out of the feeding control strategies, the DO-stat and pH-stat methods are very accessible as DO and pH sensors are standard sensors that fermenters are already equipped with, and they are simple to implement. The effectiveness of these strategies has been shown by Chen et al. (1997) as the feedback control from these sensors provided a higher cell density culture and significantly higher plasmid yields compared to a manual stepwise feeding strategy [50]. This showed that the lower growth rate with this feedback control strategy can achieve high cell density and product yield without needing pure oxygen aeration while being reproducible in both 7 L and 80 L scales [50]. Similar results were shown with DO-stat control with the use of a standard DO sensor where feed rate is decreased when oxygen transfer limits are reached [51]. This was done because growth must be slowed down by reducing substrate feed when oxygen demand is unable to be met to a level that is able to be maintained. This strategy detects acetate accumulation

and consumption as well because they lead to a lower DO reading, which triggers the feed rate to be lowered so that growth rate is slowed down to prevent acetate production. The main purpose of this is to keep the growth rate high to avoid long cultivation time and low productivity while keeping it low enough to prevent overflow metabolism, oxygen transfer limitations, and starvation zones [51].

2.4 Bioreactor Design

In addition to good operation and feeding strategy, the design of a bioreactor is crucial for optimal cell growth and product generation. Bioreactors have many parameters to control including agitation, air flow rate, pH, DO, nutrient supply, and temperature. There are many types of bioreactors including (but not limited to) the stirred tank reactor (STR), modified STR, airlift bioreactor, bubble column bioreactor, wave bioreactor, disposable bioreactor, membrane bioreactor, solid-state fermentation, and three dimensional (3D) printed bioreactors [52]. Aerated STRs are the most common type of bioreactor as they are simple, versatile, scalable, easy to control, and have a low risk of contamination [53]. The agitation system of STRs is very important because it is responsible for keeping the nutrients well-mixed, for providing good distribution of oxygen, and for maintaining ideal conditions throughout the entire reactor. Common impellers for agitation are the Rushton turbine and the pitched blade impellers. Rushton turbines are used for bacteria or yeast cultures as they are able to withstand the high shear mixing from them, whereas pitched blade impellers are used for shear sensitive cells, such as mammalian and insect cells [53]. For mammalian cells that are more shear sensitive, modified STRs are used.

Modifications include a height to diameter ratio that is less than two, usage of perforated-type sprinklers for aeration, and marine-type impellers [54]. Airlift bioreactors have an aerated cylinder where gas flows in from the bottom and comes out the top with a descending tube surrounding it [55]. Bubble column bioreactors are similar, but the aeration system is at the bottom of the reactor and does not have riser and downcomer sections to create a cyclic flow [55]. These types of bioreactors have high mass transfer of oxygen, good mixing with low shear stress, low energy consumption, simple aseptic operation, and simple design, but they are difficult to scale up for industrial applications [53, 55]. Wave bioreactors are used for cultures that are sensitive to shear and require low oxygen demand. They consist of a sterile plastic bag that is permeable to allow for gas exchange, and a rocking table for imparting oscillatory motion and temperature control capability. These reactors are also difficult to scale up as they are limited to a 500 L scale [56]. Disposable bioreactors are made of plastic, are pre-sterilized, and can come in sizes up to 2,000 L [57]. They have gained popularity in industrial applications due to their efficiency and ability to be designed based on the application, thus allowing for flexibility for various geometries [58, 59]. They are convenient to use because they do not need to be cleaned or sterilized, and they can be recycled, which reduces waste. Membrane bioreactors have semi-permeable membranes which keep cells in the bioreactor while allowing substances of a specific size to pass through. They are an excellent choice for efficient separation, possible continuous operation, contamination control, and reduction in space usage [60]. The three main caveats are that they are expensive, complex to maintain, and have flow limitations [60]. Solid-state fermentation typically involves trays, fixed beds, or stirred drums. It is usually used for fungal growth, and the challenges

associated with this include: the hyphae of the fungi are very delicate, sterilization is difficult, and the solid medium can agglomerate, which can cause uneven growth, aeration, and temperature control [61]. With the development of printing technology, customized printed bioreactors have been gaining traction as well for both micro and macro-scale bioreactors due to their customizability [62]. The key parameters to look at when choosing between these bioreactors for particular applications include mass transfer, heat transfer, shear stress, medium homogeneity, scalability, and oxygen transfer [52]. Artificial intelligence and machine learning have been successfully used to improve the efficiency of bioreactors by adjusting parameters in real time [63].

When considering the overall design of bioreactors, they require aseptic operation, agitation, aeration, efficient energy consumption, temperature control, pH control, sampling ports, low evaporation loss, minimal labor requirements, smooth interior surfaces, seals for containment, and aseptic protection [64]. The vessels of bioreactors are typically made of glass in the smaller lab scale due to its non-toxicity, corrosion resistance, and transparency. Stainless steel is common in large scale operations due to its longevity, corrosion resistance, and pressure resistance. Heat is removed by using cooling jackets, silicone shirts, or internal coils when necessary. Heat is supplied through thermostatic baths or internal coils. Usually, internal coils will be necessary in the large scale due to reduced heat transfer area per reactor volume. Sealing assemblies for the agitator are made of gland packing, mechanical seals, or magnetic actuators which use magnets to rotate the shaft. Baffles made of stainless-steel metal strips are installed radially on the vessel walls to prevent swirling, to increase mixing and mass transfer, and to improve aeration. The impellers are made of paddles attached to the agitator shaft

and are used for keeping the bioreactor well-mixed as mentioned before. They also reduce the air bubble size to improve mass transfer, and the number, size, and shape of the impellers vary based on the application. Disc turbines and variable pitch open turbines are commonly used depending on the sensitivity to shear of the culture. The sparger delivers sterile air with bubble size in the range of 5-10 mm. Three common types of atomizers are used, including porous bubblers, nozzle sprayers, or combined bubbler-agitators. Feeding ports are necessary to be able to supply sterile nutrients, control pH through acid or base addition, and control foaming through antifoam addition. Foaming control is important to keep levels down for better process performance and is done using foam or level sensors, which control the addition rate of antifoam, foam traps, or foam skimmers. Valves are another important component and are essential for controlling flow rate, direction, and pressure management of fluids in the bioreactor. Some common valves include ball valves, butterfly valves, diaphragm valves, and safety valves. Finally, the usage and placement of online sensors are critical in order to control the bioreactor environment effectively during a fermentation process. The usual sensors on a bioreactor are temperature, DO, pH, and level sensors, however, carbon dioxide, cell density, and nutrient concentration sensors are other sensors that can greatly improve process performance [64]. The placement of these sensors are an important consideration as readings may be different throughout other regions of the bioreactor, especially in large-scale vessels due to gradient formation.

2.5 Heterogeneities in Bioreactors

Gradient formation in bioreactors generally depends on the mass transfer and consumption time. If the characteristic time for mass transfer is longer than the characteristic time for reaction, gradients will occur, whereas they are likely to not occur if the time for consumption is longer [65]. Substrate and oxygen gradients in bioreactors are the most widely examined due to their importance in aerobic fermentations [66, 67]. The characteristic time for substrate consumption, τ_c can be given by the expression shown in Equation 2.2 below, where S is the substrate concentration, q_S is the specific substrate consumption rate, and X is the cell density.

$$\tau_c = \frac{S}{(q_S X)} \tag{2.2}$$

It is evident that when the cell concentration is high, the characteristic consumption time will be low, which means that gradients will likely occur [68]. Correspondingly, the characteristic consumption time for oxygen will be low because the solubility of oxygen is low in fermentation media, approximately in the order of about 8 mg/L at 1 atmosphere of pressure [69]. The relation between oxygen transfer rate and mixing time is very important because of the low characteristic consumption time of oxygen. For example, large bioreactors in the range of 100 m^3 will realistically have an oxygen transfer rate of 2-5 kg/m^3h, which result in characteristic mass transfer times of about 10-20 seconds, and mixing times in the range of 10-1000 seconds [65, 68, 70] thus resulting in significant oxygen gradients. The mixing time will also depend on the feeding port location, the

sensor location, and the sampling location [71, 72]. This is because the mixing time measurement will vary based on the location in which the sample or reading is collected due to the complex hydrodynamics and the location of the feeding port. For example, if the feeding port and the sensor or sample are both at the top, the mixing time may appear to be short, but if the sensor or sample was at the bottom of the bioreactor, the mixing time will appear to be much longer. The length scale of substrate transport is in the order of 10-100 metres because it is typically fed at a single point. The length scale of oxygen transport has a smaller length scale in the order of 0.01-0.1 metres because the oxygen transfer is dispersed in small bubbles throughout the bioreactor [68]. Other considerations of substrate and oxygen gradients will be that cells will likely not be exposed to high enough levels of oxygen to cause physiological problems, making oxygen transfer to be a major consideration, whereas for substrate, high levels will lead to overflow metabolism, so the concentration of substrate must be ideally kept under a critical value [68, 73].

The main factors that influence the occurrence of gradients include aeration rate, agitation speed, feeding rate, headspace pressure, impeller type and number, reactor design, reactor type, and the physical properties of the medium [68]. An increase in aeration rate will lead to a higher gas holdup, higher oxygen transfer rate, and shorter mixing times, but this has the downside of increased energy demand, increased likelihood of foaming, and possible impeller flooding [74, 75, 76, 77]. The agitation speed will affect the flow pattern and intensity in the bioreactor. An increase in the speed will shorten the mixing time, decrease the air bubble size (which improves oxygen transfer), and increase volumetric power output (which increases $k_L a$ for oxygen transfer). However, this

increases the power demand and shear stress thus requiring more energy and increasing damage of shear sensitive cells [71, 75, 77, 78]. The substrate concentration in the feed, the feeding rate, and the feed port location will affect the substrate distribution in the bioreactor. These parameters must be managed to prevent starvation and overfeeding, which would lead to substrate limitation and overflow metabolism, respectively [67, 79, 80]. For example, a highly concentrated feed at the top of the reactor may cause overfeeding at the top while starving cells at the bottom. An increase in headspace pressure will decrease the bubble size and increase the oxygen saturation concentration. This increases the driving force for oxygen transfer; however, it requires more energy to compress the air, and the vessel will be more expensive due to the requirement of thicker walls to be able to handle the higher pressures [69]. The impeller size and number affect the mixing time and air bubble size, but increasing the number of impellers increases power requirements [81, 82, 83]. The design of all internal components in the bioreactor including the location and size of the impeller, sparger, baffles, and coils will affect the mixing time, oxygen transfer rate, and substrate distribution. On the other hand, having many internal components complicates cleaning post-operation [69, 71, 79, 84]. The reactor type affects the flow pattern, mixing time, and the gas holdup, which affects the k_La and oxygen transfer rate [69, 71, 85, 86]. The physical properties of the medium, such as the viscosity, can negatively affect the oxygen transfer rate and mixing time [87, 88, 89]. In this case, a high viscosity will impact the agitation by making it more difficult to break up air bubbles and slow down mixing. All these factors must be managed to lower the occurrence of gradients and fluctuations in the bioreactor environment.

In a large bioreactor where it is difficult to completely eliminate gradient formation, biological responses from cells have been seen due to the fluctuations in the bioreactor environment [68]. Changes in the metabolome have been observed at a time scale of seconds, where insufficient oxygen will result in fermentative metabolism, which generates by-products such as ethanol or acetate [90]. Another case would be excess substrate, which causes overflow metabolism, generating acetate. This lowers the cell growth rate, cell yield, and product yield, which overall will reduce the economics of the process [37, 91]. Exposure to gradients can also result in changes in the transcriptome, where stress genes have been shown to be expressed in *E. coli* within seconds of the fluctuations. This led to reduced product formation and increased energy demand for cell maintenance by 40-50% [92, 93, 94]. These kind of changes in the transcriptome also led to changes in the proteome, which has been shown to lead to a "tenfold increase in the incorporation of non-canonical amino acids in recombinant proinsulin produced using *E. coli* along with an 18% decrease in product yield" [68, 95]. In longer time scales, there have been increased mutation rates, which have caused heterogeneities in cell populations. Cell populations that can best handle the fluctuations from gradients are favoured to grow [96, 97, 98]. While heterogeneities have shown to produce many negative effects, some positive effects have been also observed, such as higher cell viability, improved product quality, and reduced media viscosity. The negative effects observed were lower biomass yield and morphological changes in cell size [99, 100, 101, 102, 103].

Heterogeneities are however often difficult to investigate as there is a lack of experimental data in industrial scale bioreactors. A reason for this is that they would be very expensive to run as it would require a large volume of media and a lot of time and

resources which would also contribute to down time for a company. Another reason is that publication of such industrial data would be subject to confidentiality. Scale down reactors are often used to replace large-scale experiments, but they require multiple replicate parameters, or they do not truly reflect what may happen in an actual industrial large-scale bioreactor [68], especially in terms of the formation of gradients. There are several published results for large scale bioreactor experiments for various cell lines where heterogeneities have been investigated, but it would be beneficial to have more studies to be comprehensive. In a 3-5 m^3 CHO culture, it was found that hypoxia was detected compared to no oxygen limitation in a 20 L culture [104]. For an 8-9 m^3 *E. coli* culture, the biomass yield was shown to be 20% lower, acetate accumulation occurred, and the product formation rate was unaffected [105]. In two other *E. coli* cultures in 22 m^3 bioreactors, formate accumulation was observed, which confirmed oxygen depleted zones [5, 66]. The biomass was also reduced due to acetate production and re-assimilation from overflow metabolism and mixed acid fermentation. The biomass was reduced by 12%, acetate accumulated up to 300 mg/L, and formate accumulated up to 50 mg/L. Four stress induced genes were detected and the lowest concentration was furthest away from the feeding port, showing that overfeeding caused stress on the cells. The cell membrane potential and integrity were reduced as well [5, 66]. In a 54 m^3 Penicillium chrysogenum culture, 57% of cells were starved and 7% was overfed, where the feeding was done at the top of the reactor [106, 107]. As expected, the cells in the neighborhood of the feeding port were overfed. In a 19.8 - 22.1 m^3 Saccharomyces cerevisiae culture, glucose concentration peaks ranged between 40 - 80 mg/L, and this fluctuation depended on the turbulence at the feed port location. This was scaled up to a 215 m^3 culture and higher

concentrations were found close to the feed port [67, 101]. pH gradients were investigated in a 0.7 m^3 Streptococcus thermophilus culture, but there were no significant gradients found [108, 109]. There was also no significant DO gradients found in a 20 m^3 Trichoderma reesei culture [110]. Based on the experiments in literature so far, gradient formation will vary by application due to the differing cell lines and reactor type and size.

As mentioned earlier, scale down experiments are another option to analyze heterogeneities, and they are still an attractive alternative because of the lack of industrial scale experimental data. They have the advantage of being able to control fluctuations that would occur in large scale bioreactors with precision while also being easy to sample and analyze [68]. There are typically two types of scale down reactors. Pulse feeding reactors are when a variable of choice (such as carbon source, pH, or DO) is pulsed into the reactor at defined intervals [40, 111]. Multicompartment simulators are when two or more reactors are connected. Common configurations are a plug flow reactor (PFR) and a stirred tank reactor connection (PFR-STR) and two STRs in connection (STR-STR); each reactor attempts to mimic a different region in a large-scale bioreactor [100, 112, 113, 114]. Usually, one reactor attempts to simulate a feeding area with higher concentration of the controlled variable while the other attempts to simulate a well-mixed region. The downsides of scale down reactors include the inability to sample at sub-second time scales, inability to replicate flow phenomena and oxygen transfer rates occurring at the larger scale, direct scale down is often designed based on educated guesses which may not be a true reflection of real large-scale reactors, and the number and size of compartments in a large-scale bioreactor can vary, which is difficult to replicate [68, 115, 116]. Scale down cultures of *E. coli* have shown 15% increases in cell

maintenance, 11% decreased growth, 23% increase in acetate, and lower biomass yields in comparison to homogeneous bioreactors [114, 117, 118]. The accumulation of acetate and decrease in growth and biomass match with the large-scale experiments, which show that scale down experiments can still show the effects of heterogeneities in industrial scales. The motivation for many of these experiments, either in large-scale or scale down experiments, is to be able to validate models. The interaction between cells and their environment must be modeled accurately to account for gradients in bioreactors [68].

2.6 Metabolic and Hydrodynamic Modeling of Bioreactors

Computational fluid dynamics (CFD) and compartmental model (CM) approaches have been used to model and study gradients [68]. They are usually coupled with a metabolic model to account for both the fluid phenomena and the metabolism of the cells in a bioreactor. A simple metabolic model typically involves Monod kinetics within mass balances on the bioreactor, typically operated in batch or fed-batch modes. Modifications on Monod kinetics are usually necessary to account for differences that may occur in the bioreactor. Some modifications can include self-growth inhibition, metabolic switching in diauxic growth, and an addition of a lag function for delays in growth or metabolism of acetate [119, 120, 121, 122, 123]. Self-growth inhibition is added to account for slower growth rates at higher cell densities while substrate concentrations are still substantial [123]. According to Monod kinetics, a substantial substrate concentration would normally

keep the growth rate high. In diauxic growth, a cell will undergo a lag phase as it switches from a primary carbon source to a secondary carbon source after the primary source is depleted, such as the switching from glucose to acetate [120, 121] consumption when glucose is depleted. In this case, a metabolic switch is added to the model to account for the lag as the cell switches carbon sources. Lag functions are added to model sigmoidal lag patterns in parameters such as growth rate, as it can gradually increase to adapt to the environment [122, 123]. The types of sigmoidal lag functions include the logistic, Gompertz, Richards, Stannard, and Schnute functions, and the Gompertz function tends to be the most frequently used due to good fit for a variety of experiments [122, 123]. In Monod kinetics, the growth rate would start at a high value and decrease as the substrate concentration goes down, so it would not account for an initial increase in the growth rate. These lag functions also predict the minimum cell density required to switch to acetate metabolism and the effect of high glucose levels that can delay acetate metabolism [120, 122, 123].

CFD involves numerical methods to evaluate the Navier-Stokes equations to determine the hydrodynamics in a system [68]. CFD provides high levels of detail and accuracy about flows in the system to predict local values of parameters throughout a bioreactor volume. The most common numerical method is the finite volume method, where the reactor geometry and time are discretized to obtain a solution. Higher levels of discretization create smaller cells in the mesh and smaller time steps, which increase the computational demand, which is not favorable; however, a certain level of discretization is required to prevent numerical errors. Moreover, small time steps of 5-10 milliseconds are also required for accuracy due to the simulation of the fast-moving rotation of impellers.

The gas-liquid system in bioreactors is modeled with the Euler-Euler or the Euler-Lagrange approach. The Euler-Euler method treats the phases "as interpenetrating continua, with each phase having a volume fraction" [68]. The Euler-Lagrange method calculates the displacement of particles by integrating the particle momentum equation. This method is useful for tracking cells moving throughout the bioreactor, which can be used to account for the time and history of the cells [79, 85, 124]. However Euler-Lagrange methods are significantly more computationally expensive as compared to Euler-Euler methods since they require tracking a large population of individual cells exposed to different environmental conditions.

Several CFD studies of bioreactors have shown that gradients exist, however, they have not shown gradients in pH and DO [80, 108, 109, 110]. Those that have reported gradients showed that biomass yield decreased, transcription changed, and the loss in yield was a function of the feeding port location [79, 107, 125, 126]. CFD models, however, are not a very favorable method of modeling hydrodynamics as they are very computationally intensive by themselves and have long calculation times due to high mesh densities [80].

To reduce computational demand and calculation times, compartmental models (CMs) have been developed. CMs involve a network of homogeneous zones that exchange flows to represent the overall hydrodynamics of the reactor [127]. CMs do not have to simulate complex fluid phenomena since the zones are all homogeneous, so they only need to solve mass balances of the fluid flows between compartments in the network. This allows for computation times in the scale of a few seconds without needing sophisticated computing hardware [108]. The challenge with CMs is identifying compartment volumes

and flow between the compartments as there is no standard approach due to the variety of applications and the need for accuracy [128]. CMs were originally built empirically using knowledge of global flow patterns in a reactor [129]. These global flow patterns include circulation flow, exchange flow, and induced flow. Circulation flow is caused by the impeller, creating a loop above and below the impeller planes. Exchange flow is caused by the intensity of the liquid flow between neighbouring compartments axially. Induced flow is a result of density differences during aeration [129]. More recently, CFD simulations have enabled the automation of developing compartments based on homogeneity tolerance levels [80]. A CM is now initiated by selecting a group of target variables, and then CFD zones are created and compartmentalized. These zones are then connected to exchange flows if they share an interface [80]. Compartmentalization was found to be 4500 times faster than regular CFD simulations while still showing high levels of accuracy [80]. CMs can also be combined with population balance models, where cells are differentially treated based on their growth rate. A time delay is introduced to the response of the cells to a fluctuating environment, which decouples the actual growth rate from location concentrations. This improved the accuracy of modeling acetate production and biological behavior, but fitting to the data was not very accurate [4]. It was shown in the same study that the growth rate distribution widened when cells were constantly exposed to changing substrate concentrations, which meant that fluctuations caused heterogeneous cell populations in terms of growth rate [4]. Flux balance analysis metabolic models were also used to further increase the accuracy of biological kinetics, where a metabolic flux is balanced around each metabolite in a network of enzyme catalyzed reactions and transport processes. However, it does not account for reaction

kinetics and regulation, which limits insight into dynamic responses [130, 131]. When these metabolic flux models were coupled with a compartmental hydrodynamic model, good fitting to experimental data from a 30 m^3 bioreactor culture of *E. coli* was obtained. This fitting was realized for 40 hours of simulated operation, and it was evaluated in a few minutes using a binary search tree method by Promma et al. (2024) [132]. This model was able to correctly predict glucose gradients, acetate peaks in oxygen deficient zones, and biomass concentrations observed in experiments [132].

Chapter 3

Flask and Bioreactor Experiments

3.1 Overview

The goal of this work is to run a bioreactor culture in a 19.5 L vessel (New Brunswick Scientific 19.5 L BioFlo 415 SIP Fermentation System) and determine whether heterogeneities will form, and if they do, to measure them. To begin, a characterization of the *E. coli* strain through 50 mL flask cultures was performed. The growth rate was measured, and this was also treated as initial practice to learning how to grow and sample small scale cultures. As a next step, the bioreactor was run in a 7.5 L batch operation to further characterize the culture growth rate and substrate consumption rate in a larger scale. This allows for a good approximation of the feeding rate required in fed-batch operation. The goal of operating in fed-batch mode is to grow the culture to a sufficiently high density to potentially create gradients along the height of the bioreactor.

The gradients of interest are the pH, DO, cell density, glucose and acetate concentrations, and differences in k_La at three different heights (top, middle, and bottom). The sensor and sampling ports were modified to allow for measurement at these three heights. Using the information from the batch operation, an appropriate feeding rate was estimated and used in a 13.5 L fed-batch operated bioreactor. pH, DO, and k_La gradients were confirmed and measured. This was performed once more in a 14 L fed-batch operated bioreactor, where the cell density, glucose, and acetate concentrations at the top and bottom of the reactor were measured as well. To summarize, the objectives that will be achieved in this chapter are the first five objectives that were mentioned in Chapter 1.

3.2 Methodology

3.2.1 Media Preparation for Flask Cultures

M9 media was prepared in a 400 mL batch using deionized water, 4.512 g of 5X M9 powder (Sigma-Aldrich), 1.6 g of glucose (Sigma-Aldrich), 0.4 mL of stock solution A (SSA), and 0.8 mL of stock solution B (SSB). This was then sterile filtered using a vacuum filter unit (Thermo Fisher) and stored in an autoclaved 500 mL media bottle. 50 mL of SSA was prepared by dissolving 0.15 g calcium chloride (Sigma-Aldrich), 0.025 g iron (II) sulfate heptahydrate (Sigma-Aldrich), and 0.025 g thiamine (Sigma-Aldrich) in deionized water. 100 mL of SSB was prepared by dissolving 24.65 g magnesium sulfate heptahydrate (Sigma-Aldrich) in deionized water. Both SSA and SSB were sterile filtered (Fisher Scientific) by syringe. 1 mL vials of kanamycin monosulfate (Wisent Bioproducts)

were prepared by dissolving 0.5 g into 10 mL of deionized water (50 mg/mL kanamycin monosulfate (KM50)). This was sterile filtered (Fisher Scientific) by syringe and pipetted into 1.5 mL storage vials. The final concentrations of each ingredient in the media are as follows:

- 6.78 g/L Na_2HPO_4
- 3 g/L KH_2PO_4
- 1 g/L NH_4Cl
- 0.5 g/L NaCl
- 4 g/L glucose
- 0.493 g/L (2 M) $MgSO_4 \cdot 7\,H_2O$
- 3 mg/L $CaCl_2$
- 0.5 mg/L $FeSO_4 \cdot 7\,H_2O$
- 0.5 mg/L thiamine-HCl
- 50 µg/mL kanamycin monosulfate

3.2.2 Flask Cultures

50 mL flask cultures were prepared in 250 mL Erlenmeyer flasks. 50 mL of the media prepared for flask cultures was put in the flask under aseptic conditions. 50 µL of KM50

was mixed into the media, and it was inoculated with 1 mL of frozen *E. coli BL21 (DE3) PET-VP1* stock. An initial 1 mL sample of inoculated media and 1 mL of the regular media (as a control) were put in cuvettes to measure the initial optical density at 600 nanometres (OD_{600}) with a spectrophotometer (Beckman Coulter DU530 Life Science UV/Vis Spectrophotometer). The flask was placed in a shaker incubator at 250 revolutions per minute (rpm) and 37°C. 1 mL samples were taken approximately once every hour until stationary phase. Samples were diluted by 10x once the OD_{600} was expected to be greater than 0.6 as the accuracy beyond this point fails to capture the true cell density of the culture. A growth curve was established to obtain the growth rate of the bacterial strain in the small scale. This was done for two flask cultures.

3.2.3 Media Preparation for Bioreactor Batch Culture

8 L of M9 media were prepared for batch operation. A 20 L carboy was filled in 1 L increments to prepare the media. To account for water loss in sterilization in the bioreactor, the media was diluted based on the recommendation by the manufacturer (Eppendorf). 11.28 g of 5X M9 powder (Sigma-Aldrich) and 4 g of glucose (Sigma-Aldrich) was used per each 1 L increment up to 7 L, then diluted by 1 L of deionized water (as the manual indicated to expect up to 1 L of media loss during sterilization). The 8 L was pumped into the bioreactor with a peristaltic pump, and then the sterilization in place (SIP) procedure was begun on the bioreactor. This consisted of a cooling jacket draining phase for 2 minutes, then two heating phases which bring the temperature up to 121.5°C (sterilization temperature), and finally a sterilization phase

for 45 minutes. Once this is complete, two cooling phases bring the temperature down to 37°C (growth temperature) using cooling water. 7.5 mL and 15 mL of sterile filtered SSA and SSB, respectively, were added aseptically after the SIP procedure, using a propane torch to keep the environment sterile. 7.5 mL of a prepared KM50 solution was added aseptically as well. The bioreactor had a final volume of approximately 7.5 L as only 500 mL of fluid was lost during sterilization.

3.2.4 Bioreactor Batch Operation

To prepare inoculum for the batch operation, three 50 mL flask cultures were grown overnight and concentrated into one 50 mL falcon tube to obtain a density that would be suitable for inoculating into 7.5 L of media. This was done by centrifuging the three flask cultures in three 50 mL falcon tubes, then decanting the supernatant, and finally, resuspending the cell pellets in 50 mL of fresh media. Once one cell pellet was resuspended using a vortexer, the culture was transferred to the next falcon tube to resuspend the second cell pellet. The same was done for the third cell pellet. This resulted in a cell density of approximately $OD_{600} = 7$. Sterile antifoam 204 (Sigma-Aldrich) and 29% w/w ammonium hydroxide (Sigma-Aldrich) was connected to the peristaltic pumps and feeding port of the bioreactor with sterile tubing and addition bottles. Approximately 0.075 mL of the antifoam was pumped into the bioreactor. The initial setpoints of the bioreactor were set to 37°C, 250 rpm, pH of 7.0, DO of 30%, and an air flow rate of 0 standard litres per minute (SLPM). The DO was controlled by a cascaded control system which changes the agitation and air flow rate between 250-350

rpm and 0-15 SLPM respectively based on the output of the controller. The bioreactor was then inoculated using a sterile syringe. An initial sample was taken and measured against a control to obtain the starting OD_{600} of the culture. The first sample was taken after 2.3 hours, and the following samples were taken in approximately 1-hour increments. Samples were diluted by 10x once the OD_{600} was about to surpass 0.6. The samples were collected in 50 mL falcon tubes and put in an ice box to stop any further growth. Approximately 40 mL of sample was taken each sampling period, with 5 mL being drained initially to replace the fluid that was stagnant inside the sampling tube. The OD_{600} was measured after each sample was collected using a spectrophotometer (Beckman Coulter DU530 Life Science UV/Vis Spectrophotometer). The bioreactor was terminated and cleaned after the culture reached stationary phase. The agitation, temperature, air flow, DO, pH, and base pump profiles were extracted from the bioreactor as well. The samples were centrifuged for 30 minutes at 3500 rpm and sterile filtered to obtain the supernatant. These samples were then analyzed with an high performance liquid chromatography (HPLC) (HPLC (Agilent 1260 Infinity II with Aminex HPX-87H Column, 300 x 7.8 mm) to obtain the glucose and acetate concentration profile during the run.

3.2.5 Media Preparation for Bioreactor Fed-Batch Culture 1

14.5 L of M9 media were prepared for fed-batch operation. A 20 L carboy was filled in 1 L increments to prepare the media. To account for water loss in sterilization in the bioreactor, the media was diluted based on the recommendation by the manufacturer

(Eppendorf). 11.28 g of 5X M9 powder (Sigma-Aldrich) was used per each 1 L increment up to 13.9 L (last volume was 900 mL but still using the same amount of M9 powder), then diluted by 500 mL of deionized water as the previous sterilization showed a 500 mL loss of media. The 14.4 L was pumped into the bioreactor with a peristaltic pump, and then the SIP procedure was begun. A separate 100 mL containing 14 mL SSA, 28 mL SSB, and 56 g of glucose (Sigma-Aldrich) was prepared and sterile filtered using vacuum filter units (Fisher Scientific). This was then similarly added as before aseptically to the bioreactor post-sterilization. The final volume was 13.5 L as 1 L of media was lost due to sterilization as it had to be run twice (first sterilization failed to reach 121.5°C). 13.5 mL of a prepared KM50 solution was added aseptically as well. 500 mL of feed solution was prepared; the feed solution includes deionized water, 250 g of glucose (Sigma-Aldrich), 4.512 g 5X M9 powder (Sigma-Aldrich), 0.2465 g magnesium sulfate heptahydrate (Sigma-Aldrich), and 0.5 mL of KM50. The concentrations of the feeding solution components were as follows:

- 500 g/L glucose
- Regular M9 media component concentrations (first four bullet point listed ingredients in 3.2.1)
- 0.493 g/L (2 M) $MgSO_4 \cdot 7\,H_2O$
- 50 µg/mL kanamycin monosulfate

3.2.6 Bioreactor Fed-Batch Operation 1

To prepare inoculum for the batch operation, six 50 mL flask cultures were grown overnight and concentrated into one 50 mL falcon tube to obtain a density that would be suitable for inoculating into 13.5 L of media. Sterile antifoam 204 (Sigma-Aldrich), 29% ammonium hydroxide (Sigma-Aldrich), and the 500 mL of feed was connected to the peristaltic pumps and feeding ports of the bioreactor with sterile tubing and addition bottles. Approximately 0.135 mL of the antifoam was pumped into the bioreactor. The initial setpoints of the bioreactor were set to 37°C, 200 rpm, pH of 7.0, DO of 30%, and an air flow rate of 5 SLPM. The DO was controlled by a cascaded control system with an agitation range of 200-500 rpm, and an air flow rate range of 5-20 SLPM. The bioreactor was then inoculated using a sterile syringe. An initial sample was taken and measured against a control to obtain the starting OD_{600} of the culture. The first sample was taken after 1.35 hours, and the following samples were taken in approximately 1-hour increments. Samples were diluted by 10x or 20x as needed by the criteria given in Section 3.2.2. The sampling was performed in the same way as in the batch operation. The feed rate was established based on the consumption of glucose in the batch operation, where feeding starts at a cell density between 0.15 – 0.25 g/L. The feed rate was a stepwise function, where the rate was set to:

- 0.036 L/h between 4.72 h – 7.68 h
- 0.072 L/h until 8.72 h
- 0.108 L/h until 9.63 h

- 0.144 L/h until approximately 11.2 h (where the feed was exhausted)

This feeding profile was estimated to attempt maintaining a glucose profile that would be approximately constant. Approximately 9 hours into the fermentation, it was assumed that the cell density may be sufficiently high to produce gradients along the height of the reactor, so modifications were made to the heights of the DO and pH sensors. The DO% and pH measurements were noted at heights of 0.14 m, 0.305 m, and 0.47 m (heights of the bottom, middle, and top of the reactor). The k_La was also measured at these heights by shutting off the air supply, then resupplying it again once the DO% was sufficiently low (<10%). This was measured by calculating the uptake rate when the air was shut off, then finding the k_La by having the change in oxygen over time equal to 0 when the reading settles back to 30%. These were also done at approximately 11 hours into the fermentation as well. The bioreactor run was terminated and cleaned once the culture reached stationary phase, and the samples were processed and analyzed as before in the batch operation. The samples from this were also used to create a calibration curve between the OD_{600} and the cell concentration in g/L. This was done by noting the total sample volume, then freeze drying the cell pellet to obtain the dry cell weight.

3.2.7 Media Preparation for Bioreactor Fed-Batch Culture 2

The methodology was the same as in the first fed-batch culture, however, the intended volume of 14 L was achieved as sterilization was successful in one attempt. 14 mL of a prepared KM50 solution was added aseptically. The feeding solution was also kept the same.

3.2.8 Bioreactor Fed-Batch Operation 2

The culture was initialized in the same manner as the first fed-batch experiment. After the first samples were taken post-inoculation, the next sample was taken after 2 hours of growth. Subsequent samples were taken in 1-hour increments and diluted as necessary. The feed rate was established based on the modeling of consumption of glucose in the first fed-batch operation, where feeding started at a cell density between 0.35-0.55 g/L. The feed rate was a stepwise function, where the rate was to be set to 0.0216 L/h between 5.7 h – 9 h, 0.036 L/h until 14.5 h, then 0.0504 L/h until 19 h. This feeding schedule attempts to maintain the glucose profile to be constant. However, due to some issues with the feeding tube being occluded, the feeding was not performed on time. Thus, the rates were increased sooner than intended. Glucose test strips were also used to monitor the concentration; however, they showed concentrations of 0, so the feeding was further accelerated, and the feeding profile became as follows (where the first 5 flows may not have been on for 100% of the time due to tube occlusion):

- 0.0216 L/h between 5.7 h – 8.5 h
- 0.036 L/h until 10.25 h
- 0.0504 L/h until 11.9 h
- 0.072 L/h until 12.27 h
- 0.108 L/h until 13.35 h
- 0.144 L/h until 16 h

At 16 h, the solution was exhausted. Approximately 12 hours into the fermentation, it was assumed that the cell density may be sufficiently high to produce gradients along the height of the reactor, so modifications were made to the heights of the DO and pH sensors. In this experiment, sampling was done at the top and bottom of the reactor as well, starting at this point in time. The DO% and pH measurements were noted at heights of 0.14 m, 0.305 m, and 0.47 m (heights of the bottom, middle, and top of the reactor), and the k_La was also measured as in the first experiment. These measurements were conducted several times before the termination of the culture, until 19.3 h. The bioreactor run was terminated and cleaned once the culture reached stationary phase, and the samples were processed and analyzed as before.

3.3 Results and Discussion

3.3.1 Characterizing the *E. coli* Culture Through Flask Culture and Bioreactor Batch Operation

Two 50 mL flask cultures were performed in 250 mL Erlenmeyer flasks at 250 rpm and 37°C in a shaker incubator for a basic initial study in the small scale and to practice working with cell culture. A growth curve was constructed using the OD_{600} of the samples taken from the flask cultures. The initial OD_{600} was 0.046 for both flasks, and the final density was 2.17 and 2.09. Using the calibration curve shown in Figure 3.1 (where X is the dry weight cell density), the equivalent cell density was 0.023 g/L, 1.08 g/L, and 1.04 g/L, respectively.

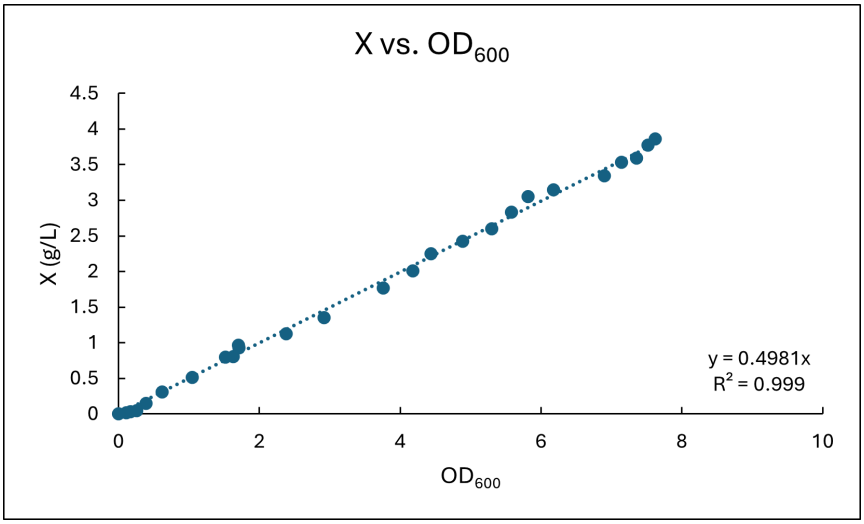


Figure 3.1: Calibration curve between optical cell density and dry cell weight density. Freeze dried cell pellet samples from the first fed-batch experiment were used to construct this plot.

The specific growth rate during exponential phase was 0.498 h^{-1} and 0.489 h^{-1}. The plots shown in Figure 3.2 and Figure 3.3 show the growth curve and fitting of the growth rate during exponential phase of the first flask culture. The curves for the second flask culture may be found in Appendix A.1. It is evident in these figures that exponential phase started almost immediately after inoculation.

The apparent biomass yield on glucose was estimated to be 0.264 and 0.254 g cell/g glucose based on a 4 g/L glucose concentration becoming depleted at the end, and the peak cell densities. The yield is lower than what is reported for wild type strains that report a yield of 0.5 g cell/g glucose, and the growth rate lies in a typical range for various *E. coli* strains [37]. With this as a base for understanding the growth kinetics of the culture, a batch operation of the culture was prepared.

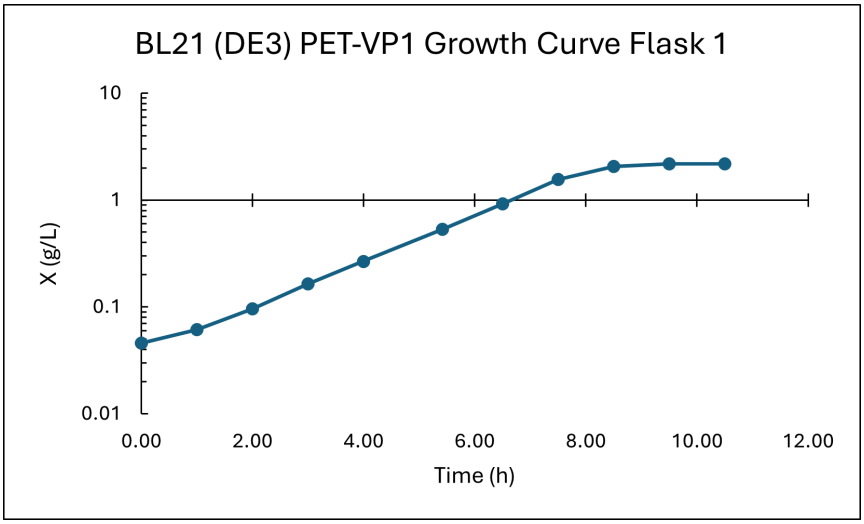


Figure 3.2: Growth curve of *E. coli BL21 (DE3) PET-VP1* flask culture 1 at 250 rpm and 37°C.

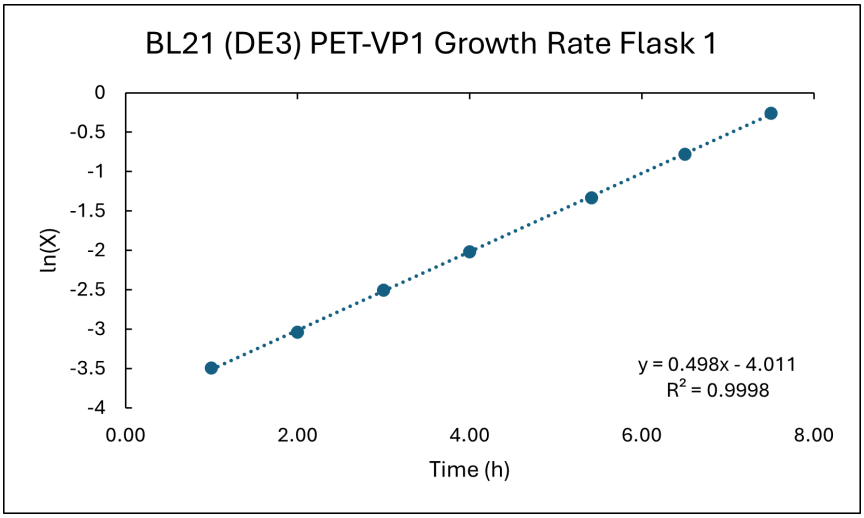


Figure 3.3: Exponential phase of the growth curve to calculate the growth rate of the first flask culture.

A 7 L batch operation was intended; however, the final volume was approximately 7.5 L as there was less water loss than expected during sterilization. Due to this reason, the final concentration of glucose and other nutrients were about 7% less of what they

normally should be. The glucose, in this case, was also heat-sterilized as it was assumed to not affect the culture significantly. The inoculation and final cell densities were 0.022 g/L and 0.852 g/L, respectively. Figure 3.4 shows the plotted growth curve of the bioreactor and the flask cultures, and it is seen that the initial growth rate at the first two hours shows more lag compared to the growth in the flasks. It is also evident that the flask cultures grew faster and to a higher cell density, however, this result may be attributed to the lower nutrient concentration due to the excess water. The specific growth rate was measured to be 0.3768 h^{-1} as shown in Figure 3.5. The apparent biomass yield on glucose was estimated as 0.232 g cell/g glucose, which is slightly lower than the yield coefficients from the flasks.

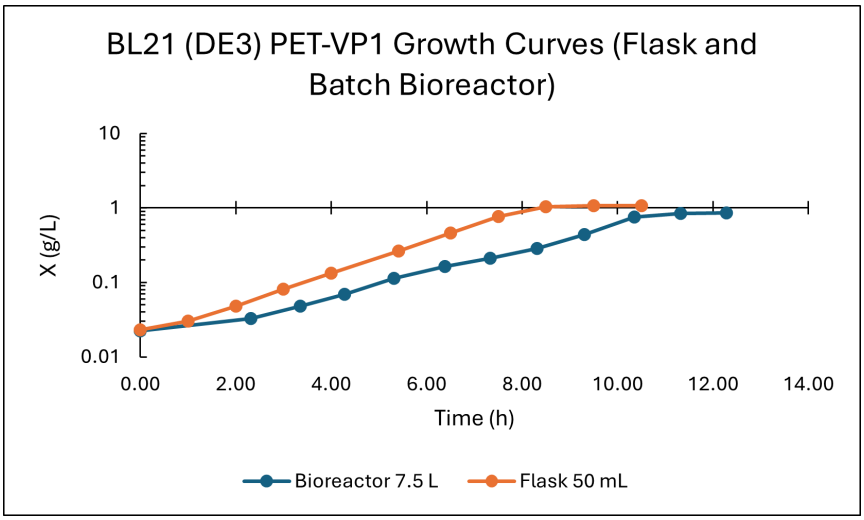


Figure 3.4: Growth curve comparison between flask culture 1 and the 7.5 L batch operation at 37°C.

There is likely some error in this measurement as there were some issues with the glucose measurement on the HPLC. The reported concentrations were much lower than

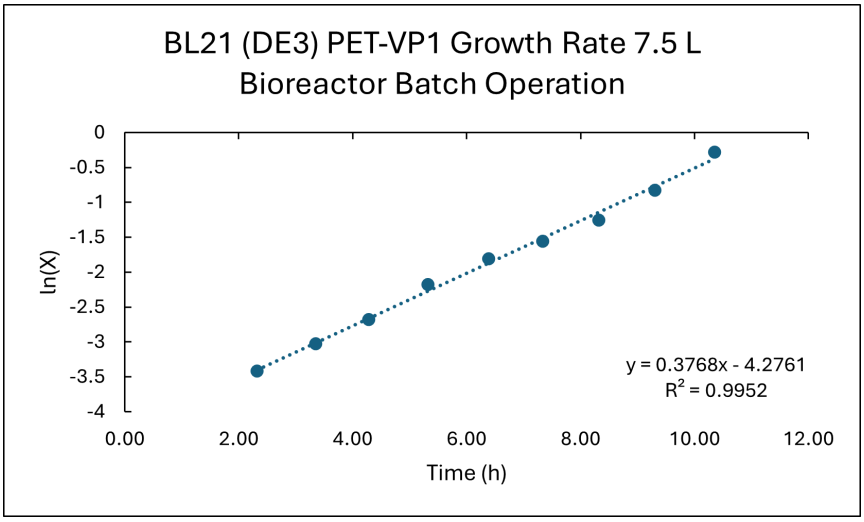


Figure 3.5: Exponential phase of the growth curve to estimate the growth rate of the 7.5 L batch culture.

they were expected to be, so they were multiplied by a constant factor of 2.48 for the entire profile, with the assumption that the initial glucose concentration was 3.7 g/L. Figure 3.6 shows the biomass, glucose, and acetate concentration profiles throughout the fermentation. As expected, acetate is produced as the glucose is consumed in the early to late stages of the culture; however, once the glucose is nearly depleted, there is a metabolic switch to the consumption of acetate at about 10.35 h. The acetate production also shows that this growth rate is higher than the critical growth rate, where acetate starts to be produced [37]. The glucose was also not fully consumed (as was assumed in the flask culture) and was left at 0.138 g/L. The peak acetate concentration was 0.546 g/L before it was consumed until a final concentration of 0.272 g/L.

The glucose consumption rate was then calculated based on the change in glucose concentration over time and the optical cell density (as the calibration between optical

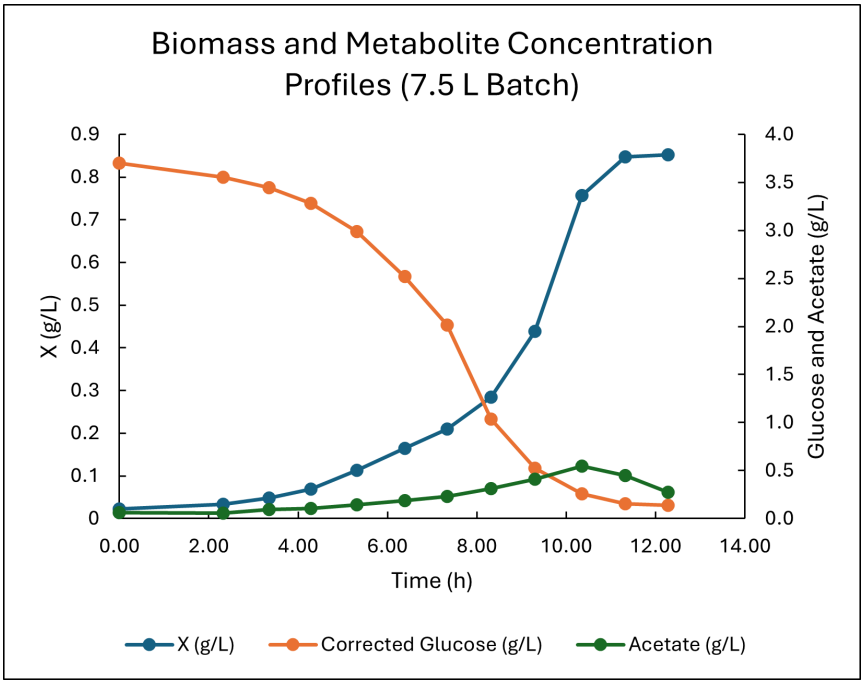


Figure 3.6: Biomass and metabolite concentrations over time for the 7.5 L batch culture. The glucose is labeled as corrected because the measurement from the HPLC needed a correction factor of 2.48, and it was corrected based on an assumed initial glucose concentration of 3.7 g/L.

density and dry cell weight density has not been made at this time yet). An appropriate feeding rate was calculated for by using Equation 2.1, where the glucose feed concentration was set to 500 g/L, the yield coefficient was assumed to be constant at 0.232 g cell/g glucose as calculated earlier, the cell maintenance coefficient was assumed to be negligible, the initial cell density was set to the same density as in the batch culture (0.022 g/L), the initial volume was set to 14 L, and the growth rate was chosen to be 0.4 h^{-1}. This was chosen arbitrarily based on the growth rates calculated from the flask cultures and the batch culture, where a growth rate closer to the batch culture was chosen. This was because it was assumed that the growth rate would normally be higher

if the batch culture had the correct initial glucose concentration of 4 g/L rather than 3.7 g/L. The feed flow rates that were calculated were then converted to pump flow setpoints that would approximately match the necessary flow that was required to keep the glucose concentration constant throughout the culture.

Plots of the agitation, temperature, air flow rate, dissolved oxygen, pH, and the base addition pump were also extracted from the bioreactor, which can be found in Appendix A.2. As this was the first attempt to operate the bioreactor, the agitation and air flow rate had many fluctuations due to the cascaded control of the DO being managed under very small controller output responses. This was an attempt to learn how to control the cascaded control which changes the agitation rate and air flow rate to control the DO to a specific setpoint of 30%. Another observation was that the agitation and air flow rate decreased near the end of the culture, which signified a lesser demand for oxygen, which was expected of a culture reaching stationary phase. The pH had a downward trend during growth as the culture produced acetate over time; however, it started to rise as the culture reached stationary phase, and ammonium is released from the cells when carbon source is depleted [37]. The pH was also initially at a value of 8, rather than 7, which would have been ideal. A combination of the suboptimal agitation, air flow control, and a higher initial pH may have also caused a longer lag time in the bioreactor in comparison to the flask culture growth. Another small issue that occurred was that the base feed tubing was occluded for almost one hour, so the pH had dropped to about 6.58 before base was added to bring it back to a pH of 7. This happened due to the tubing being squeezed with no motion under the peristaltic pump on the bioreactor. The control of temperature was nearly perfect, with a 0.1°C deviation from 37°C in either

direction. Temperature control on the bioreactor is done automatically through a heater and a cooling water jacket.

This successfully completed the objective of characterizing the *E. coli* strain growth characteristics to perform a fed-batch culture. This experiment also served as a learning experience for how to operate and control a bioreactor, especially one of a larger scale compared to bench scale bioreactors typically found in labs.

3.3.2 Bioreactor Fed-batch Operation for Potential Heterogeneity Measurement

With the feeding strategy from the batch experiment, a fed-batch experiment was performed in attempt to obtain a culture of higher cell density to potentially measure gradients along the height of the bioreactor. The initial cell density was approximately 0.037 g/L, and it had a maximum cell density of 3.80 g/L. As shown in Figure 3.7, the culture lasted for 10 hours longer than the batch operation, and a diauxic growth is observed. A slight increase in the growth rate is also observed in the first few hours, and due to the diauxic growth, the growth rate was approximated in two separate intervals of time as shown in Figure 3.8. The first average growth rate was 0.4464 h^{-1}, and the second average growth rate was 0.07 h^{-1}, which is significantly lower than the first rate. The initial growth rate is also higher than the rate from the batch operation as expected due to having the appropriate initial nutrient concentrations similar to the flask experiments.

The apparent yield coefficient was approximated at 0.168 g cell/g glucose, which was 38% lower than the yield from the batch operation. The metabolite concentration profiles

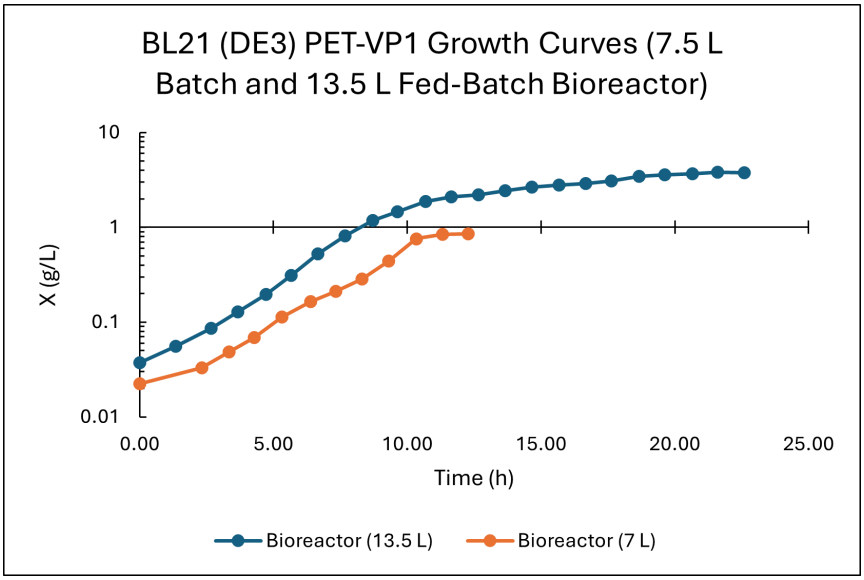


Figure 3.7: Growth curve comparison between the 7.5 L batch operation and the 13.5L fed-batch operation at 37°C.

are shown in Figure 3.9, and it is clear that the feeding strategy developed was too high. The peak glucose concentration was 15.07 g/L, which is much higher than the target of 4 g/L as originally intended. It was noticed afterwards that the feeding calculation was approximately one hour ahead of schedule, which caused the large discrepancy over time. This may also be an explanation as to why the growth rate was very low in the second half of the culture as there is constant adaptation with the large changes in glucose levels over time. The excess glucose causes overflow metabolism, producing acetate, which is known to decrease the growth rate and cell yield [37, 91]. There is about 1.17 g/L of acetate when the growth rate decreases at 11.65 h, and it peaks at 5.84 g/L at the end of the culture, which is a significant amount of acetate accumulation compared to the batch experiment. The acetate accumulation is also where a lot of carbon flux went to instead

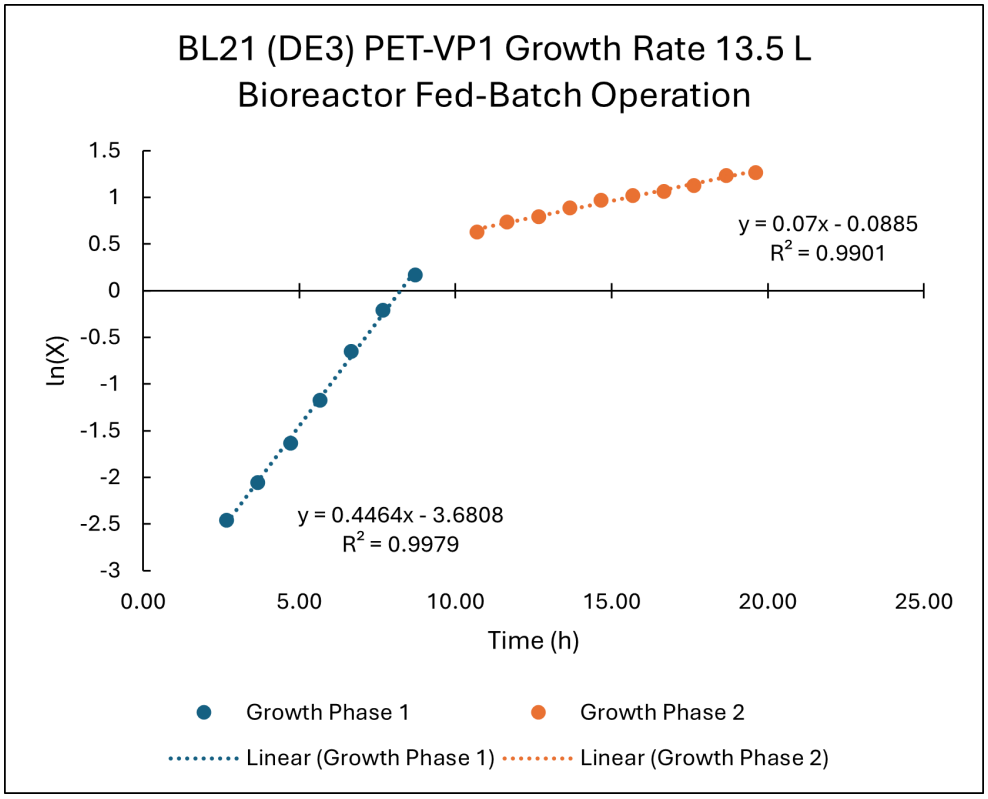


Figure 3.8: Approximate growth rates during each growth phase as observed in the diauxic growth trend for the 13.5 L fed-batch culture.

of biomass, which reduced the overall yield as well. An ammonia assay was done as well to be certain that there is no nitrogen limitation causing the decrease in growth. The concentration profile showed no limitation as shown in Appendix B.1.

Plots of the agitation, temperature, air flow, DO%, pH, feed pump, and base pump were extracted from the bioreactor and may be found in Appendix B.1. The agitation and air flow trends are more of a gradual trend upwards in comparison to the fluctuations in the batch culture as control of the DO% has been more refined. Similar to the batch culture, the agitation and air flow requirement drops significantly at the end of the culture

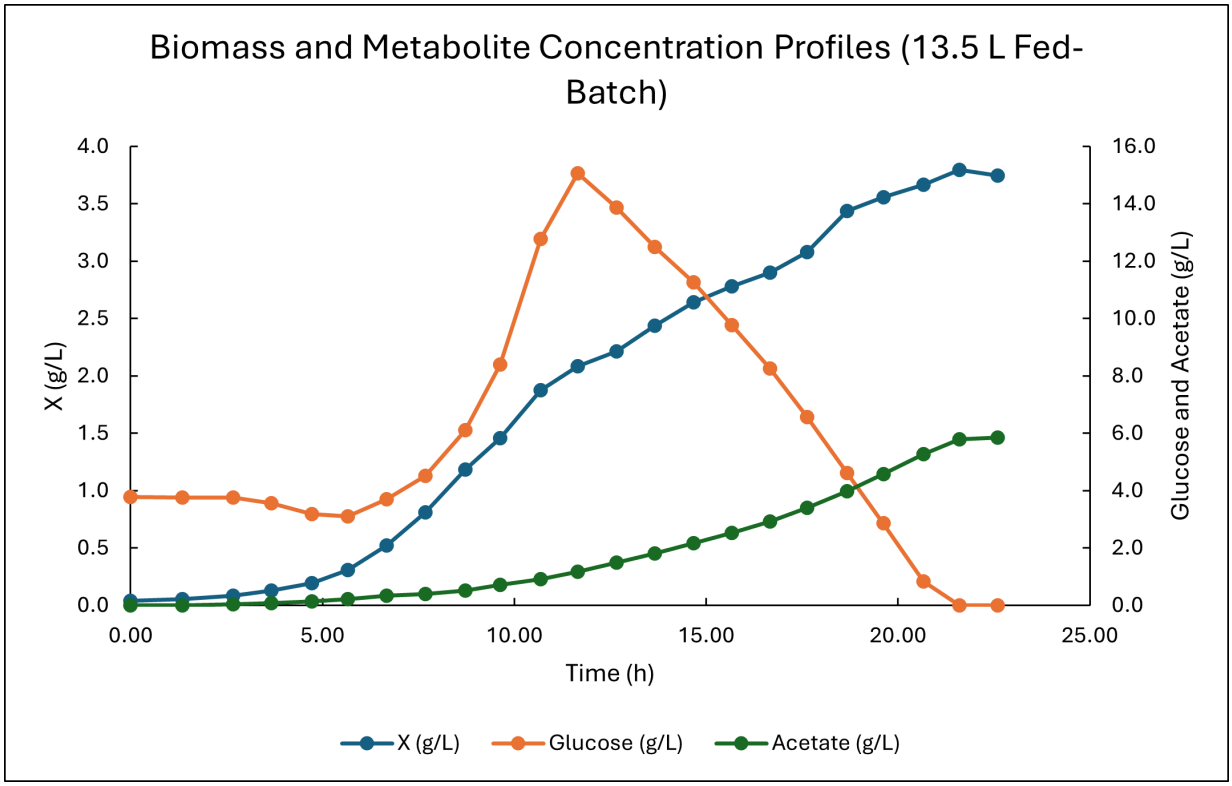


Figure 3.9: Biomass and metabolite concentrations over time for the 13.5 L fed-batch culture.

as oxygen demand is reduced considerably at stationary phase. The two drops and peaks in the air flow and DO% graphs are when the k_La was attempted to be measured; this will be explained further later. The temperature control was nearly perfect as it was in the batch culture. The pH showed a large increase at the start of the culture, which was due to addition of ammonium hydroxide. This was an error caused while priming the base addition tubing, which can be seen in the base pump trend. The tubing was occluded at approximately 8.1 h when the pH started to dip below 7, so it had dropped to 6.71 before this issue was resolved. The fluctuations between 9 h and 12 h were from

sensor movement experiments which will be explained later. The cause for the increase in pH starting from 14.4 h is not clear, however, known reasons for this could include metabolism of nitrogenous compounds such as ammonium, which releases ammonia, or a sudden increase in acetate metabolism, which would both increase the pH of the culture medium. However, the acetate trend and the ammonia trend do not provide any significant evidence for this sudden pH increase. Finally, the decrease in pH at 19.1 h was caused by the need to replenish the addition bottle with ammonium hydroxide solution. The supplement feed pump profile shows the feeding schedule, and the increase in glucose concentration during the addition times, which occurred as the culture grew denser.

Sensor height changes were performed on the DO and pH sensor to measure gradients in the DO, pH, and the $k_L a$. The sensor heights are categorized as bottom, middle, and top, at heights of 0.14 m, 0.305 m, and 0.47 m. The impeller heights of the reactor are at 0.09 m, 0.29 m, and 0.51 m. A rough schematic of the reactor is shown in Figure 3.10. The first changes made for the DO sensor height were bottom, middle, top, middle, and back to the bottom between 8.98 h and 9.05 h. The DO% differences were quite noticeable, where the general trend was that the bottom had the lowest DO%, and the top had the highest DO%. The average difference between the bottom and middle was about 16%, and it was about 14% between the middle and the top. The second change that was made was from middle, top, then bottom between 11.07 h and 11.12 h. The same trend was observed, but with greater differences. The difference between the bottom and the middle was about 17%, and it was about 21% between the middle and the top. The conditions of the agitation, cell density, pH, and air flow rate were approximately equal for each DO sensor height change. The conditions in which the sensor change

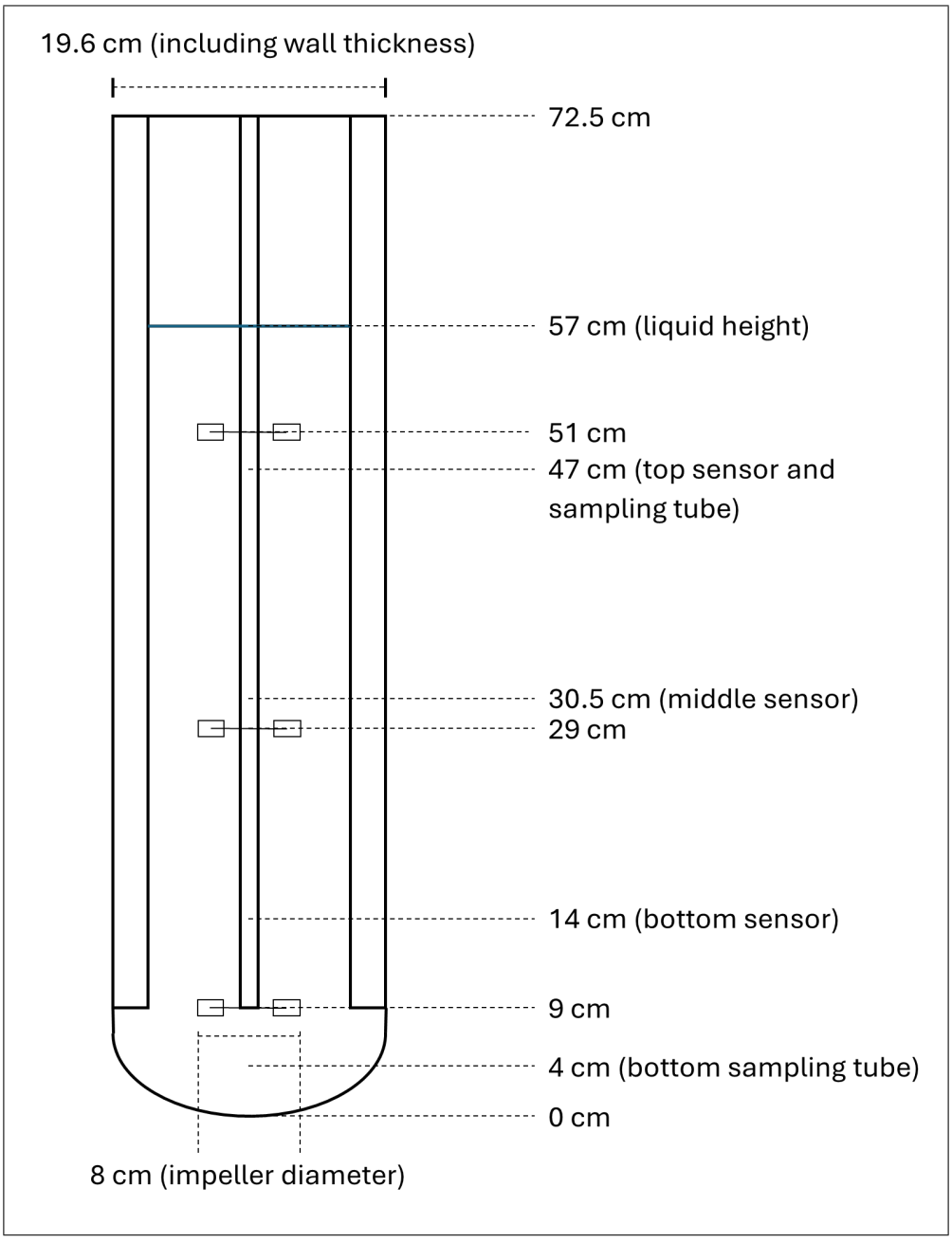


Figure 3.10: Approximate schematic of the bioreactor including the impellers, sensor and sampling locations, reactor diameter, and approximate liquid height for the fed-batch culture.

readings were performed can be found in Table B.1 in Appendix B.1. Figure 3.11 shows the DO% readings at each height and sensor change. As the cell density conditions were not known for these specific times, a rough curve fit was performed to estimate the cell density at the exact time points. The DO% may be higher at the top of the reactor as the air bubbles go through two impellers, reducing the bubble size, and the third impeller is just above the sensor location. There is also headspace pressure for more oxygen transfer from the top. At the bottom of the reactor, the air bubbles may be larger as they only pass through one impeller. The extra pressure from the medium is likely negligible to affect the solubility of oxygen compared to the other heights. In the middle section, the bubbles pass through two impellers, which is likely the reason for the higher DO% compared to the bottom, but less than the top as it is not exposed to the headspace.

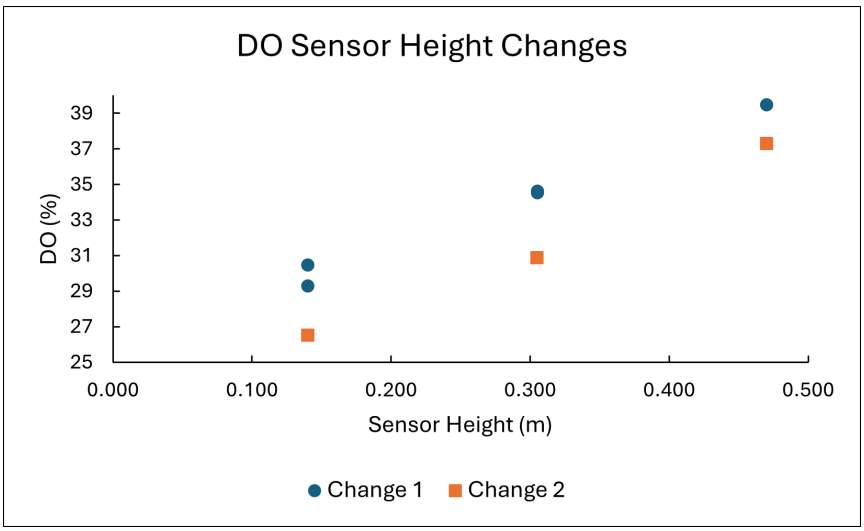


Figure 3.11: DO% sensor height changes for the 13.5 L fed-batch culture at 8.98 h – 9.05 h (change 1), and 11.07 h - 11.12 h (change 2).

The pH changes along the height were less prominent than the DO%, however they

were still noticeable with consistent trends. The height changes were performed four times at the time intervals of:

- 9.37 h – 9.46 h (bottom, middle, top, middle)
- 11.12 h – 11.16 h (bottom, middle, top)
- 11.26 h – 11.31 h (top, middle, bottom, middle)
- 11.53 h – 11.58 h (bottom, middle, top, middle, bottom)

The changes are shown in Figure 3.12 below. Each change displays an increase in pH as the sensor is moved up higher, which can be explained by the base feeding being done at the top. The base is gradually mixed from the top to the bottom to increase the pH at the bottom as it is evident that the mixing time was significant enough to see the pH differences. A table of the conditions is shown in Table B.2 in Appendix B.1, similar to the conditions for the DO sensor changes earlier. On average, the pH difference between the bottom and middle and the middle and top were 0.34% and 0.43%, respectively. These changing conditions along the height of the bioreactor are very promising results as many CFD models have not shown gradients in DO or pH during fermentation simulations [80, 108, 109, 110].

The k_La was estimated with the limitation that the bioreactor records data every 15 seconds at each height as well, since there should be a difference as there was a difference in the DO% reading. The measured k_La values did not show a consistent trend to make concrete conclusions; however, the two changes did seem to reveal that the k_La was lower

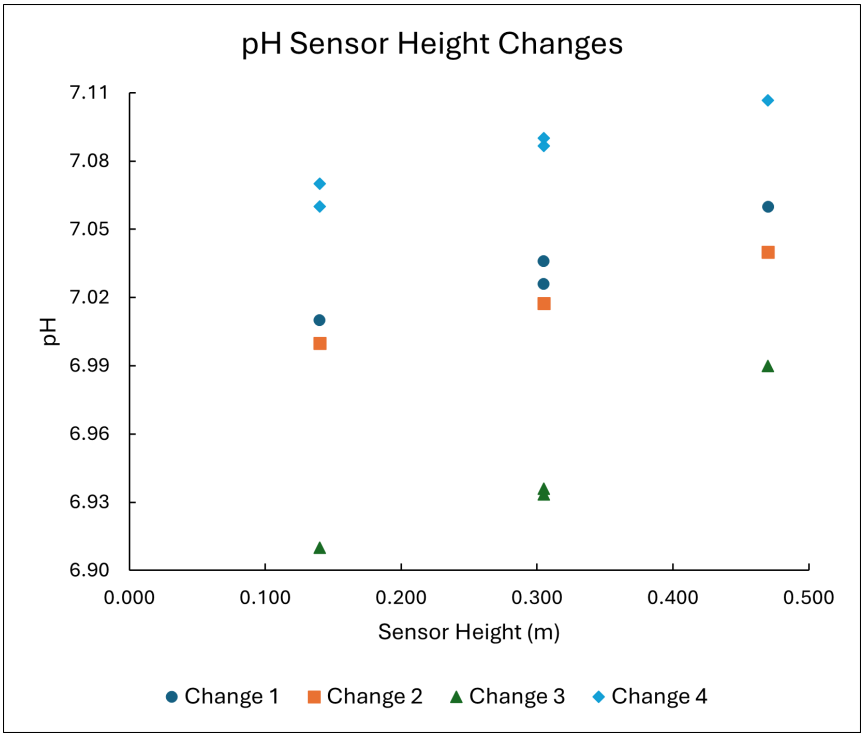


Figure 3.12: pH sensor height changes for the 13.5 L fed-batch culture at 9.37 h – 9.46 h (change 1), 11.12 h – 11.16 h (change 2), 11.26 h – 11.31 h (change 3), and 11.53 h – 11.58 h (change 4).

in general at the bottom of the bioreactor, which is consistent with the lower DO% at the bottom compared to the top of the bioreactor. Figure 3.13 below shows the measured k_La values at each height. A sample of the air flow rate and DO% profile is shown in Figure B.9 in Appendix B.1, where the air shut off and on is displayed to obtain the oxygen uptake rate and transfer rate as DO% reaches steady state afterwards. The conditions in which these measurements were taken are also shown in Table B.3 in Appendix B.1. Additional sensor changes and k_La measurements could have been performed to obtain more data, however, slow down in growth, the sudden increase in pH

(at 15 h), and pause in agitation and air flow increases (at 15 h) led to the belief that the culture was nearing stationary phase, so further measurements were not taken in case that the culture no longer shows any growth while the measurements were being taken. With the knowledge that the culture will likely last over 20 hours, additional measurements were planned in the next fed-batch experiment to obtain concrete data.

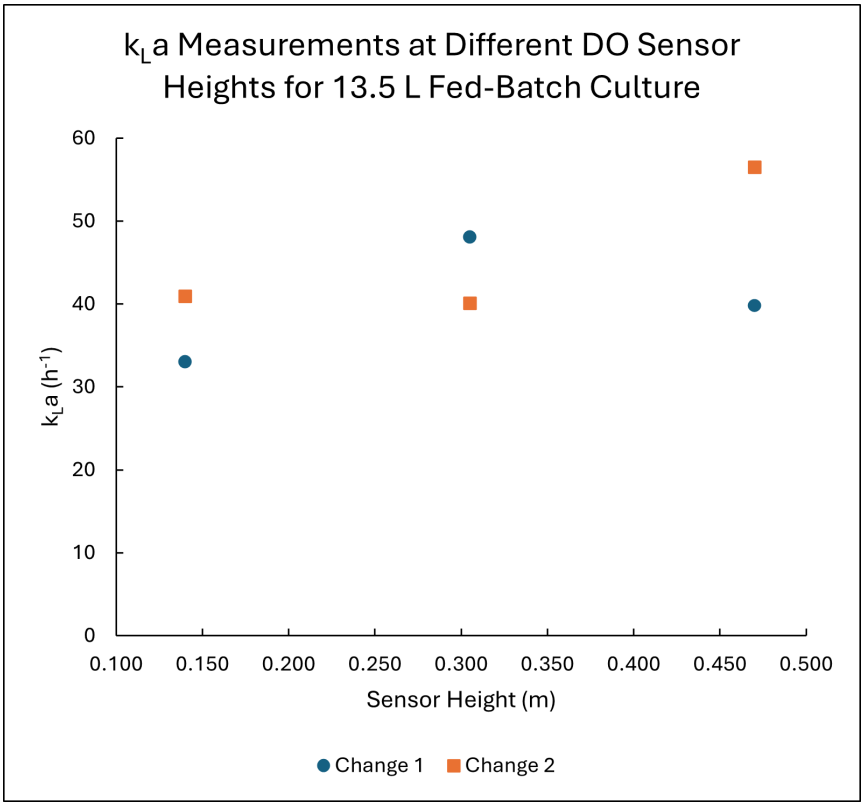


Figure 3.13: k_La measurements at different DO% sensor heights for the 13.5 L fed-batch culture at 9.09 h – 9.32 h (change 1), and 10.81 h – 11.03 h (change 2).

3.3.3 Bioreactor Fed-batch Operation to Verify Heterogeneities

To verify the findings in the first fed-batch experiment, a second fed-batch experiment was performed with more sensor changes, sampling at different heights, and a better feeding control was attempted. Sampling was done at the top starting at 12 h into the culture. The initial cell density was about 0.061 g/L, and it had a maximum cell density of 6.759 g/L at the bottom and 6.931 g/L at the top of the bioreactor. Figure 3.14 shows that the culture was 1.7 h shorter than the first fed-batch culture, however, there was a 78% increase in cell density.

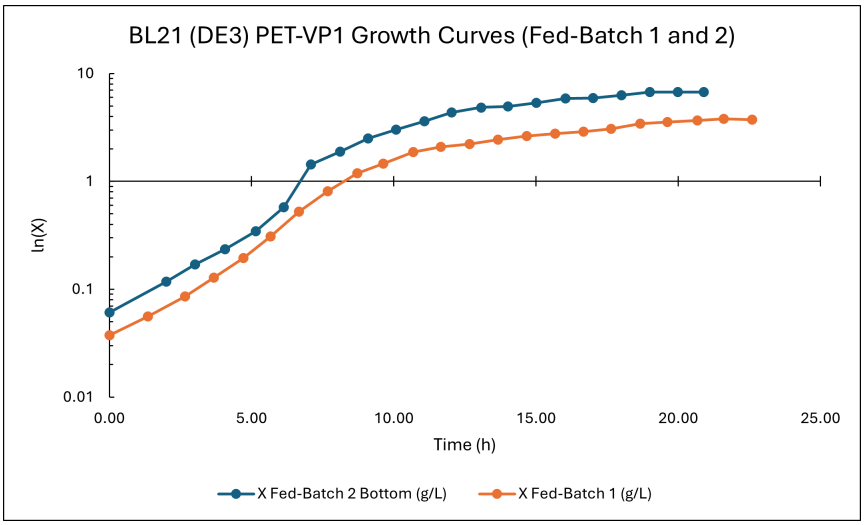


Figure 3.14: Growth curve comparison between the two fed-batch operations at 37°C.

There were three different average growth rates observed in Figure 3.15: 0.3569 h^{-1}, 0.2228 h^{-1}, and 0.0521 h^{-1}. This culture had an initial cell density that was 65% higher and a larger growth rate on average for a long period of time, so there was a larger increase in cell density over time. However, the third growth rate showed a similar slow

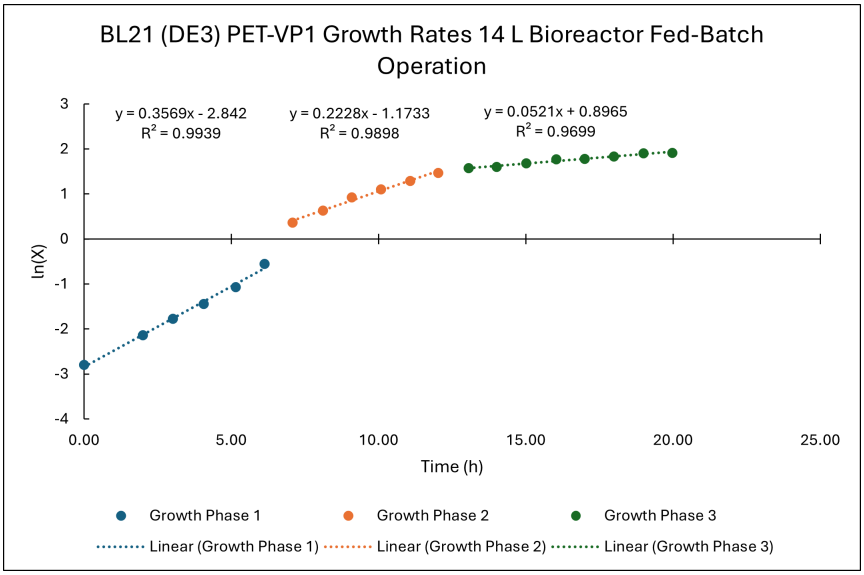


Figure 3.15: Approximate growth rates during each growth phase as observed in the 14 L fed-batch culture.

down as the first fed-batch culture. The initial growth rate was about 25% lower than the initial growth rate in the first fed-batch culture. The main differences in the initial conditions were a higher cell density, higher pH, higher DO%, and higher glucose concentration. The higher pH and DO% (as shown in Appendix B.1) potentially could have caused a lower growth rate as the starting pH of 7 is ideal, and a 90% starting DO% may be too high causing stress to the cells, however, there is little evidence to make these conclusions. The apparent yield coefficient was approximated at 0.273 g cell/g glucose, which is the highest yield out of all the experiments. This shows that a better control of glucose feeding leads to a higher yield, as opposed to overfeeding, which would cause overflow metabolism, thus reducing the yield [37, 91]. Figure 3.16 shows the metabolite concentration profiles and the feeding profile. While they were not ideal due to the mishap, there was improvement in terms of less overfeeding overall. There is a region of

glucose depletion from 9 h – 13 h, which may have caused the second, slightly lower growth rate, as acetate was also being consumed as a secondary carbon source at this time. Once the glucose concentration significantly increased due to overfeeding, acetate accumulation started to occur once again, and the growth rate started to decrease at 13 h. The peak glucose concentration was 6.96 g/L, and the peak acetate accumulation was 1.33 g/L, which were much lower than the 15.07 g/L overfeeding and 5.84 g/L from the first fed-batch experiment, respectively. Minimizing the glucose overflow and the acetate accumulation showed clearly that carbon flux is directed to biomass more favourably.

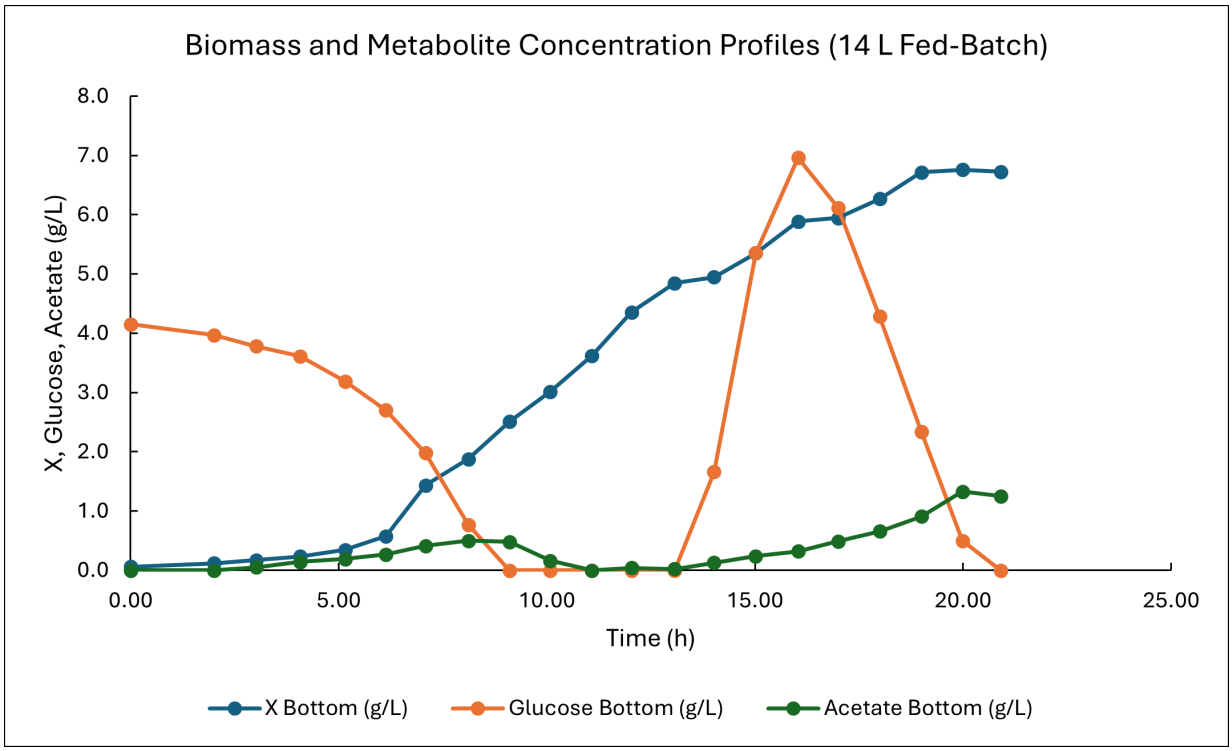


Figure 3.16: Biomass and metabolite concentrations over time for the 14 L fed-batch culture.

Plots of the agitation, temperature, air flow, DO%, pH, feed pump, and base pump

were extracted from the bioreactor and may be found in Appendix B.1. As previously, the agitation and air flow rate demands increased as the culture grew denser and decreased sharply once the culture reached stationary phase where oxygen demand is decreased. Several fluctuations occurred in the DO% compared to the previous fed-batch experiment prior to 12 h, so the P value of the DO% controller was increased for a more aggressive response from the agitation and air flow rate, which decreased the fluctuations slightly. The several low points are from the k_La measurements. The pH was very steady for the entire culture and rose at stationary phase as primary carbon source is depleted. The feeding pump profile shows a steady increase in feeding, however, as mentioned previously in the methodology, there was a mishap with the tubing becoming occluded. As a result, the feeding was not performed continuously throughout the feeding period as shown in the plot, except for 13.35 h and onwards. This was also the cause of glucose depletion between 9 h – 13 h. The deviation from the original feeding schedule resulted in overfeeding as well.

Samples were taken from the top of the bioreactor from 12 h until the end of the culture. This allowed for the measurement of cell density, glucose, and acetate concentrations at the top to investigate potential formation of gradients in biomass and metabolites. A limitation of this was that sampling could not be done instantaneously, and there were gaps of approximately 3 minutes between the bottom and top sampling as only one sampling needle was available at a time. Given this limitation, these measurements may not truly show the presence or absence of gradients. The bottom and top measurements for cell density are shown in Figure 3.17, and it is consistently higher at the top compared to the bottom. This may potentially be due to higher levels of

oxygen and glucose at the top compared to the bottom. It was shown that DO% is higher at the top in prior DO% sensor changes, and since the glucose is fed from the top, the top of the bioreactor will be met with glucose first, which may cause the cells to migrate there. It is also possible that the mixing in the bioreactor counters cell settling to the extent that cells are more suspended near the top. Another potential reason is that the cells may have been physically different, which could contribute to differences in the optical density measurement.

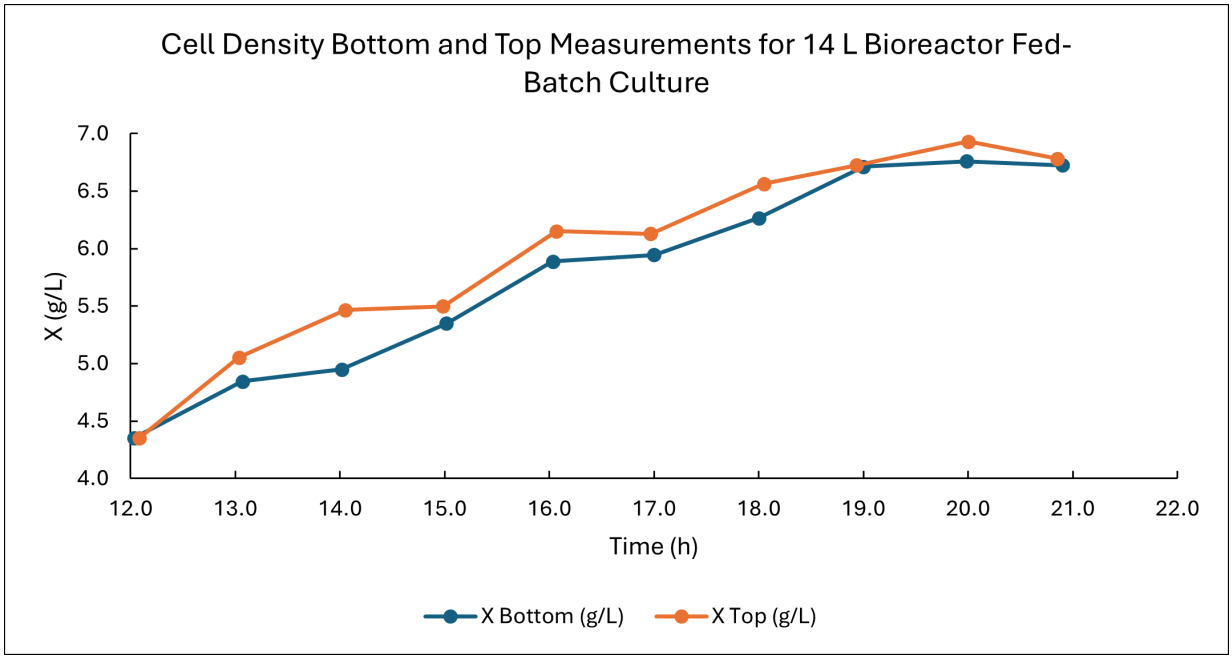


Figure 3.17: Bottom and top measurements of cell density to investigate gradient formation.

Figure 3.18 shows the bottom and top measurements of the glucose and acetate concentrations. They do not show any consistent pattern, and it is likely that mixing between the sampling times may have caused the fluctuating responses or there are no

gradients to be seen, and the differences are a result of sample variance.

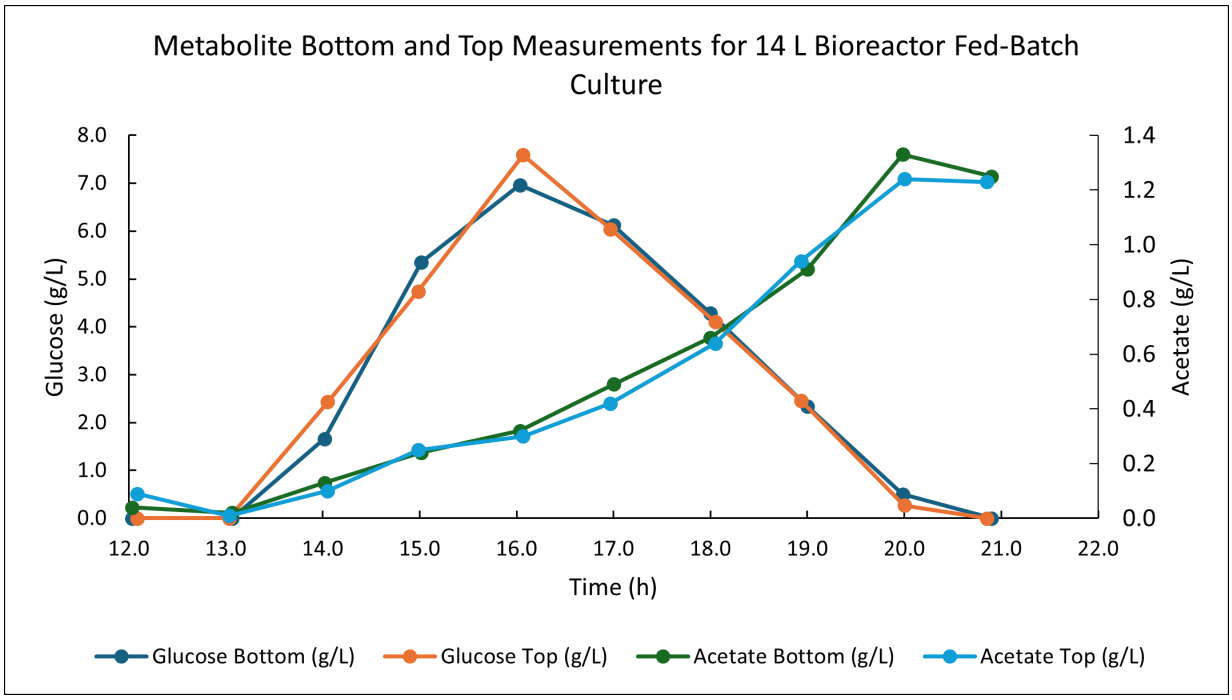


Figure 3.18: Bottom and top measurements of metabolite concentrations to investigate gradient formation.

Sensor height changes were performed similarly to the first fed-batch experiment. There were 11 height changes on the DO sensor at intervals between 11.517 h – 19.45 h. Details on the conditions at which they were measured are listed in Table B.4 in Appendix B.1. The average difference from all 11 changes between the bottom and middle was about 12%, and it was about 15% between the middle and the top. While the average differences were slightly different compared to the first fed-batch culture, the trend is the same, where the DO% at the top is the highest, and it is lowest at the bottom. Figure 3.19 shows the DO% readings for each height change with a mean trend and a 95% confidence interval. This confirms that gradients in DO% do occur in

pilot-scale bioreactors for *E. coli*, where DO increases along the height of the reactor.

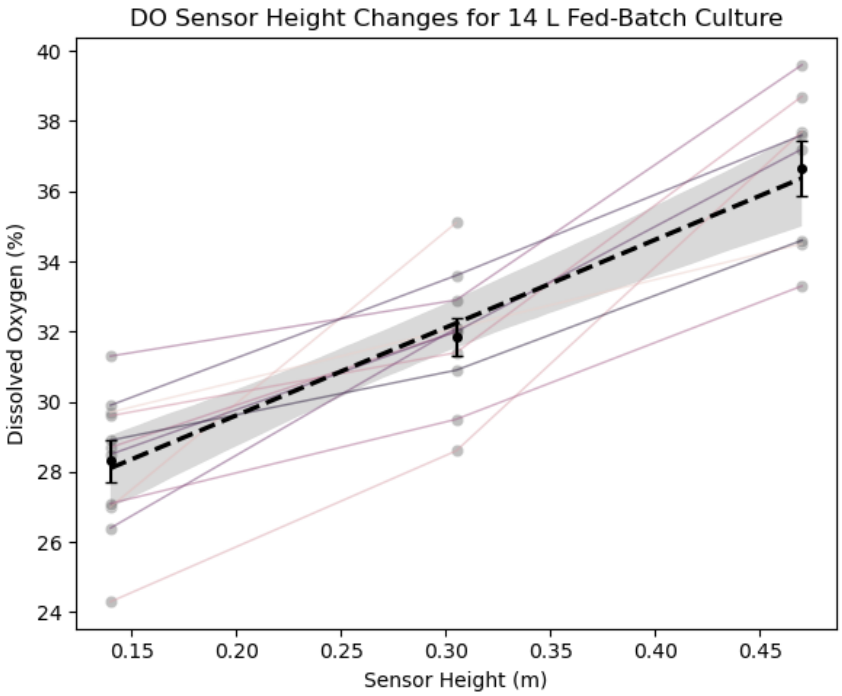


Figure 3.19: DO% sensor height changes for the 14 L fed-batch culture at various times between 11.5 h – 19.5 h. A mean trend and 95% confidence interval are shown.

The pH differences once again were not very prominent compared to the DO%; however, they maintained the same trend shown previously in the first fed-batch experiment. The height changes were performed eight times between 11.33 h – 19.52 h. The changes are shown in Figure 3.20 below. On average, between the 8 changes, the difference between the bottom and middle was 0.47%, and it was 0.35% between the middle and top. This shows that there are small pH gradients that form due to the location of the feeding port of the base (or acid depending on culture medium). However, this may also strongly depend on the concentration of the acid or base being added, as

higher concentrations will likely induce larger gradients as the pH fluctuation would be greater with each addition. The conditions in which these measurements are taken can be found in Table B.5 in Appendix B.2. These results confirm that pH gradients can be measured along the height of pilot-scale bioreactors for *E. coli*, where pH increases along the height of the reactor.

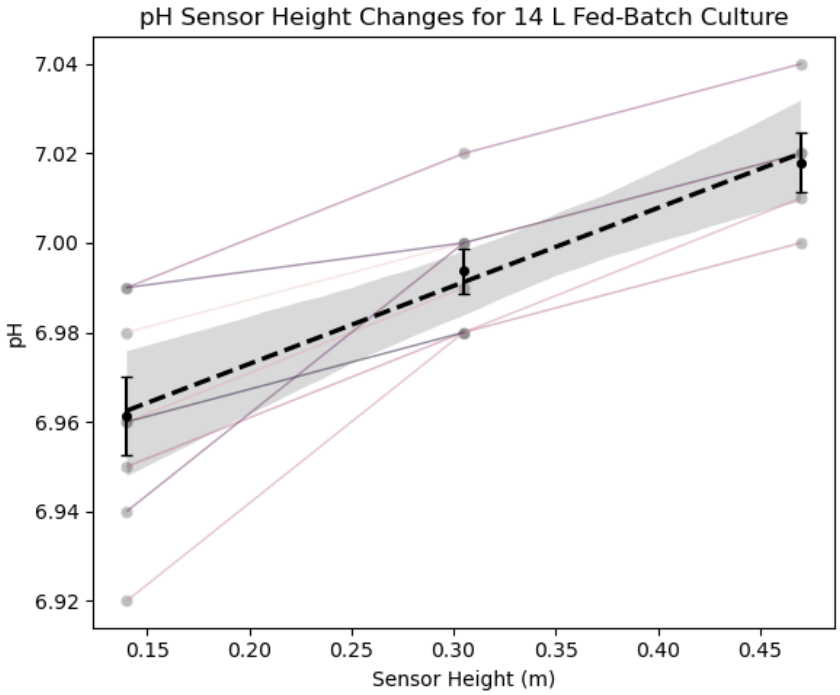


Figure 3.20: pH sensor height changes for the 14 L fed-batch culture between 11.33 h – 19.52 h. A mean trend and 95% confidence interval are shown.

The k_La measurements were attempted once more with 5 different height changes. This time, there was a clear trend, with the exception of an outlier where the middle k_La was much larger than every other measured k_La. The k_La showed increases as the height increased, which is once again consistent with the increasing DO% as the height

increases. Figure 3.21 below shows the measured k_La values at each height with a mean trend and 95% confidence intervals. The conditions in which these measurements are taken can be found in Table B.6 in Appendix B.2.

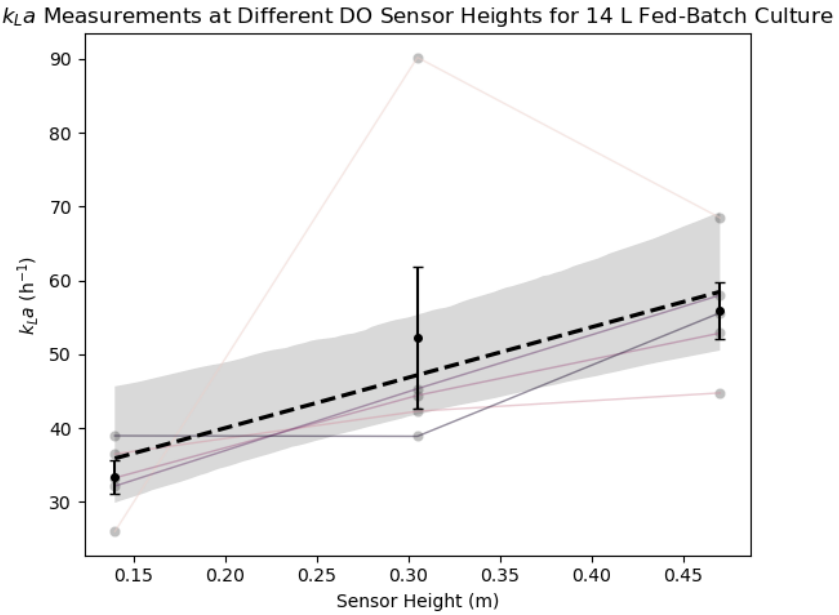


Figure 3.21: k_La measurements at different DO% sensor heights for the 14 L fed-batch culture between 11.62 h – 19.36 h. A mean trend and 95% confidence interval are shown.

Overall, the results from each experiment showed the dynamic responses that can occur depending on the control of the concentration of the carbon source, and that gradients are measurable in a 20 L pilot-scale bioreactor. Overflow metabolism significantly reduces the biomass yield through acetate accumulation, and good substrate control prevents acetate from accumulating too much. Gradients in DO, pH, and k_La are very clear in the measurements; however, it is recommended that a second sampling needle be used along with a second hand to assist in order to sample two heights

simultaneously to investigate the presence of cell density and metabolite concentration gradients. It would also be recommended to measure a more realistic k_La by obtaining smaller time steps for the DO readings given by the bioreactor for oxygen uptake rate measurements as this was limited to 15-second intervals.

Chapter 4

Modeling of the Fed-Batch Experiments

4.1 Overview

A model of the two fed-batch bioreactor cultures was developed for the following goals: i- to quantify the variability among experiments, ii- to identify the relative contributions of glucose and acetate to growth including the occurrence of diauxic switch, and iii- to elucidate the implications of a lumped model assumption vis-à-vis the observed experimental gradients. As it was shown that gradients can form in smaller scale bioreactor cultures of *E. coli*, it would be beneficial to model key parameters to be able to understand the limitations of a model that ignores these gradients. Initially, the time evolutions of biomass, glucose, and acetate were modeled based on simple Monod kinetic

rates with mass balances on the fed-batch bioreactor. A simple oxygen balance was then performed to model the oxygen and k_La. As there were clear limitations with the simple model, modifications were made to the metabolic model, specifically, self-growth inhibition, metabolic switching for diauxic growth, and a lag function based on the cell density for growth and metabolism of acetate. This chapter will discuss the results related to the final objective stated in Chapter 1.

4.2 Model Development for Fed-Batch Cultures

Initially, a simple system of ordinary differential equations (ODEs) was coded in Python including mass balances for biomass, glucose, and acetate for a fed-batch operated bioreactor using Monod kinetics. The cell growth is represented by the following:

$$\frac{dX}{dt} = \mu X - \frac{X}{V} \cdot \frac{dV}{dt} \tag{4.1}$$

$$\mu = \mu_{\text{glucose}} + \mu_{\text{acetate}} \tag{4.2}$$

$$\mu_{\text{glucose}} = \frac{\mu_{m_{\text{glucose}}} S}{K_S + S} \cdot \frac{K_a}{K_a + A} \tag{4.3}$$

$$\mu_{\text{acetate}} = \frac{\mu_{m_{\text{acetate}}} A}{K_{a2} + A} \cdot \frac{K_g}{K_g + S} \tag{4.4}$$

Where X is the cell density, S is the extracellular glucose concentration and A is the acetate concentration. μ is the overall growth rate, whereas the subscript m denotes the maximum growth rate for $\mu_{\text{m,glucose}}$ and $\mu_{\text{m,acetate}}$. The various K constants (K_a, K_{a2}, K_G, K_S) are affinity or inhibition coefficients defined in the Monod model, where the growth rate for glucose is assumed to be inhibited by acetate and the growth rate for acetate is assumed to be inhibited by glucose [4]. The changing volume in the culture was defined as:

$$\frac{dV}{dt} = F_1 + F_2 - F_3 \tag{4.5}$$

Where F_1 is the feeding schedule, F_2 is the base addition, and F_3 is the volume taken out from sampling. The glucose and acetate balance were given by the following:

$$\frac{dS}{dt} = -\frac{\mu_{\text{glucose}} X}{Y_{X/S}} - m_X X + \frac{F_1}{V} S_0 - \frac{S}{V} \cdot \frac{dV}{dt} \tag{4.6}$$

$$\frac{dA}{dt} = q_A \mu_{\text{glucose}} X - \frac{A}{V} \cdot \frac{dV}{dt} \tag{4.7}$$

Where $Y_{X/S}$ is the yield coefficient on glucose, m_X is the cell maintenance coefficient, S_0 is the glucose concentration in the feed, and q_A is the growth-associated acetate yield. This system was solved using the built-in initial value problem solver in Python (ivpsolve). However, this simple model clearly lacked the ability to match the experimental data, so modifications were required to the equations above.

The first set of modifications was made to Equations 4.3 and 4.7, where a substrate

inhibition constant (K_I) was added to the growth on glucose, and the growth rate and biomass yield on acetate was added to the acetate mass balance as follows:

$$\mu_{\text{glucose}} = \frac{\mu_m S}{K_S + S + \frac{S^2}{K_I}} \cdot \frac{K_a}{K_a + A} \tag{4.8}$$

$$\frac{dA}{dt} = q_A \mu_{\text{glucose}} X - \frac{\mu_{\text{acetate}} X}{Y_{X/A}} - \frac{A}{V} \cdot \frac{dV}{dt} \tag{4.9}$$

These modifications showed significant improvements in the fitting of the model, but it was still not sufficient to obtain a good fit. To further improve the fit, Equation 4.8 was reverted back to Equation 4.3, and instead Equation 4.4 was modified to include the inhibition term as follows:

$$\mu_{\text{acetate}} = \frac{\mu_{m_{\text{acetate}}} A}{K_{a2} + A + \frac{A^2}{K_I}} \cdot \frac{K_g}{K_g + S} \tag{4.10}$$

This latter change was based on the hypothesis that higher acetate concentrations would have a larger inhibitory effect on the growth rate compared to higher glucose levels. To better fit the time changes in volume observed in the experiments, an approximate curve was fit in Excel by a function of V with respect to time, and then the derivative of this function was calculated to obtain the $\frac{dV}{dt}$ term. This resulted in a close fit for the glucose concentration and biomass over time, but the time profiles for the biomass and acetate could still not fit the experiments well. The model fitting procedure was also attempted in the Excel environment using the built-in solver as it allowed faster and easier experimentation with the parameters. This showed more favorable results on

the biomass, but the acetate profile did not fit the data. The model parameters obtained from the Excel solver were then used in the Python solver, and the oxygen balance and k_La were added to the model. These were represented by the following equations:

$$\frac{dC_{O_2}}{dt} = k_La(C_{O_2}^{\text{sat}} - C_{O_2}) - q_{O_2}X - \frac{C_{O_2}}{V} \cdot \frac{dV}{dt} \tag{4.11}$$

$$\frac{dk_La}{dt} = \frac{q_{O_2}X + \frac{C_{O_2}}{V} \cdot \frac{dV}{dt}}{C_{O_2}^{\text{sat}} - C_{O_2}} \tag{4.12}$$

Where C is the concentration, O_2 and sat denote oxygen and saturation respectively, k_La is the liquid mass transfer coefficient, and q_{O_2} is the specfic oxygen uptake rate.

Since the DO set-point was set to 30%, the model was set so that dk_La is 0 and k_La is equal to a set initial value while the oxygen is consumed until 30%, and then once it reaches 30%, dC_{O_2} is set to 0, while Equation 4.12 gets activated. This models a constant k_La until the controller increases the agitation and air flow rate to keep the DO constant at 30% thus increasing k_La.

The model was then further developed with the modifications mentioned in the Overview, and the parameters were further optimized using a genetic algorithm in Python. Since the fitting of dissolved oxygen to the data was not good, the oxygen balance and k_La equations were also changed to depend on the modeled growth rate rather than a separate oxygen uptake coefficient to link the growth to the oxygen balance. This oxygen balance has the assumption that oxygen consumption is purely growth-related for simplification, and this is not necessarily true, as oxygen consumption

could also be related to cell maintenance. Equations 4.11 and 4.12 were modified as follows:

$$\frac{dC_{O_2}}{dt} = k_L a(C_{O_2}^{\text{sat}} - C_{O_2}) - Y_{O_2/X}\mu X - \frac{C_{O_2}}{V} \cdot \frac{dV}{dt} \tag{4.13}$$

$$\frac{dk_L a}{dt} = \frac{Y_{O_2/X}\mu X + \frac{C_{O_2}}{V} \cdot \frac{dV}{dt}}{C_{O_2}^{\text{sat}} - C_{O_2}} \tag{4.14}$$

The first modification made to the Monod kinetics is the addition of a growth inhibition term, where slower growth is observed at higher cell densities. The latter may be caused by a variety of reasons, which may include competition for limited nutrients and oxygen, the accumulation of toxic by-products, reduced mixing, or specific internal systems that suppress growth [119]. This decrease in growth was represented by a Hill-type self-growth inhibition term, as shown below:

$$\text{Self Growth Inhibition} = \frac{1}{1 + \left(\frac{X}{K_X}\right)^{n_X}} \tag{4.15}$$

Where K_X is the cell density at which inhibition becomes significant, and n_X controls the strength of the inhibition.

The next modification that was considered was a metabolic switch function, where a Hill-type repression function is used to control the growth rate on acetate based on the glucose concentration. This expression provides a sharper inhibition than the original more gradual substrate inhibition term in Equation 4.10. The term is similar to the one

given by Equation 4.15, as shown below:

$$\text{Acetate Switch} = \frac{1}{1 + \left(\frac{S}{K_G}\right)^{n_G}} \tag{4.16}$$

Where K_G is the substrate concentration at which growth on acetate is inhibited. In contrast, when substrate concentrations are below K_G, the growth on acetate becomes activated. The n_G term controls the strength of the switch. This switch is commonly considered to describe diauxic growth, where growth can occur on a secondary carbon source once the primary source is depleted [120, 121].

The final modification that is considered is an addition of a state-dependent lag function to the growth rate to capture the occurrence of a lag-phase before exxponential growth starts. Out of the four sigmoidal lag functions (Logistic, Richards, Stannard, and Gompertz), the Gompertz model was selected as it seemed to fit best with the experimental data. The base form of the Gompertz model $W(t)$ shown in Equation 4.17 is as follows [123]:

$$W(t) = A_1 \cdot \exp\left(-\exp\left[-k_G \cdot (t - T_i)\right]\right) \tag{4.17}$$

Where A_1 represents the scale of the upper asymptote, exp is the exponential function with base e, k_G is the growth rate coefficient, t is time, and T_i is the inflection point. However, this was modified to shift the lower asymptote of the curve with the addition of A_1, as the initial growth rate is nonzero, and the lag function should depend on the state variables rather than time, since a predictive model should be determined by the states

and not be governed by time. A compression factor of $(1-A_1)$ was also added to maintain the original scale of the upper asymptote. The following equation is the result of these modifications:

$$\text{lag} = A_1 + (1 - A_1) \cdot \exp\left(-\exp\left[-\lambda_{\text{lag}} \cdot (w \cdot g(X, S, A, C_{O_2}) - \beta)\right]\right) \tag{4.18}$$

Where A_1 shifts the lower asymptote and maintains the scale of the upper asymptote, λ_{lag} controls the steepness of the curve, w is a scaling factor, β is the inflection point, and $g(X, S, A, C_{O_2})$ is a state dependent function that replaces the time dependency. This function was found through a search algorithm which generated and found an optimal form among all possible combinations of expressions from the Monod, Hill, and inhibition functions based on the state variables of cell density, glucose, acetate, and oxygen concentrations. The best fit was obtained with a function that depended on just the cell density as follows:

$$g(X) = \frac{1}{1 + (\frac{K_{X_2}}{X})^{n_{X_2}}} \tag{4.19}$$

Where $g(X)$ represents a biomass-dependent activation of the lag function. This is a Hill-type activation function that reflects the requirement of a minimum cell density to start growing efficiently. To further simplify the lag function, λ_{lag} was also removed from the lag function since its effect was small, resulting in the following expression:

$$\text{lag} = A_1 + (1 - A_1) \cdot \exp\left(-\exp\left[-(w \cdot \frac{1}{1 + (\frac{K_{X_2}}{X})^{n_{X_2}}} - \beta)\right]\right) \tag{4.20}$$

In summary, the resulting final system of ODEs is listed below:

$$\frac{dX}{dt} = \mu X - \frac{X}{V} \cdot \frac{dV}{dt} \tag{4.21}$$

$$\frac{dS}{dt} = -\frac{\mu_{\text{glucose}} X}{Y_{X/S}} - m_X X + \frac{F_1}{V} S_0 - \frac{S}{V} \cdot \frac{dV}{dt} \tag{4.22}$$

$$\frac{dA}{dt} = q_A \mu_{\text{glucose}} X - \frac{\mu_{\text{acetate}} X}{Y_{X/A}} - \frac{A}{V} \cdot \frac{dV}{dt} \tag{4.23}$$

$$\frac{dC_{O_2}}{dt} = k_L a (C_{O_2}^{\text{sat}} - C_{O_2}) - Y_{O_2/X} \mu X - \frac{C_{O_2}}{V} \cdot \frac{dV}{dt} \tag{4.24}$$

$$\frac{dk_L a}{dt} = \frac{Y_{O_2/X} \mu X + \frac{C_{O_2}}{V} \cdot \frac{dV}{dt}}{C_{O_2}^{\text{sat}} - C_{O_2}} \tag{4.25}$$

$$\frac{dV}{dt} = F_1 + F_2 - F_3 \tag{4.26}$$

$$\mu = (\mu_{\text{glucose}} + \mu_{\text{acetate}}) \cdot (A_1 + (1 - A_1) \cdot \exp(-\exp[-(w \cdot \frac{1}{1 + (\frac{K_{X_2}}{X})^{n_{X_2}}} - \beta)])) \tag{4.27}$$

$$\mu_{\text{glucose}} = \frac{\mu_m S}{K_S + S} \cdot \frac{K_a}{K_a + A} \cdot (\frac{1}{1 + \left(\frac{X}{K_X}\right)^{n_X}}) \tag{4.28}$$

$$\mu_{\text{acetate}} = \frac{\mu_{m_{\text{acetate}}} A}{K_{a2} + A} \cdot \left(\frac{1}{1 + \frac{S}{K_G}^{n_G}}\right) \cdot \left(\frac{1}{1 + \left(\frac{X}{K_X}\right)^{n_X}}\right) \tag{4.29}$$

$$g(X) = \frac{1}{1 + \left(\frac{K_{X_2}}{X}\right)^{n_{X_2}}} \tag{4.30}$$

This model was applied for both fed-batch experiments. The following genetic algorithm parameters were used in the first fed-batch experiment: population size of 200, 100 generations, 200 offspring, tournament-style selection, crossover and mutation probabilities of 0.8 and 0.2 respectively, and a fitness function using the sum of squared errors of X, S, A, μ, and C_{O_2}. The algorithm was implemented using the Distributed Evolutionary Algorithms Python (DEAP) library. The parameters were bound on the basis of what may be possible biologically. Once the parameters were optimized, the system was then solved using those parameters with the built-in initial value problem solver in Python.

It should be noticed that, to reduce the possibility of overfitting noisy data, it is desirable to reduce the number of parameters. Toward that end, a parametric sensitivity analysis was performed to identify redundant parameters that can be eliminated without a major impact on the model. In this analysis, no parameters were found to be redundant.

4.3 Results and Discussion

4.3.1 Modeling the First Fed-Batch Experiment

The resulting parameters of the modeling for the experiments are shown in Table 4.1 below.

Table 4.1: Best fit model parameters and descriptions for the first and second fed-batch experiment.

Parameter	**Value**	**Description**
$\mu_{\mathrm{m,glucose}}$	0.680	Max growth rate on glucose (h^{-1})
$\mu_{\mathrm{m,acetate}}$	0.600	Max growth rate on acetate (h^{-1})
K_S	0.00100	Monod constant on glucose (g/L)
K_a	0.700	Acetate inhibition constant on glucose growth (g/L)
K_{a2}	0.0400	Monod constant on acetate (g/L)
$Y_{X/S}$	0.500	Yield coefficient on glucose (g cell/g glucose)
$Y_{X/A}$	0.400	Yield coefficient on acetate (g cell/g acetate)
$Y_{\mathrm{O_2}/X}$	0.180	Yield coefficient of oxygen on biomass (g oxygen/g cell)
q_A	0.500	Growth associated acetate yield (g acetate/g cell)
m_X	0.180	Cell maintenance coefficient (h^{-1})
K_X	3.400	Self-growth inhibition constant (g/L)
n_X	3.800	Hill coefficient for self-growth inhibition
K_{X2}	0.300	Biomass constant for lag function (g/L)
n_{X2}	2.400	Hill coefficient for biomass in lag function
K_G	0.200	Glucose constant for acetate switch (g/L)
n_G	2.950	Hill coefficient for acetate switch
A_1	0.550	Lower asymptote in lag function
w	7.900	Scaling factor in lag function
β	2.800	Inflection point in lag function

The key results to note are the comparison between the experiment and the fit of the model for cell density, glucose and acetate concentrations, growth rate, DO, and k_La.

Figure 4.1 shows the model fit for the cell density. It was able to show the initial faster growth rate, then a transition to a slower growth in the latter half of the culture, which is consistent with the self-growth inhibition term. However, the model shows an over-prediction in the final cell density.

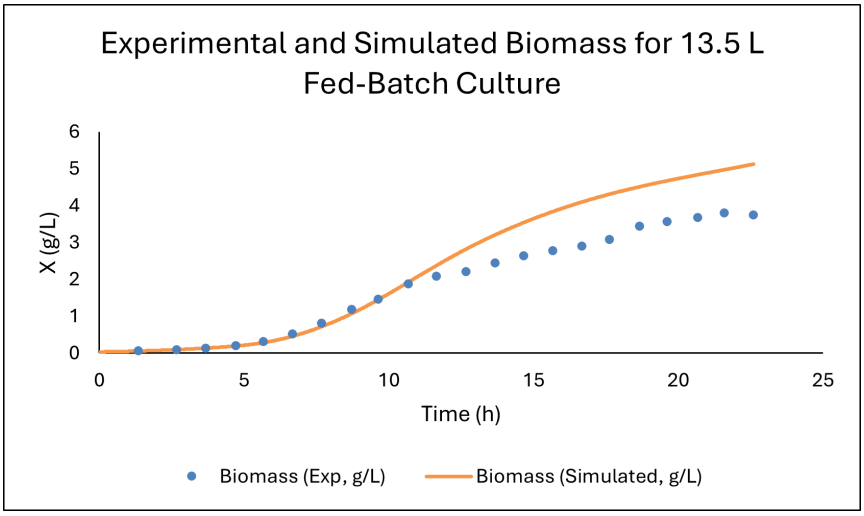


Figure 4.1: Experimental and simulated cell density for first fed-batch culture.

Figure 4.2 shows the growth rate over time and clearly shows the effectiveness of the lag function in the early stages of the culture, where growth is not yet at its maximum as the culture adapts to its new environment. The growth rate reaches its maximum once the cell density reaches a minimum, after which the growth rate is observed to show a decline as it normally would in Monod kinetics.

Figure 4.3 shows the fit for the glucose concentration, where the feeding and consumption trends were accurately captured, but there were noticeable over-predictions during the feeding and latter consumption portions of the profile. This may be due to the difficulty in balancing the acetate production and cell growth during the feeding and the

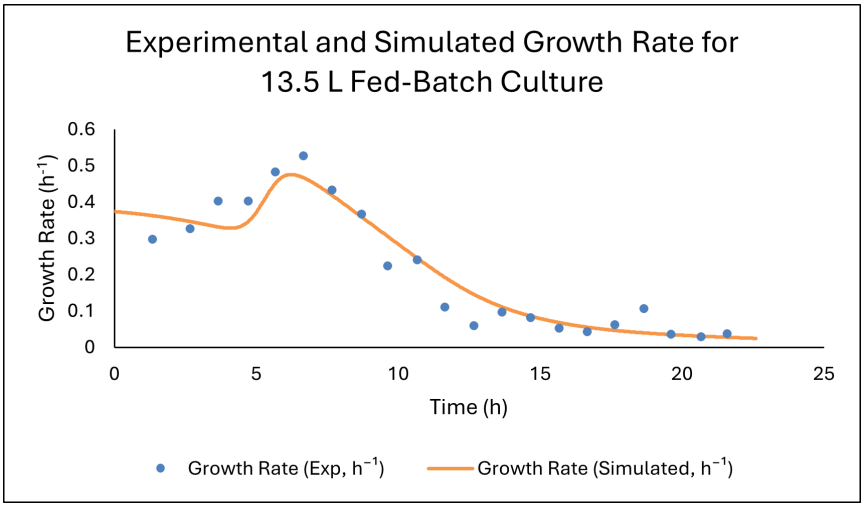


Figure 4.2: Experimental and simulated growth rate for first fed-batch culture.

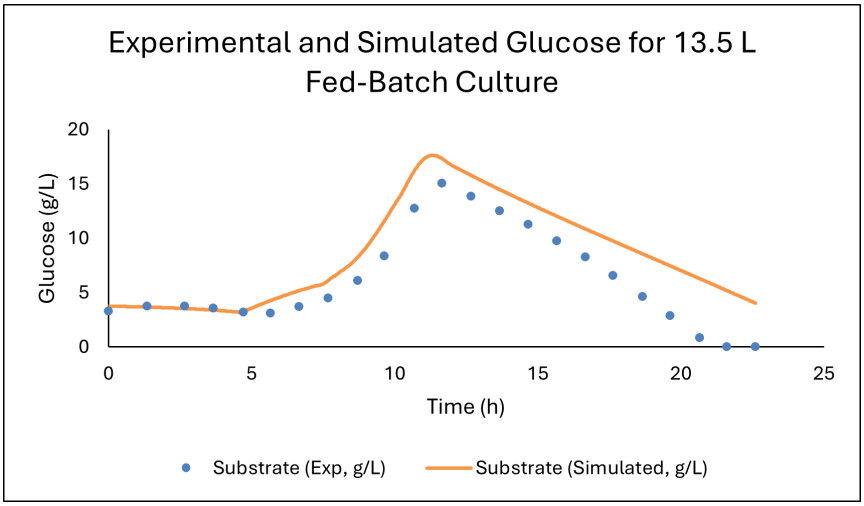


Figure 4.3: Experimental and simulated glucose concentration for first fed-batch culture.

consumption as these may vary due to overflow metabolism and adaptation of the cells. This applies for the cell maintenance coefficient as well, and may also be the reason for the over-prediction of the biomass earlier in Figure 4.1. Figure 4.4 shows the acetate profile was not able to be fit as well as the others, as it could not accurately capture the

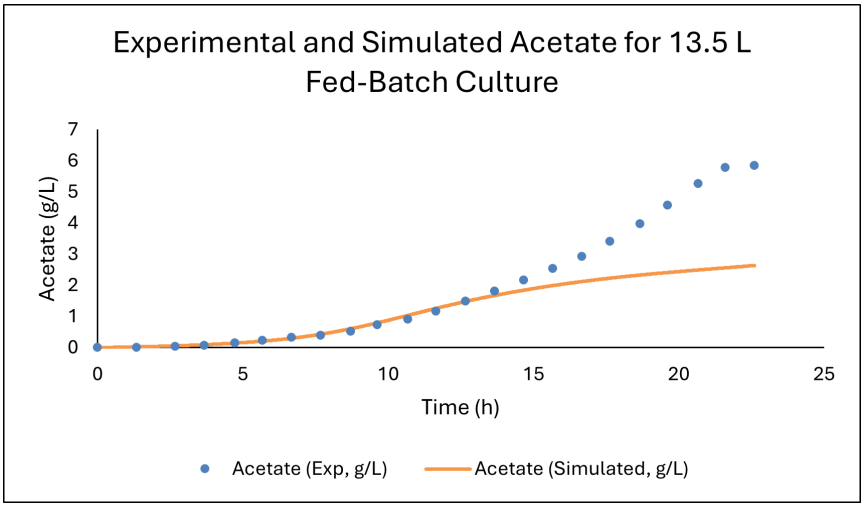


Figure 4.4: Experimental and simulated acetate concentration in first fed-batch culture.

gradual exponential accumulation throughout the entire time profile, and the final peak concentration observed in the experiment. A reason for this could be that a constant growth-associated yield of acetate is used, whereas the actual production rate of acetate may depend on other factors, such as overflow metabolism (high glucose levels) and stress factors which would lower biomass yield, redirecting glucose to acetate production. However, this may result in tradeoffs with the fit to the biomass profile. This is also evident when the model shows extra glucose that could be consumed to produce acetate, and the over-prediction in biomass could have gone towards acetate accumulation instead of the extra biomass. Figure 4.5 and Figure 4.6 show the DO profile, and the predicted k_La profile associated with the DO requirements. The DO was modeled using the strategy of switching from a constant k_La for the initial drop to a 30% DO, then moving to a constant DO and changing k_La over time to account for the DO control that occurs in the bioreactor. The consumption of oxygen until the plateau is under-estimated by the

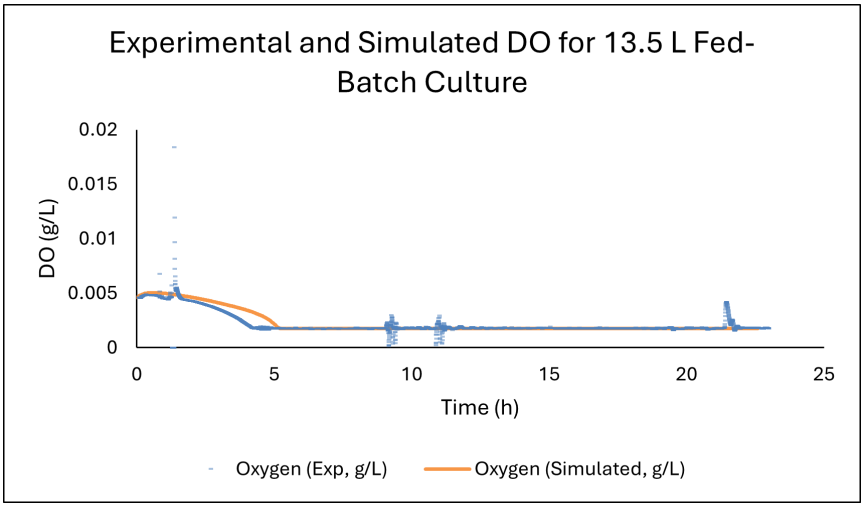


Figure 4.5: Experimental and simulated DO profile in the first fed-batch culture.

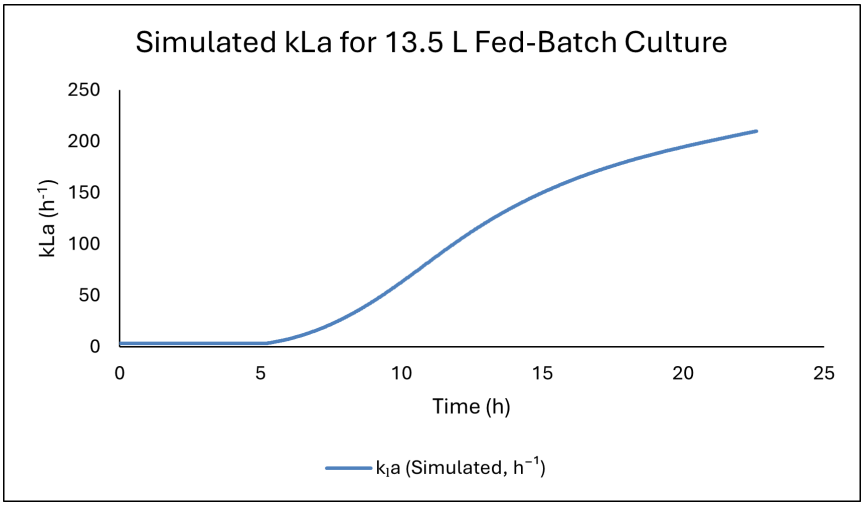


Figure 4.6: Simulated k_La for the first fed-batch culture.

model, as it is not reached until later, and this would be attributed to the inability of the model to show a gradual increase in the growth rate at the start, which directly affects the slower oxygen consumption predicted by the model. The prediction of the k_La depends on the initial value prediction, model growth rate, and yield on oxygen, as an

experimental value is not available due to sampling rates that are not sufficiently small to provide an accurate value. However, the overall trend seems to be reasonable as oxygen requirements increase over time in proportion to the biomass. The range of k_La values are also reasonable for a bioreactor of this size, where a k_La of up to 360 h^{-1} is reported for bioreactors between 1 – 30 L in volume [38].

4.3.2 Modeling the Second Fed-Batch Experiment

The best-fit model parameters for the second fed-batch experiment are shown in Table 4.1 in Section 4.3.1.

Evidently for this experiment, the model fitting has some trade-offs in order to fit with the first experiment as well. Figure 4.7 and Figure 4.8 show the cell density and growth rate fits, and an under-prediction of the biomass is observed. This starts to occur as the model starts to switch to acetate as a secondary carbon source, which is shown by the plateau during the time when glucose is almost fully consumed.

The growth rate was over-predicted in the middle of the culture, where a spike is shown, while a relatively good fit was obtained only near the end of the culture. It is likely that the model has difficulty in accurately capturing the more complex dynamics of this experiment, where there is a very evident switch between carbon sources during growth, as shown in Figure 4.9 and Figure 4.10, where glucose and acetate concentration profiles are displayed.

Plateaus in cell density were observed during acetate consumption along with sharp increases between plateaus where glucose is being fed into the bioreactor. The glucose

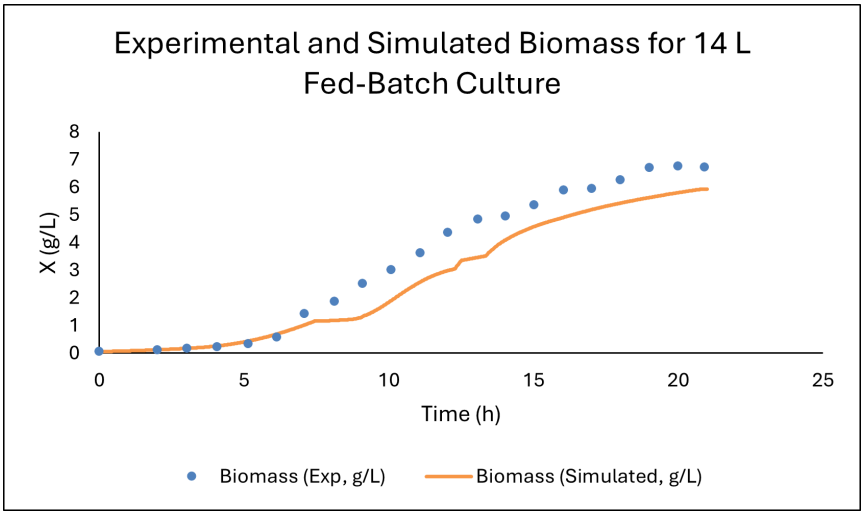


Figure 4.7: Experimental and simulated cell density for second fed-batch culture.

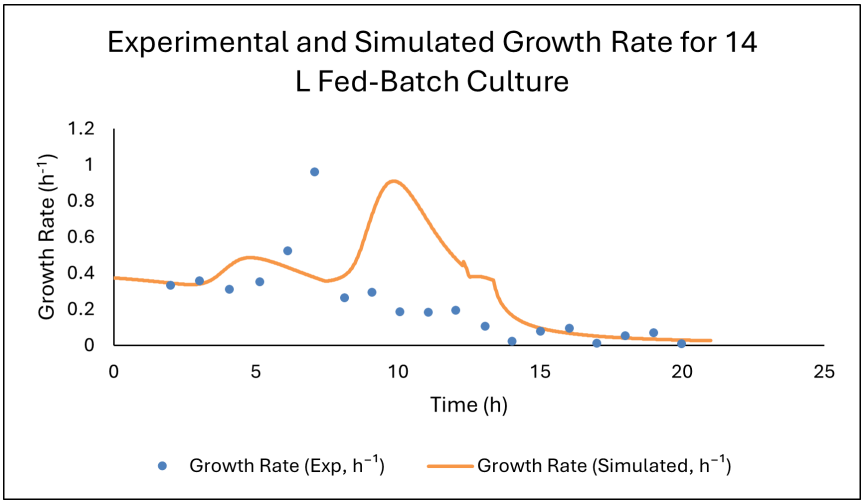


Figure 4.8: Experimental and simulated growth rate for second fed-batch culture.

feeding is also evident in the growth rate profile in Figure 4.8 as a large spike is observed during the same time frame. It is also likely that the lag function is not as well defined in this experiment as the sharp increase in growth at 7 h may be an outlier since the rest of the data shows a gradual downward trend. The glucose profile in Figure 4.9 fitted

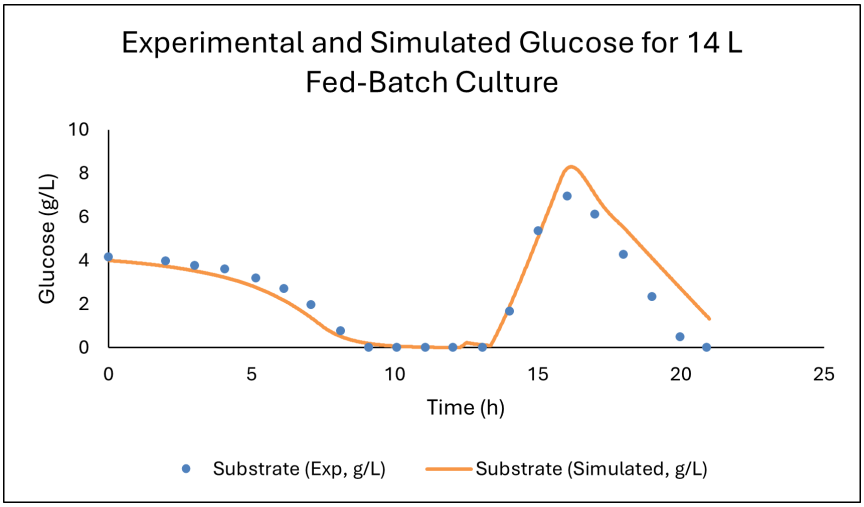


Figure 4.9: Experimental and simulated glucose concentration in second fed-batch culture.

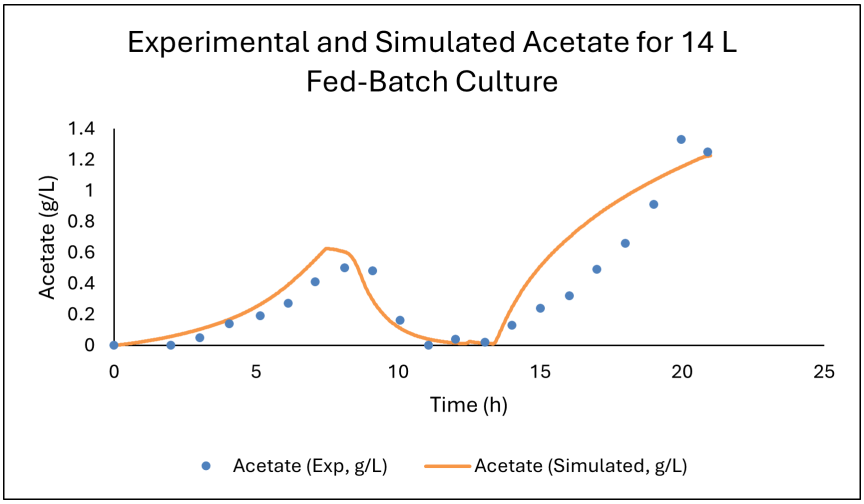


Figure 4.10: Experimental and simulated acetate concentration in second fed-batch culture.

relatively accurately by correctly capturing the initial depletion, then accumulation during a high feeding rate followed by consumption towards the end of the culture. Similar limitations of the model was observed for the first fed-batch experiment related to over-predictions in the end of the profile. However, it is especially evident that for this

experiment, the acetate switch is clearly occurring as observed in the acetate profile in Figure 4.10. This shows an initial accumulation, then consumption during the absence of glucose, followed by a new accumulation once glucose is present, all while the cell density is increasing. Despite this, the observed acetate accumulation towards the end of the culture was very abrupt. This is likely once again because of a constant q_A, and this model also has the possibility of showing a sudden over-consumption if the glucose levels fall too low, which would trigger the consumption of acetate due to the acetate switch. The latter would be difficult to model with the current setup, as the model would have to describe different consumption rates between the exponential and stationary phase of the culture, e.g. it will be required to turn off the acetate consumption when stationary phase is reached. Overall, the sudden feeding of glucose challenges this model as Monod kinetics generally refer to balanced growth, whereas the sudden over-feeding of glucose generates unbalanced growth.

Figure 4.11 and Figure 4.12 show the DO and the predicted k_La profile associated with the DO requirements for the second fed-batch culture. The DO was modeled with an over-prediction in the consumption this time, and the k_La showed a similar trend within reasonable ranges. The differences in growth rate and higher initial cell density in this experiment made it difficult to accurately capture the oxygen consumption dynamics at the start of both experiments. On the other hand, the range of values are very similar between the two experiments despite the much higher cell density in this experiment compared to the first fed-batch experiment due to the closed-loop control actions that maintain the oxygen close to a prescribed set-point. This is also evident in the agitation and air flow rates shown in Appendix B, where they are higher in the second fed-batch

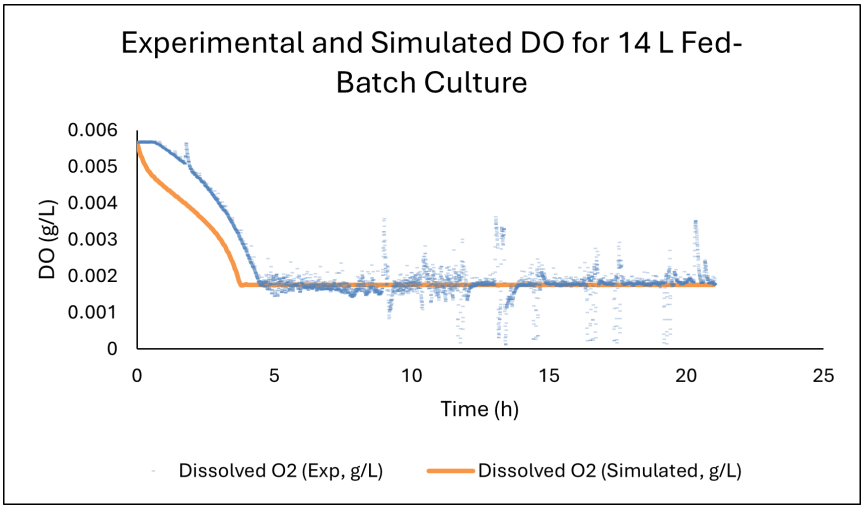


Figure 4.11: Experimental and simulated DO profile in the second fed-batch culture.

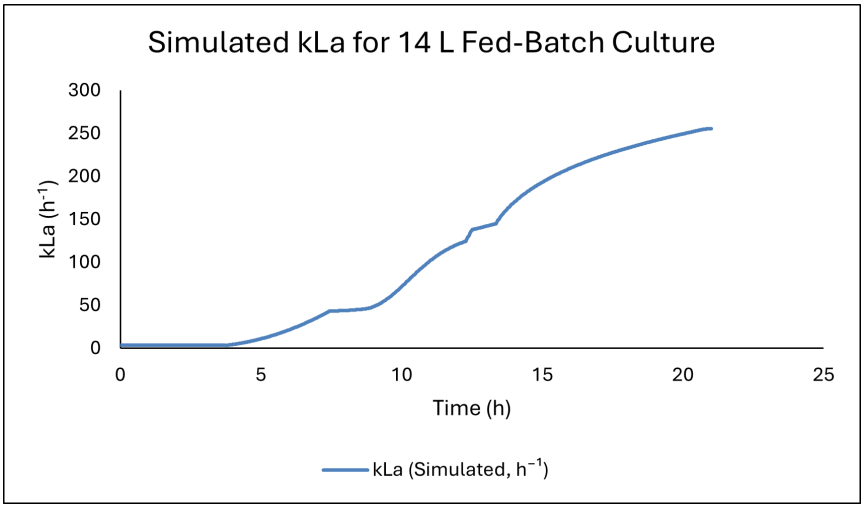


Figure 4.12: Simulated k_La for the second fed-batch culture.

experiment compared to the first fed-batch experiment, which correlates to a higher k_La. This shows how the simulated k_La is heavily dependent on the parameters used for the oxygen balance and the initial guesses, as there were no concrete k_La measurements other than the estimated trend of k_La along the height of the reactor.

In summary, the model was able to fit the experimental data well despite the difference in complex dynamics in the two experiments with the help of the modifications to the Monod kinetic model. Although there were still some significant inaccuracies and room for improvement, this model shows promise in being able to reflect the complex metabolic patterns that occur in *E. coli* when faced with changing extracellular conditions such as glucose overfeeding and depletion. Coupling this metabolic model with hydrodynamic models may serve to predict heterogeneities in large-scale bioreactors [132].

Chapter 5

Conclusions and Recommendations

5.1 Conclusions

In this work, an *E. coli* culture was characterized and grown in a 20 L pilot-scale bioreactor in order to investigate the possibility of gradient formation as seen in industrial bioreactors. The reaction kinetics of the culture were identified experimentally from batch experiments, which allowed for a calculation of a feeding rate for a fed-batch experiment. The fed-batch experiment allowed for higher cell density cultures in comparison to the batch culture, which gave an opportunity to investigate gradient formation in DO, k_La, pH, cell density, glucose, and acetate. These measurements are typically not performed in lab-scale studies because it is generally expected that gradients do not form in smaller-scale bioreactors such as the one used in this work. On the other hand, from measurements of DO and pH at different heights, this work clearly

shows that gradients can form in a 20 L bioreactor. The observed metabolism was then modeled and fitted to data from two fed-batch bioreactor fermentations. This work has resulted in the following conclusions:

- The growth rate and yield are shown to significantly depend on the extracellular environment in terms of cell and metabolite concentrations. The first fed-batch experiment showed that the high level of glucose overfeeding significantly reduces yield as a result of acetate accumulation from overflow metabolism, while the second fed-batch experiment showed that better glucose feeding allowed for reassimilation of acetate and a significantly higher cell density.

- Gradients in DO and pH can be measured in 13.5 – 14 L bioreactor cultures, and an approximate k_La trend was identified based on the assumed oxygen balance. This was achieved by positioning the probe at different heights and by shutting off the air intake for a short period of time and turning it back on. These measurements have shown that the DO, pH, and k_La are lowest at the bottom of the bioreactor and highest at the top of the bioreactor. It was inferred that the DO and k_La were highest at the top due to the head-space and the number of impellers the air bubbles pass through, allowing for a higher rate of mass transfer. The observed pH measurements were shown to correlate with the proximity to the location where acid or base is fed for pH control.

- Although we attempted to measure gradients in cell density and metabolites at different heights, gradients were not observed. There was a consistent trend where cell density was higher at the top compared to the bottom of the bioreactor, but

there was no consistent trend with the glucose and acetate measurements. This was likely due to the time needed to sample the top and bottom of the bioreactor (sampling at both heights was not simultaneous). However, the observed differences in concentrations between top and bottom motivate further investigation by additional experiments.

- Simple models based on Monod kinetics were not able to accurately describe the data, but certain additional modifications of the model were shown to improve the fit. Specifically, the addition of self-growth inhibition, an acetate metabolic switch, and a cell density-dependent lag function allowed the effects of overflow metabolism to be modeled, where there is a large accumulation of acetate. In addition, better glucose control in experiments may promote balanced growth, which can be more easily described by traditional substrate-biomass models.

These results show that fed-batch experiments can be performed at this scale to measure gradients, which can be used to fit metabolic models. The measurement of the gradients and the metabolic models can then be used to potentially assist in validating coupled hydrodynamic models to predict the gradients, which normally are not studied in bioreactors of this scale.

5.2 Recommendations

While the experiments and modeling have shown good results, the experimental conditions could have been controlled more effectively to obtain a more consistent glucose

profile. For example, it would be of interest to obtain metabolic data where glucose is kept consistently close to the original 4 g/L. It would also be of interest to find the critical growth rate at which acetate production is prevented, and feed glucose with respect to that growth rate. Another factor would be that instantaneous sampling for the cell density and metabolite measurements would allow for a more accurate data set. The k_La measurements can potentially be measured accurately as well with a smaller data sampling interval, as the bioreactor software has a limitation of recording data points every 15 seconds, which is longer than what it actually took to consume the oxygen between the data points. For example, the real time to consume oxygen during no aeration may have been approximately 3 seconds rather than 30 seconds, which would mean the measured k_La was ten times greater. With the knowledge that oxygen and k_La gradients occur, an experiment in which the DO probe is kept at the top of the reactor would provide insight into the importance of sensor location in the presence of gradients in terms of metabolic responses, as this will force different conditions throughout the bioreactor. For example, having a set point of 15% DO may create oxygen-depleted zones at the bottom of the bioreactor, causing changes in metabolic responses. The inclusion of product generation into the metabolic dynamics would be another area of interest as this is a key area of interest in industry. Furthermore, replications of these experiments would allow for better validation of these results.

The accurate measurement of k_La would also allow for better modeling so that it can be based on an experimentally measured oxygen uptake rate of the culture, which can be used to develop a correlation between k_La, the agitation, and the air flow rate of the bioreactor. The consideration of cell maintenance in the oxygen balance may further

improve the fitting of the DO and k_La prediction. The model could also be coupled with a hydrodynamic model to test the validity of it for predicting gradients which would occur in industrial bioreactors, such as the model presented by Promma et al. (2024) [132].

Finally, studies with a retrofitted bioreactor which include sensors and feeding ports at different heights of the bioreactor could be done in order to compare results with a traditional bioreactor such as the one used in this work. The idea would be to attempt to maintain homogeneity by having more controlled zones along the height of the bioreactor to investigate the effectiveness of the retrofitting.

References

[1] M. Faizullabhoy and G. Wani. Biopharmaceutical market size & share report, 2025 - 2034, April 2025.

[2] Grand View Research Inc. Biopharmaceutical market size, share: Industry report, 2030, 2025.

[3] World Health Organization. Who releases first data on global vaccine market since covid-19, November 2022.

[4] Maxime Pigou and Jérôme Morchain. Investigating the interactions between physical and biological heterogeneities in bioreactors using compartment, population balance and metabolic models. *Chemical Engineering Science*, 126:267–282, April 2015.

[5] B. Xu, M. Jahic, G. Blomsten, et al. Glucose overflow metabolism and mixed-acid fermentation in aerobic large-scale fed-batch processes with *Escherichia coli*. *Applied Microbiology and Biotechnology*, 51:564–571, 1999.

[6] Neil A. Campbell and Jane B. Reece. *Biology*. Pearson Education Inc., San Francisco, 2002.

[7] A. R. Tuttle, N. D. Trahan, and M. S. Son. Growth and maintenance of *Escherichia coli* laboratory strains. *Current Protocols*, 1(1), 2021.

[8] Britannica. Facts about *E. coli*: Dimensions as discussed in bacteria: Diversity of structure of bacteria, June 2015.

[9] C. D. Köhler and U. Dobrindt. What defines extra intestinal pathogenic *Escherichia coli*? *International Journal of Medical Microbiology*, 301:642–664, 2011.

[10] W. C. Van Dijk, H. A. Verbrugh, M. E. Tol, R. Peters, and J. Verhoef. Role of *Escherichia coli* k capsular antigens during complement activation, c3 fixation, and opsonization. *Infection and Immunity*, 25(2):603–609, 1979.

[11] Z. D. Blount. The unexhausted potential of *E. coli*. *eLife*, 25(4):e05826, 2015.

[12] V. N. Idalia and F. Bernardo. *Escherichia coli as a Model Organism and Its Application in Biotechnology*. Intech Open, London, 2017.

[13] Microbiology Online. Bacteria, 2014. Archived from the original on 27 February 2014.

[14] K. L. Elbing and R. Brent. Recipes and tools for culture of *Escherichia coli*. *Current Protocols in Molecular Biology*, 125(1):83, 2019.

[15] K. Muhammad, S. Zohra, L. Ji Xiu, I. Taj, M. H. Taj, and Y. Wei. *Escherichia coli* as a model organism. *International Journal of Engineering Sciences & Research Technology*, 3:3–8, 2014.

[16] M. N. I. Vargas and B. Franco. *Escherichia coli as a Model Organism and Its Application in Biotechnology*. IntechOpen, July 2017.

[17] D. C. Williams, R. M. Van Frank, W. L. Muth, and J. P. Burnett. Cytoplasmic inclusion bodies in *Escherichia coli* producing biosynthetic human insulin proteins. *Science*, 215:687–689, 1982.

[18] V. Gupta, M. Sengupta, J. Prakash, and B. C. Tripathy. Production of recombinant pharmaceutical proteins. *Basic and Applied Aspects of Biotechnology*, pages 77–101, October 2016.

[19] M. N. Baeshen, A. M. Al-Hejin, R. S. Bora, M. M. Ahmed, H. A. Ramadan, K. S. Saini, N. A. Baeshen, and E. M. Redwan. Production of biopharmaceuticals in *E. coli*: Current scenario and future perspectives. *Journal of Microbiology and Biotechnology*, 25(7):953–962, 2015.

[20] N. K. Tripathi and A. Shrivastava. Recent developments in bioprocessing of recombinant proteins: Expression hosts and process development. *Frontiers in Bioengineering and Biotechnology*, 7:420, 2019.

[21] İ. İncir and Ö. Kaplan. *Escherichia coli* in the production of biopharmaceuticals. *Biotechnology and Applied Biochemistry*, 72(2):528–541, 2024.

[22] İ. İncir and Ö. Kaplan. *Escherichia coli* as a versatile cell factory: Advances and challenges in recombinant protein production. *Protein Expression and Purification*, 219:106463, 2024.

[23] J. F. Kane. Effects of rare codon clusters on high-level expression of heterologous proteins in *Escherichia coli*. *Current Opinion in Biotechnology*, 6:494–500, 1995.

[24] W. Jeong and H. C. Shin. Supply of the argu gene product allows high-level expression of recombinant human interferon-alpha-2a in *Escherichia coli*. *Biotechnology Letters*, 20:19–22, 1998.

[25] C. A. Valente, D. M. F. Prazeres, J. M. S. Cabral, and G. A. Monteiro. Translation feature of human alpha 2b interferon production in *Escherichia coli*. *Applied and Environmental Microbiology*, 70:5033–5036, 2004.

[26] M. M. Carrio and A. Villaverde. Role of molecular chaperones in inclusion body formation. *FEBS Letters*, 537:215–221, 2003.

[27] B. Fahnert, H. Lilie, and P. Neubauer. Inclusion bodies: Formation and utilization. *Advances in Biochemical Engineering/Biotechnology*, 89:93–142, 2004.

[28] Y. J. Lee, D. H. Lee, and K. J. Jeong. Enhanced production of human full-length immunoglobulin g1 in the periplasm of *Escherichia coli*. *Applied Microbiology and Biotechnology*, 98:1237–1246, 2014.

[29] G. Walsh and R. Jefferis. Post-translational modifications in the context of therapeutic proteins. *Nature Biotechnology*, 24:1241–1252, 2006.

[30] N. Jenkins. Modifications of therapeutic proteins: Challenges and prospects. *Cytotechnology*, 53:121–125, 2007.

[31] L. McElwain, K. Phair, C. Kealey, and D. Brady. Current trends in biopharmaceuticals production in *Escherichia coli*. *Biotechnology Letters*, 44(8):917–931, 2022.

[32] J. D. Valderrama-Rincon, A. C. Fisher, J. H. Merritt, Y. Y. Fan, C. A. Reading, K. Chhiba, et al. An engineered eukaryotic protein glycosylation pathway in *Escherichia coli*. *Nature Chemical Biology*, 8:434–436, 2012.

[33] M. Wacker, D. Linton, P. G. Hitchen, M. Nita-Lazar, S. M. Haslam, S. J. North, et al. N-linked glycosylation in campylobacter jejuni and its functional transfer into *E. coli*. *Science*, 298:1790–1793, 2002.

[34] B. S. Vadala, S. Deshpande, and A. Apte-Deshpande. Soluble expression of recombinant active cellulase in *E. coli* using b. subtilis (natto strain) cellulase gene. *Journal of Genetic Engineering and Biotechnology*, 19:7, 2021.

[35] G. L. Rosano and E. A. Ceccarelli. Recombinant protein expression in *Escherichia coli*: Advances and challenges. *Frontiers in Microbiology*, 17:172, 2014.

[36] H. Waegeman, S. De Lausnay, J. Beauprez, J. Maertens, M. De Mey, and W. Soetaert. Increasing recombinant protein production in *Escherichia coli* k12 through metabolic engineering. *New Biotechnology*, 30:255–261, 2013.

[37] C. Fuchs, D. Koster, S. Wiebusch, K. Mahr, G. Eisbrenner, and H. Märkl. Scale-up of dialysis fermentation for high cell density cultivation of *Escherichia coli*. *Journal of Biotechnology*, 93:243–251, 2002.

[38] G. L. Rosano, E. S. Morales, and E. A. Ceccarelli. New tools for recombinant protein production in *Escherichia coli*: A 5-year update. *Protein Science*, 28:1412–1422, 2019.

[39] A. H. Romano and T. Conway. Evolution of carbohydrate metabolic pathways. *Research in Microbiology*, 147:448–455, 1996.

[40] S. Wang, P. Liu, W. Shu, C. Li, H. Li, S. Liu, J. Xia, and H. Noorman. Dynamic response of aspergillus niger to single pulses of glucose with high and low concentrations. *Bioresources and Bioprocessing*, 6(1):1–14, 2019.

[41] M. El-Mansi. Control of central metabolism's architecture in *Escherichia coli*: An overview. *Microbiological Research*, 266:127224, 2023.

[42] J. Shiloach and S. Bauer. High yield growth of *E. coli* at different temperatures in a bench scale fermentor. *Biotechnology and Bioengineering*, 17:227–239, 1975.

[43] S. Y. Lee. High cell density culture of *Escherichia coli*. *Trends in Biotechnology*, 14:98–105, 1996.

[44] J. Shiloach and R. Fass. Growing *E. coli* to high cell density—a historical perspective on method development. *Biotechnology Advances*, 23(5):345–357, 2005.

[45] I. C. Gunsalus and R. Y. Stanier. *The Bacteria, Vol. 1.* Academic Press, Inc., New York, 1960.

[46] D. Riesenberg, V. Schulz, W. A. Knorre, H. D. Pohl, D. Korz, E. A. Sanders, et al. High cell density cultivation of *Escherichia coli* at controlled specific growth rate. *Journal of Biotechnology*, 20:17–28, 1991.

[47] K. Han, H. C. Lim, and J. Hong. Acetic acid formation in *Escherichia coli* fermentation. *Biotechnology and Bioengineering*, 39:663–671, 1992.

[48] E. B. Jensen and S. Carlsen. Production of recombinant human growth hormone in *Escherichia coli*: Expression of different precursors and physiological effects of glucose, acetate, and salts. *Biotechnology and Bioengineering*, 36(1):1–11, 1990.

[49] Eppendorf Canada. Bioprocess operation modes: Batch, fed-batch, and continuous culture, n.d.

[50] W. Chen, C. Graham, and R. B. Ciccarelli. Automated fed-batch fermentation with feed-back controls based on dissolved oxygen (do) and ph for production of dna vaccines. *Journal of Industrial Microbiology and Biotechnology*, 18(1):43–48, 1997.

[51] M. Åkesson, P. Hagander, and J. P. Axelsson. Avoiding acetate accumulation in *Escherichia coli* cultures using feedback control of glucose feeding. *Biotechnology and Bioengineering*, 73(3):223–230, 2001.

[52] F. Palladino, P. R. Marcelino, A. E. Schlogl, Á. H. José, R. de Rodrigues, D. L. Fabrino, I. J. Santos, and C. A. Rosa. Bioreactors: Applications and innovations for a sustainable and healthy future—a critical review. *Applied Sciences*, 14(20):9346, 2024.

[53] M. R. Spier, L. P. D. S. Vandenberghe, A. B. P. Medeiros, and C. R. Soccol. *Application of Different Types of Bioreactors in Bioprocesses*, pages 55–90. Nova Science Publishers, Hauppauge, NY, 2011.

[54] O. Karnieli. *Bioreactors and Downstream Processing for Stem Cell Manufacturing*, pages 141–160. Elsevier, Amsterdam, 2016.

[55] J.-J. Zhong. *Bioreactor Engineering*, pages 257–269. Elsevier, Amsterdam, 2011.

[56] M. C. Decarli, D. P. dos Santos, R. M. Astray, D. C. Ventini-Monteiro, S. A. C. Jorge, D. M. Correia, J. de Sá da Silva, M. P. Rocca, H. Langoni, B. D. Menozzi, et al. Drosophila s2 cell culture in a wave bioreactor: Potential for scaling up the production of the recombinant rabies virus glycoprotein. *Applied Microbiology and Biotechnology*, 102:4773–4783, 2018.

[57] D. Pollard and C. Kistler. *Disposable Bioreactors*, pages 353–379. Elsevier, Amsterdam, 2017.

[58] J. Markarian. Sustainability in disposal of single-use systems. *BioPharm International*, 32:19, 2019.

[59] R. Sharma, S. T. L. Harrison, and S. L. Tai. Advances in bioreactor systems for the production of biologicals in mammalian cells. *ChemBioEng Reviews*, 9:42–62, 2022.

[60] K. Xiao, S. Liang, X. Wang, C. Chen, and X. Huang. Current state and challenges of full-scale membrane bioreactor applications: A critical review. *Bioresource Technology*, 271:473–481, 2019.

[61] X. Ge, J. Vasco-Correa, and Y. Li. *Solid-State Fermentation Bioreactors and Fundamentals*, pages 381–402. Elsevier, Amsterdam, 2017.

[62] E. Gkantzou, M. Weinhart, and S. Kara. 3d printing for flow biocatalysis. *RSC Sustainability*, 1:1672–1685, 2023.

[63] E. Bradford, A. M. Schweidtmann, D. Zhang, K. Jing, and E. A. del Rio-Chanona. Dynamic modeling and optimization of sustainable algal production with uncertainty using multivariate gaussian processes. *Computers & Chemical Engineering*, 118:143–158, 2018.

[64] G. Regonesi. Bioreactors: A complete review, 2023.

[65] A. P. J. Sweere, K. C. A. M. Luyben, and N. W. F. Kossen. Regime analysis and scaledown: Tools to investigate the performance of bioreactors. *Enzyme and Microbial Technology*, 9(7):386–398, 1987.

[66] S. O. Enfors, M. Jahic, A. Rozkov, B. Xu, M. Hecker, B. Jürgen, E. Krüger, T. Schweder, G. Hamer, D. O'Beirne, N. Noisommit-Rizzi, M. Reuss, L. Boone, C. Hewitt, C. McFarlane, A. Nienow, T. Kovacs, C. Trägårdh, L. Fuchs, J. Revstedt, P. C. Friberg, B. Hjertager, G. Blomsten, H. Skogman, S. Hjort, F. Hoeks, H. Y. Lin, P. Neubauer, R. van der Lans, K. Luyben, P. Vrabel, and Å. Manelius. Physiological responses to mixing in large scale bioreactors. *Journal of Biotechnology*, 85(2):175–185, 2001.

[67] G. Larsson, M. Törnkvist, E. S. Wernersson, C. Trägårdh, H. Noorman, and S. O. Enfors. Substrate gradients in bioreactors: Origin and consequences. *Bioprocess and Biosystems Engineering*, 14(6):281–289, 1996.

[68] G. Nadal-Rey, D. D. McClure, J. M. Kavanagh, S. Cornelissen, D. F. Fletcher, and K. V. Gernaey. Understanding gradients in industrial bioreactors. *Biotechnology Advances*, 46:107660, 2021.

[69] P. Doran. *Bioprocess Engineering Principles*. Elsevier, Oxford, 1995.

[70] D. Humbird, R. Davis, and J. D. McMillan. Aeration costs in stirred-tank and bubble column bioreactors. *Biochemical Engineering Journal*, 127:161–166, 2017.

[71] Y. Kawase and M. Moo-Young. Mixing time in bioreactors. *Journal of Chemical Technology and Biotechnology*, 44(1):63–75, 1989.

[72] D. D. McClure, N. Aboudha, J. M. Kavanagh, D. F. Fletcher, and G. W. Barton. Mixing in bubble column reactors: Experimental study and cfd modeling. *Chemical Engineering Journal*, 264:291–301, 2015.

[73] B. Sonnleitner and O. Käppeli. Growth of saccharomyces cerevisiae is controlled by its limited respiratory capacity: Formulation and verification of a hypothesis. *Biotechnology and Bioengineering*, 28(6):927–937, 1986.

[74] M. A. Abdullah, A. B. Ariff, M. Marziah, A. M. Ali, and N. H. Lajis. Strategies to overcome foaming and wall-growth during the cultivation of morinda elliptica cell suspension culture in a stirred-tank bioreactor. *Plant Cell, Tissue and Organ Culture*, 60(3):205–212, 2000.

[75] F. Garcia-Ochoa and E. Gomez. Bioreactor scale-up and oxygen transfer rate in microbial processes: An overview. *Biotechnology Advances*, 27(2):153–176, 2008.

[76] D. D. McClure, J. M. Kavanagh, D. F. Fletcher, and G. W. Barton. Oxygen transfer in bubble columns at industrially relevant superficial velocities: Experimental work and cfd modelling. *Chemical Engineering Journal*, 280:138–146, 2015.

[77] A. W. Nienow. Hydrodynamics of stirred bioreactors. *Applied Mechanics Reviews*, 51(1):3–32, 1998.

[78] P. Calderbank. Physical rate processes in industrial fermentation. part i: The interfacial area in gas-liquid contacting with mechanical agitation. *Transactions of the Institution of Chemical Engineers*, 36(5):433–440, 1958.

[79] D. D. McClure, J. M. Kavanagh, D. F. Fletcher, and G. W. Barton. Characterizing bubble column bioreactor performance using computational fluid dynamics. *Chemical Engineering Science*, 144:58–74, 2016.

[80] T. Tajsoleiman. *Automating Experimentation in Miniaturized Reactors*. PhD thesis, Technical University of Denmark, PROSYS - Process and Systems Engineering Centre, Kgs. Lyngby, 2018.

[81] A. W. Nienow. On impeller circulation and mixing effectiveness in the turbulent flow regime. *Chemical Engineering Science*, 52(15):2557–2565, 1997.

[82] A. W. Pacek, S. Chamsart, A. W. Nienow, and A. Bakker. The influence of impeller type on mean drop size and drop size distribution in an agitated vessel. *Chemical Engineering Science*, 54(19):4211–4222, 1999.

[83] P. Vrábel, R. G. J. M. van der Lans, K. C. A. M. Luyben, L. Boon, and A. W. Nienow. Mixing in large-scale vessels stirred with multiple radial or radial and axial up-pumping impellers: Modelling and measurements. *Chemical Engineering Science*, 55(23):5881–5896, 2000.

[84] T. P. Elson, D. J. Cheesman, and A. W. Nienow. X-ray studies of cavern sizes and mixing performance with fluids possessing a yield stress. *Chemical Engineering Science*, 41(10):2555–2562, 1986.

[85] C. Haringa, A. T. Deshmukh, R. F. Mudde, and H. J. Noorman. Euler-lagrange analysis towards representative down-scaling of a 22 m^3 aerobic s. cerevisiae fermentation. *Chemical Engineering Science*, 170:653–669, 2017.

[86] D. D. McClure, Z. Liu, G. W. Barton, D. F. Fletcher, and J. M. Kavanagh. Oxygen transfer in pilot-scale contactors: An experimental and computational investigation into the effect of contactor design. *Chemical Engineering Journal*, 344:173–183, 2018.

[87] J. C. Gabelle, F. Augier, A. Carvalho, R. Rousset, and J. Morchain. Effect of tank size on kla and mixing time in aerated stirred reactors with non-newtonian fluids. *The Canadian Journal of Chemical Engineering*, 89(5):1139–1153, 2011.

[88] H. Noorman. An industrial perspective on bioreactor scale-down: What we can learn from combined large-scale bioprocess and model fluid studies. *Biotechnology Journal*, 6(8):934–943, 2011.

[89] A. Prins and K. van't Riet. Proteins and surface effects in fermentation: Foam, antifoam and mass transfer. *Trends in Biotechnology*, 5(11):296–301, 1987.

[90] J. W. Lengeler, G. Drews, and H. G. Schlegel. *Biology of the Prokaryotes*. Thieme, Stuttgart, New York, 1999. Distributed in the USA by Blackwell Science, Malden, MA.

[91] B. Xu, M. Jahic, and S.-O. Enfors. Modeling of overflow metabolism in batch and fed-batch cultures of *Escherichia coli*. *Biotechnology Progress*, 15(1):81–90, 1999.

[92] T. Schweder, E. Krüger, B. Xu, B. Jürgen, G. Blomsten, S.-O. Enfors, and M. Hecker. Monitoring of genes that respond to process-related stress in large-scale bioprocesses. *Biotechnology and Bioengineering*, 65(2):151–159, 1999.

[93] A. R. Lara, L. Leal, N. Flores, G. Gosset, F. Bolívar, and O. T. Ramírez. Transcriptional and metabolic response of recombinant *Escherichia coli* to spatial dissolved oxygen tension gradients simulated in a scale-down system. *Biotechnology and Bioengineering*, 93(2):372–385, 2006.

[94] M. Löffler, J. D. Simen, G. Jäger, K. Schäferhoff, A. Freund, and R. Takors. Engineering *E. coli* for large-scale production – strategies considering atp expenses and transcriptional responses. *Metabolic Engineering*, 38:73–85, 2016.

[95] E. Anane, A. Sawatzki, P. Neubauer, and M. N. Cruz-Bournazou. Modelling concentration gradients in fed-batch cultivations of *E. coli* – towards the flexible design of scale-down experiments. *Journal of Chemical Technology and Biotechnology*, 94(2):516–526, 2019.

[96] R. C. Maclean, T.-B. Clara, and M. Richard. Evaluating evolutionary models of stress-induced mutagenesis in bacteria. *Nature Reviews Genetics*, 14(3):221, 2013.

[97] A.-L. Heins and D. Weuster-Botz. Population heterogeneity in microbial bioprocesses: Origin, analysis, mechanisms, and future perspectives. *Bioprocess and Biosystems Engineering*, 41(7):889–916, 2018.

[98] R. Lencastre Fernandes, M. Nierychlo, L. Lundin, A. E. Pedersen, P. E. Puentes Tellez, A. Dutta, M. Carlquist, A. Bolic, D. Schapper, A. C. Brunetti, S. Helmark, A. L. Heins, A. D. Jensen, I. Nopens, K. Rottwitt, N. Szita, J. D. van Elsas, P. H. Nielsen, and J. Martinussen. Experimental methods and modeling techniques for description of cell population heterogeneity. *Biotechnology Advances*, 29(6):575–599, 2011.

[99] C. J. Hewitt, G. Nebe-Von Caron, B. Axelsson, C. M. McFarlane, and A. W. Nienow. Studies related to the scale-up of high-cell-density *E. coli* fed-batch fermentations using multiparameter flow cytometry: Effect of a changing microenvironment with respect to glucose and dissolved oxygen concentration. *Biotechnology and Bioengineering*, 70(4):381–390, 2000.

[100] H. Onyeaka, A. W. Nienow, and C. J. Hewitt. Further studies related to the scale-up of high cell density *Escherichia coli* fed-batch fermentations. *Biotechnology and Bioengineering*, 84(4):474–484, 2003.

[101] S. George, G. Larsson, K. Olsson, and S. O. Enfors. Comparison of the baker's yeast process performance in laboratory and production scale. *Bioprocess and Biosystems Engineering*, 18(2):135–142, 1998.

[102] S. Bhargava, M. P. Nandakumar, A. Roy, K. S. Wenger, and M. R. Marten. Pulsed feeding during fed-batch fungal fermentation leads to reduced viscosity without detrimentally affecting protein expression. *Biotechnology and Bioengineering*, 81(3):341–347, 2003.

[103] S. Bhargava, K. S. Wenger, and M. R. Marten. Pulsed feeding during fed-batch aspergillus oryzae fermentation leads to improved oxygen mass transfer. *Biotechnology Progress*, 19(3):1091–1094, 2003.

[104] Y. Gao, S. Ray, S. Dai, A. R. Ivanov, N. R. Abu-Absi, A. M. Lewis, Z. Huang, Z. Xing, M. C. Borys, Z. J. Li, and B. L. Karger. Combined metabolomics and proteomics reveals hypoxia as a cause of lower productivity on scale-up to a 5000-liter cho bioprocess. *Biotechnology Journal*, 11(9):1190–1200, 2016.

[105] F. Bylund, E. Collet, S. O. Enfors, and G. Larsson. Substrate gradient formation in the large-scale bioreactor lowers cell yield and increases by-product formation. *Bioprocess Engineering*, 18(3):171–180, 1998.

[106] C. Haringa, W. Tang, A. T. Deshmukh, J. Xia, M. Reuss, J. J. Heijnen, R. F. Mudde, and H. J. Noorman. Euler-lagrange computational fluid dynamics for (bio)reactor scale down: An analysis of organism lifelines. *Engineering in Life Sciences*, 16(7):652–663, 2016.

[107] C. Haringa, W. Tang, G. Wang, A. T. Deshmukh, W. A. van Winden, J. Chu, W. M. van Gulik, J. J. Heijnen, R. F. Mudde, and H. J. Noorman. Computational fluid dynamics simulation of an industrial p. chrysogenum fermentation with a

coupled 9-pool metabolic model: Towards rational scale-down and design optimization. *Chemical Engineering Science*, 175:12–24, 2018.

[108] R. Spann, K. V. Gernaey, and G. Sin. A compartment model for risk-based monitoring of lactic acid bacteria cultivations. *Biochemical Engineering Journal*, 151:107293, 2019.

[109] R. Spann, J. Glibstrup, K. Pellicer-Alborch, S. Junne, P. Neubauer, C. Roca, D. Kold, A. E. Lantz, G. Sin, K. V. Gernaey, and U. Krühne. Cfd predicted ph gradients in lactic acid bacteria cultivations. *Biotechnology and Bioengineering*, 116(4):769–780, 2019.

[110] C. Bach. *Modelling of Gradients in Large Scale Bioreactors*. PhD thesis, Technical University of Denmark, Department of Chemical and Biochemical Engineering, Kgs. Lyngby, 2018.

[111] S. Sunya, F. Delvigne, J.-L. Uribelarrea, C. Molina-Jouve, and N. Gorret. Comparison of the transient responses of *Escherichia coli* to a glucose pulse of various intensities. *Applied Microbiology and Biotechnology*, 95(4):1021–1034, 2012.

[112] A. Amanullah, C. M. McFarlane, A. N. Emery, and A. W. Nienow. Scale-down model to simulate spatial ph variations in large-scale bioreactors. *Biotechnology and Bioengineering*, 73(5):390–399, 2001.

[113] A.-L. Heins, R. Lencastre Fernandes, K. V. Gernaey, and A. E. Lantz. Experimental and in silico investigation of population heterogeneity in continuous saccharomyces cerevisiae scale-down fermentation in a two-compartment setup. *Journal of Chemical Technology and Biotechnology*, 90(2):324–340, 2015.

[114] J. D. Simen, M. Löffler, G. Jäger, K. Schäferhoff, A. Freund, J. Matthes, J. Müller, and R. Takors. Transcriptional response of *Escherichia coli* to ammonia and glucose fluctuations. *Microbial Biotechnology*, 10(4):858–872, 2017.

[115] U. Schaefer, W. Boos, R. Takors, and D. Weuster-Botz. Automated sampling device for monitoring intracellular metabolite dynamics. *Analytical Biochemistry*, 270(1):88–96, 1999.

[116] H. J. Noorman and J. J. Heijnen. Biochemical engineering's grand adventure. *Chemical Engineering Science*, 170:677–693, 2017.

[117] A. Baez, N. Flores, F. Bolívar, and O. T. Ramírez. Simulation of dissolved co2 gradients in a scale-down system: A metabolic and transcriptional study of recombinant *Escherichia coli*. *Biotechnology Journal*, 6(8):959–967, 2011.

[118] J. T. Cortés, N. Flores, F. Bolívar, A. R. Lara, and O. T. Ramírez. Physiological effects of ph gradients on *Escherichia coli* during plasmid dna production. *Biotechnology and Bioengineering*, 113(3):598–611, 2016.

[119] E. Krichen, J. Harmand, M. Torrijos, J. J. Godon, N. Bernet, and A. Rapaport. High biomass density promotes density-dependent microbial growth rate. *Biochemical Engineering Journal*, 130:66–75, 2018.

[120] A. Kremling, J. Geiselmann, D. Ropers, and H. de Jong. An ensemble of mathematical models showing diauxic growth behaviour. *BMC Systems Biology*, 12(1), 2018.

[121] D. Chu and D. J. Barnes. The lag-phase during diauxic growth is a trade-off between fast adaptation and high growth rate. *Scientific Reports*, 6(1), 2016.

[122] M. H. Zwietering, I. Jongenburger, F. M. Rombouts, and K. Van't Riet. Modeling of the bacterial growth curve. *Applied and Environmental Microbiology*, 56(6):1875–1881, 1990.

[123] K. M. Tjørve and E. Tjørve. The use of gompertz models in growth analyses, and new gompertz-model approach: An addition to the unified-richards family. *PLOS ONE*, 12(6), 2017.

[124] A. Lapin, J. Schmid, and M. Reuss. Modeling the dynamics of *E. coli* populations in the three-dimensional turbulent field of a stirred-tank bioreactor–a structured-segregated approach. *Chemical Engineering Science*, 61(14):4783–4797, 2006.

[125] M. Kuschel, F. Siebler, and R. Takors. Lagrangian trajectories to predict the formation of population heterogeneity in large-scale bioreactors. *Bioengineering*, 4(2):27, 2017.

[126] F. Siebler, A. Lapin, M. Hermann, and R. Takors. The impact of co gradients on c. ljungdahlii in a 125 m^3 bubble column: Mass transfer, circulation time and lifeline analysis. *Chemical Engineering Science*, 207:410–423, 2019.

[127] F. Bezzo, S. Macchietto, and C. C. Pantelides. A general methodology for hybrid multizonal/cfd models: Part i. theoretical framework. *Computers & Chemical Engineering*, 28(4):501–511, 2004.

[128] N. Jourdan, T. Neveux, O. Potier, M. Kanniche, J. Wicks, I. Nopens, U. Rehman, and Y. Le Moullec. Compartmental modelling in chemical engineering: A critical review. *Chemical Engineering Science*, 210:115196, 2019.

[129] P. Vrábel, R. G. J. M. van der Lans, Y. Q. Cui, and K. C. A. M. Luyben. Compartment model approach. *Chemical Engineering Research and Design*, 77(4):291–302, 1999.

[130] R. Mahadevan, J. S. Edwards, and F. J. Doyle. Dynamic flux balance analysis of diauxic growth in *Escherichia coli*. *Biophysical Journal*, 83(3):1331–1340, 2002.

[131] C. H. Schilling, J. S. Edwards, D. Letscher, and B. Ø. Palsson. Combining pathway analysis with flux balance analysis for the comprehensive study of metabolic systems. *Biotechnology and Bioengineering*, 71(4):286–306, 2000.

[132] I. Promma, M. G. Aucoin, N. M. Abukhdeir, and H. Budman. A coupled metabolic flux/compartmental hydrodynamic model for large-scale aerated bioreactors. *Computers & Chemical Engineering*, 189, 2024.

[133] S. Mital, G. Christie, and D. Dikicioglu. Recombinant expression of insoluble enzymes in *Escherichia coli*: A systematic review of experimental design and its manufacturing implications. *Microbial Cell Factories*, 20:208, 2021.

[134] B. Özbek and S. Gayik. The studies on the oxygen mass transfer coefficient in a bioreactor. *Process Biochemistry*, 36(8–9):729–741, 2001.

APPENDICES

Appendix A

Supplementary Plots for Flask Culture 2 and Bioreactor Batch Operation

A.1 Flask Culture 2

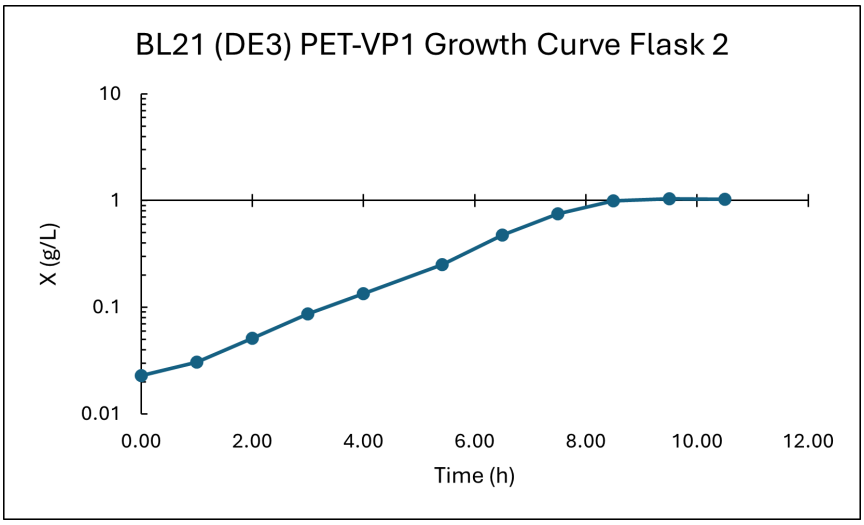


Figure A.1: Growth curve of *E. coli BL21 (DE3) PET-VP1* flask culture 2 at 250 rpm and 37°C.

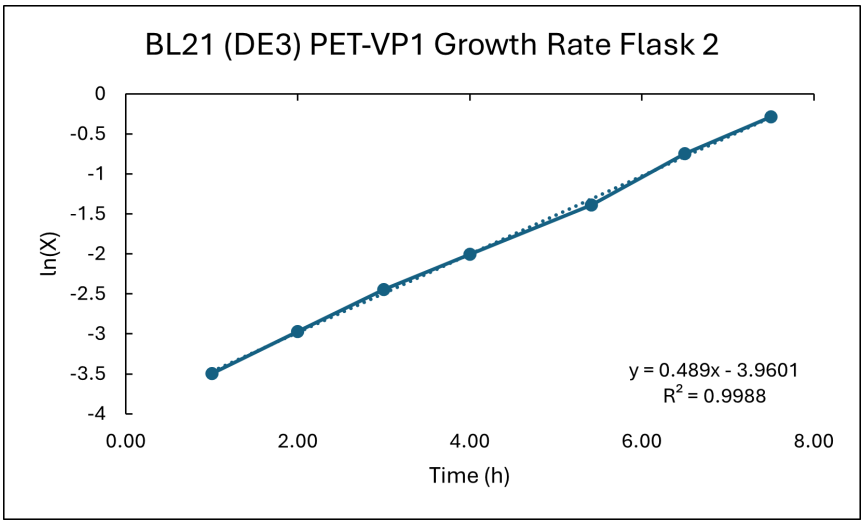


Figure A.2: Exponential phase of the growth curve to calculate the growth rate of the second flask culture.

A.2 Bioreactor Batch Operation

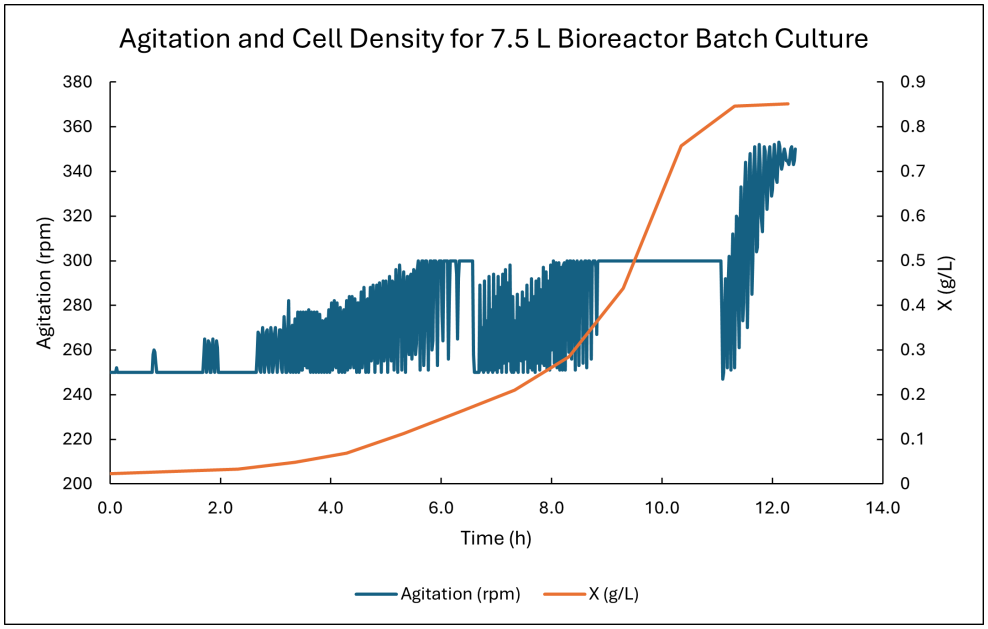


Figure A.3: Agitation rate in comparison to the cell density over time for the batch culture.

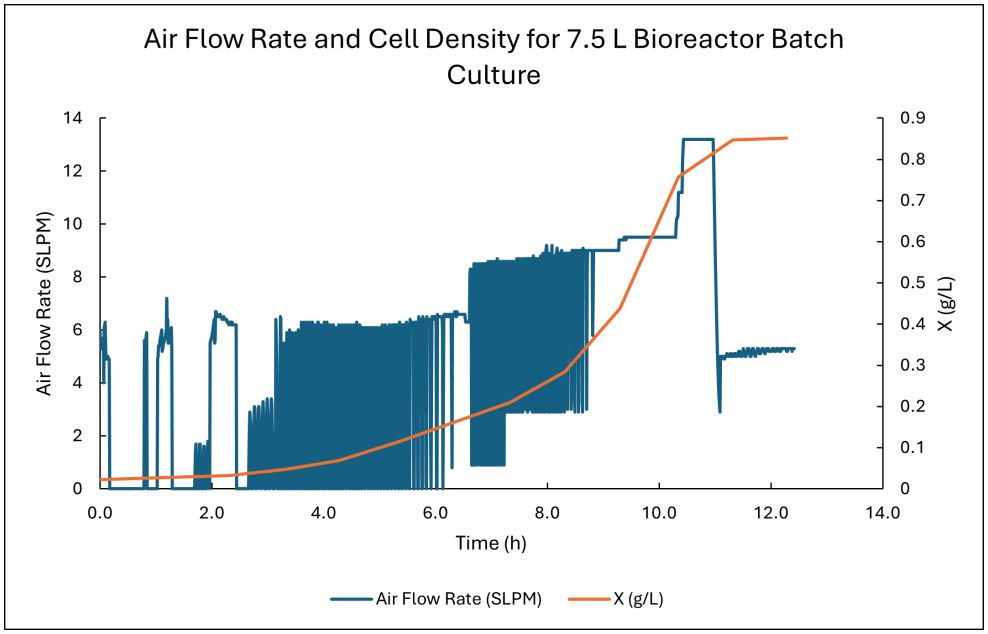


Figure A.4: Air flow rate in comparison to the cell density over time for the batch culture.

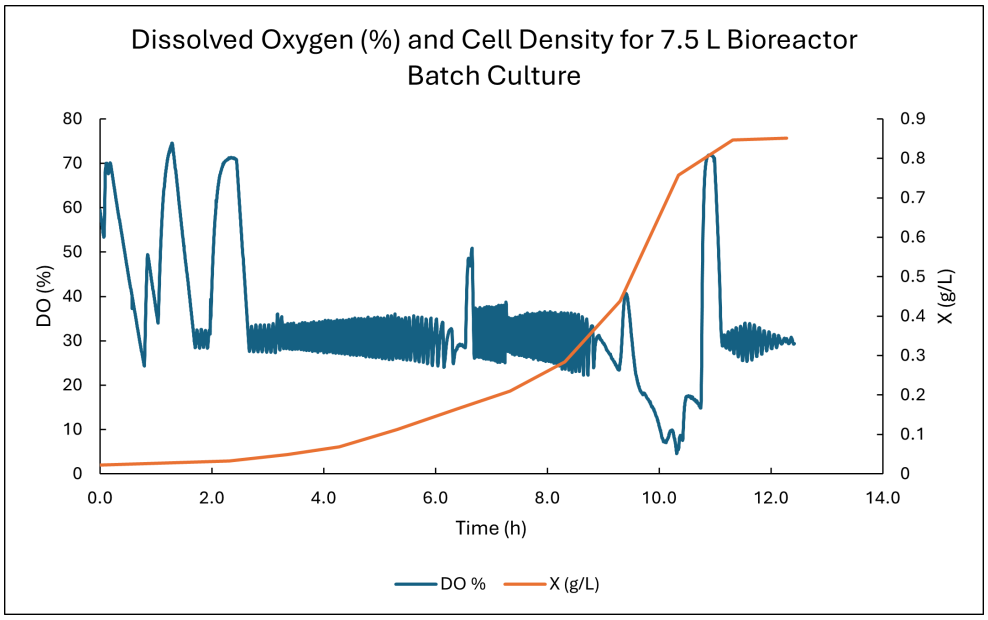


Figure A.5: DO% in comparison to the cell density over time for the batch culture.

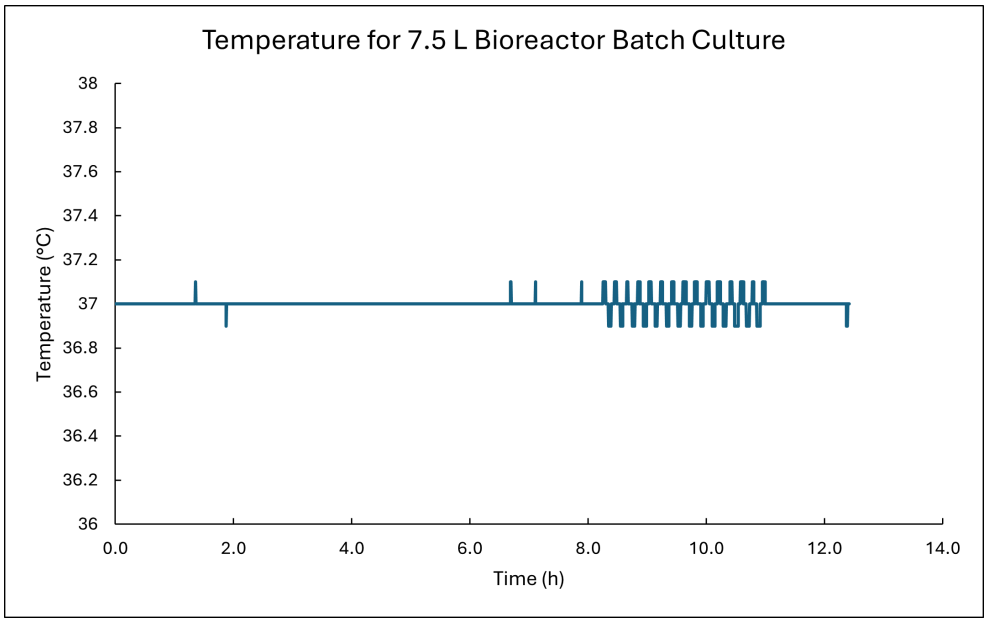


Figure A.6: Temperature of the batch culture over time.

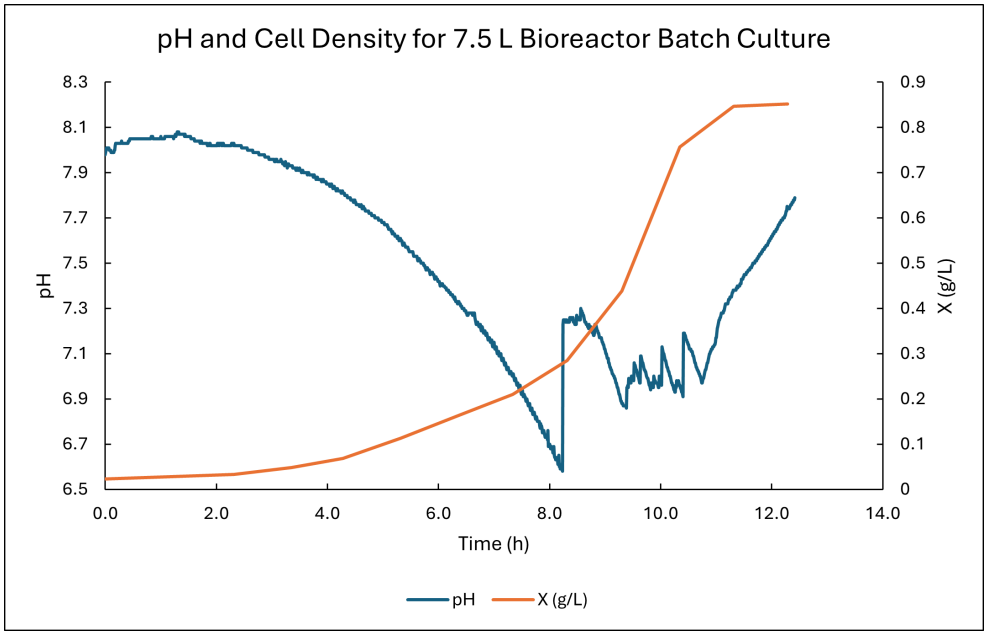


Figure A.7: pH in comparison to the cell density over time for the batch culture.

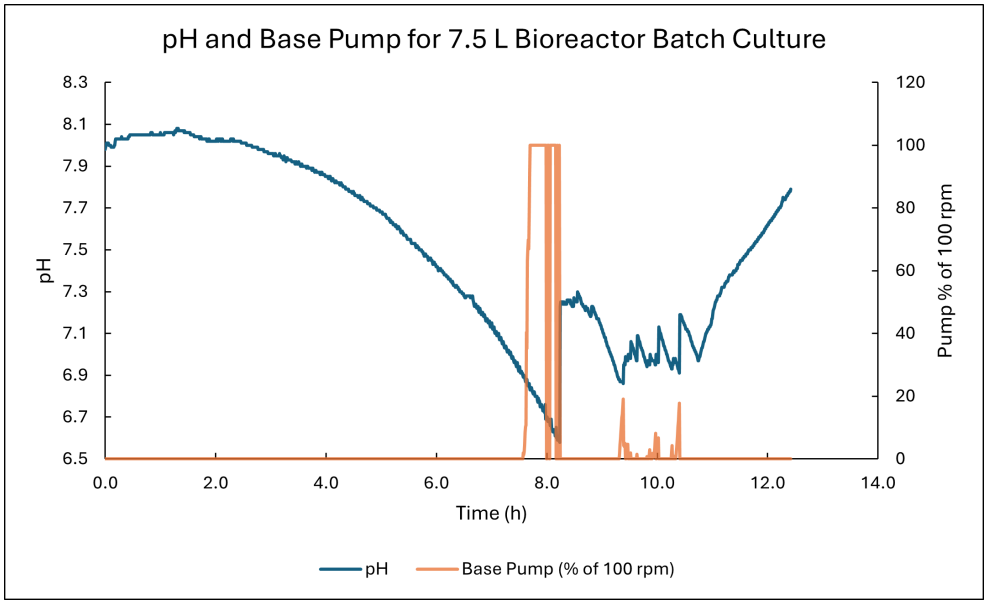


Figure A.8: pH in comparison to the base pump output over time for the batch culture.

Appendix B

Supplementary Plots and Tables for Bioreactor Fed-Batch Operation

B.1 Fed-Batch Experiment 1

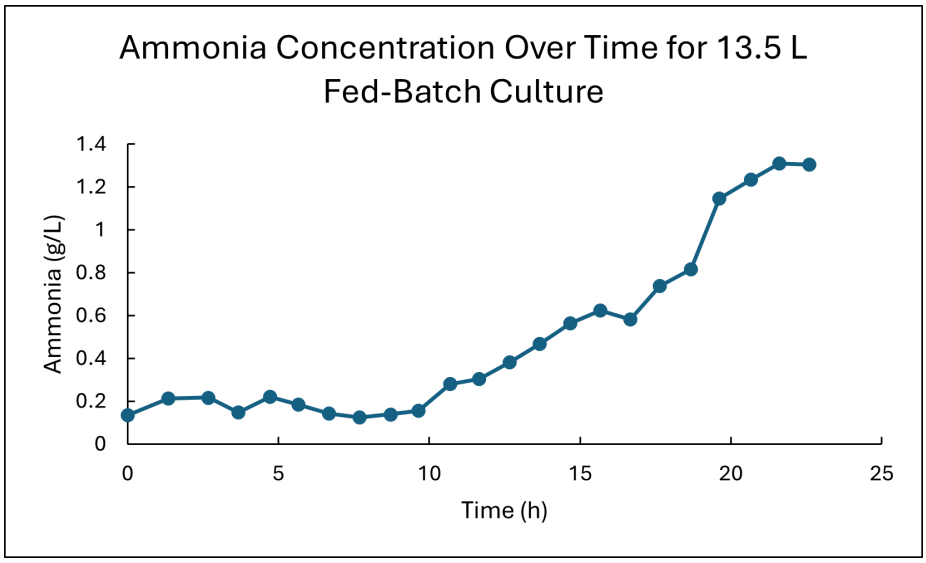


Figure B.1: Ammonia concentration profile for the 13.5 L fed-batch culture.

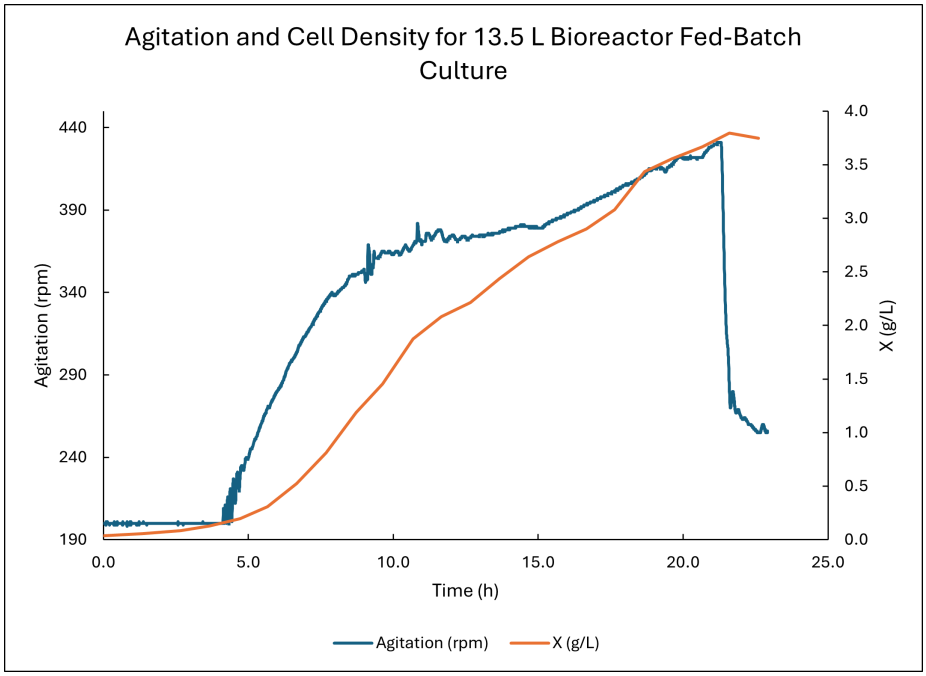


Figure B.2: Agitation rate in comparison to the cell density over time for the 13.5 L fed-batch culture.

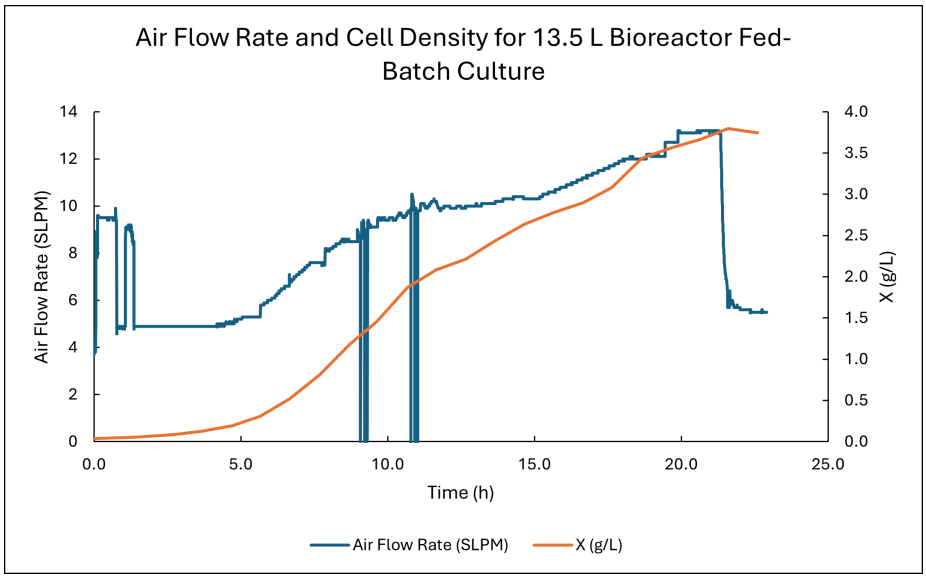


Figure B.3: Air flow rate in comparison to cell density over time for the 13.5 L fed-batch culture.

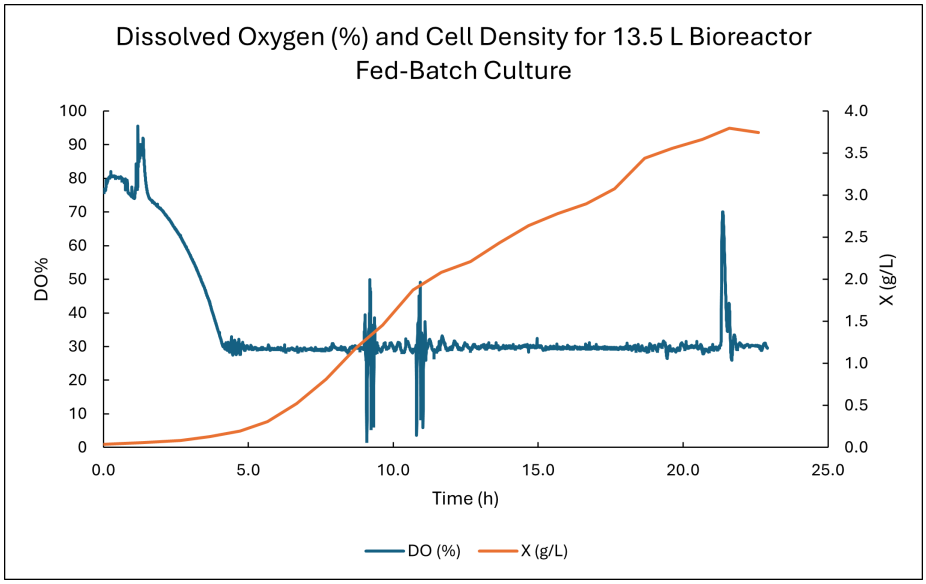


Figure B.4: DO% in comparison to cell density over time for the 13.5 L fed-batch culture.

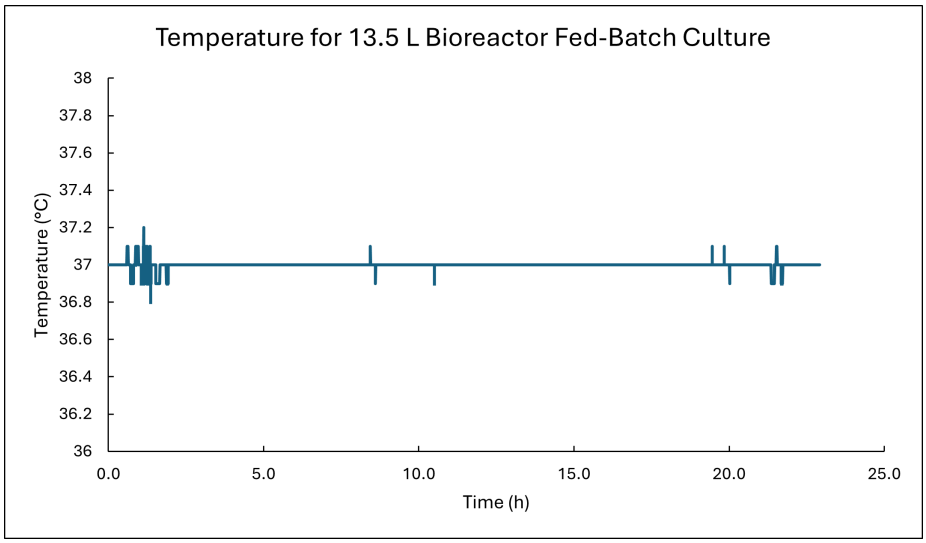


Figure B.5: Temperature of the 13.5 L fed-batch culture over time.

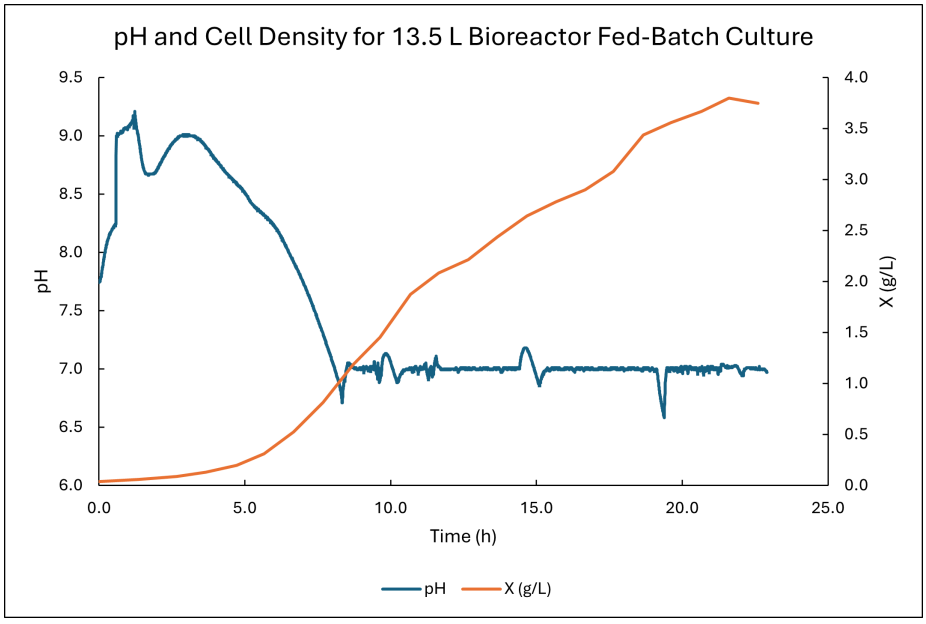


Figure B.6: pH in comparison to cell density over time for the 13.5 L fed-batch culture.

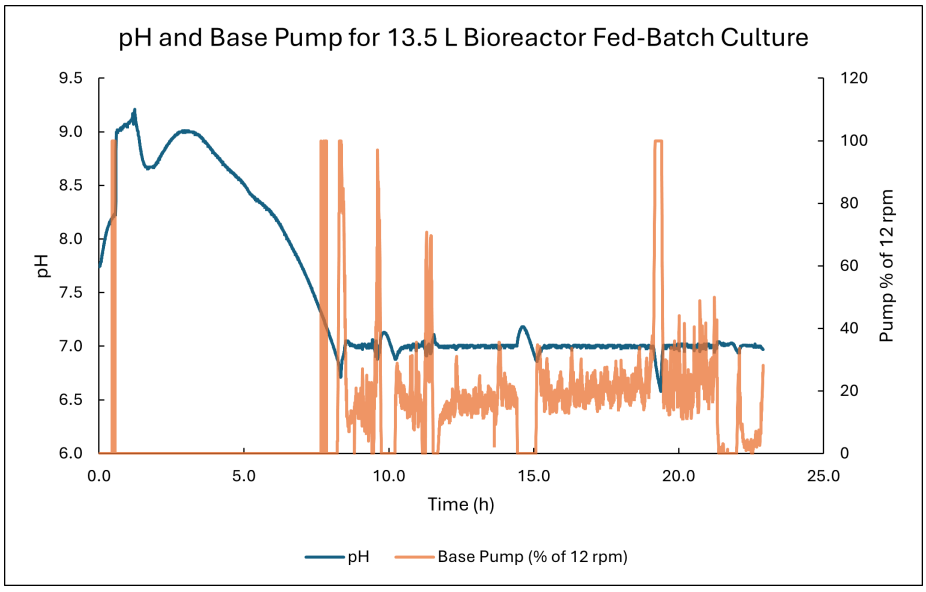


Figure B.7: pH in comparison to the base pump output over time for the 13.5 L fed-batch culture.

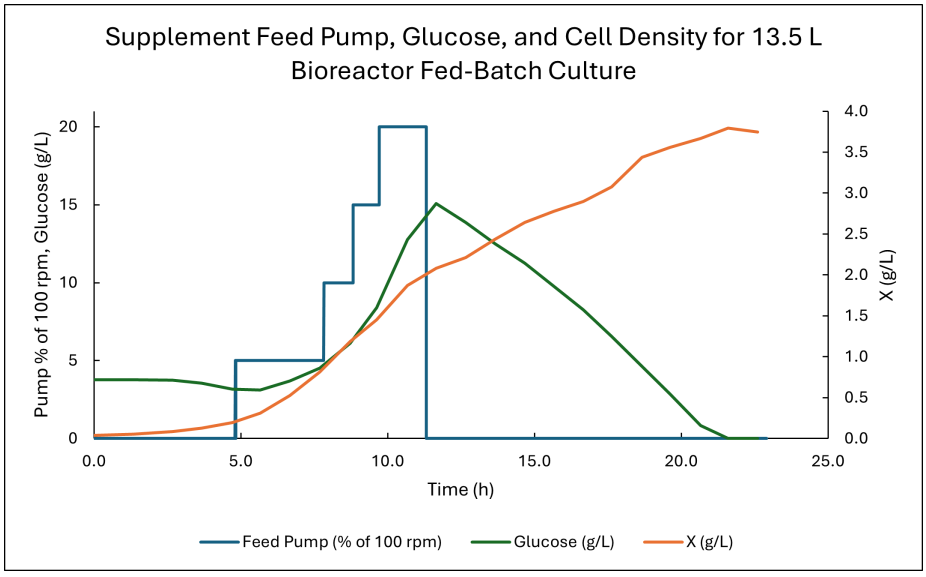


Figure B.8: Supplement feed pump output in comparison to the glucose concentration and cell density over time for the 13.5 L fed-batch culture.

Table B.1: Conditions at which the DO% sensor height changes were made and measured in the 13.5 L fed-batch culture.

DO Sensor Height Changes for 13.5 L Fed-Batch Culture							
Change Number	Time (h)	Height (m)	DO%	Agitation (rpm)	Cell Density (g/L)	pH	Air Flow Rate (SLPM)
1	8.980	0.140	29.3	353	1.258	7.00	8.9
1	9.010	0.305	34.6	352	1.268	7.00	8.8
1	9.030	0.470	39.5	348	1.275	6.99	8.6
1	9.040	0.305	34.7	347	1.279	7.00	8.5
1	9.050	0.140	30.5	346	1.282	7.00	8.5
2	11.070	0.305	30.9	371	1.953	7.00	9.8
2	11.100	0.470	37.3	371	1.961	7.01	9.8
2	11.120	0.140	26.5	372	1.967	7.00	9.9

Table B.2: Conditions at which the pH sensor height changes were made and measured in the 13.5 L fed-batch culture.

pH Sensor Height Changes for 13.5 L Fed-Batch Culture							
Change Number	Time (h)	Height (m)	pH	Agitation (rpm)	Cell Density (g/L)	DO%	Air Flow Rate (SLPM)
1	9.370	0.140	7.01	362	1.394	32.4	9.2
1	9.420	0.305	7.03	361	1.412	29.4	9.1
1	9.440	0.470	7.06	361	1.419	29.8	9.1
1	9.460	0.305	7.04	361	1.426	29.7	9.1
2	11.120	0.140	7.00	374	1.967	26.8	10.0
2	11.140	0.305	7.02	376	1.972	28.9	10.1
2	11.160	0.470	7.04	376	1.978	29.5	10.1
3	11.260	0.470	6.99	374	2.004	31.7	10.0
3	11.280	0.305	6.94	373	2.009	31.7	10.0
3	11.300	0.140	6.91	373	2.014	30.9	9.9
3	11.310	0.305	6.93	373	2.017	30.6	9.9
4	11.530	0.140	7.07	377	2.070	29.2	10.2
4	11.540	0.305	7.09	378	2.072	29.1	10.2
4	11.560	0.470	7.11	378	2.076	29.3	10.2
4	11.570	0.305	7.09	378	2.078	30.1	10.2
4	11.580	0.140	7.06	378	2.081	30.9	10.2

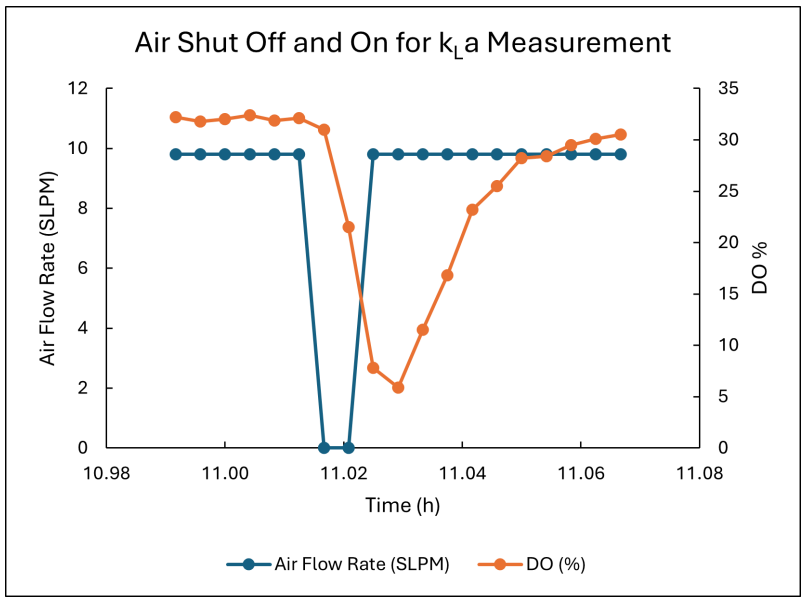


Figure B.9: Sample of air flow rate and DO% profile to show the air shut off and on to measure the $k_L a$.

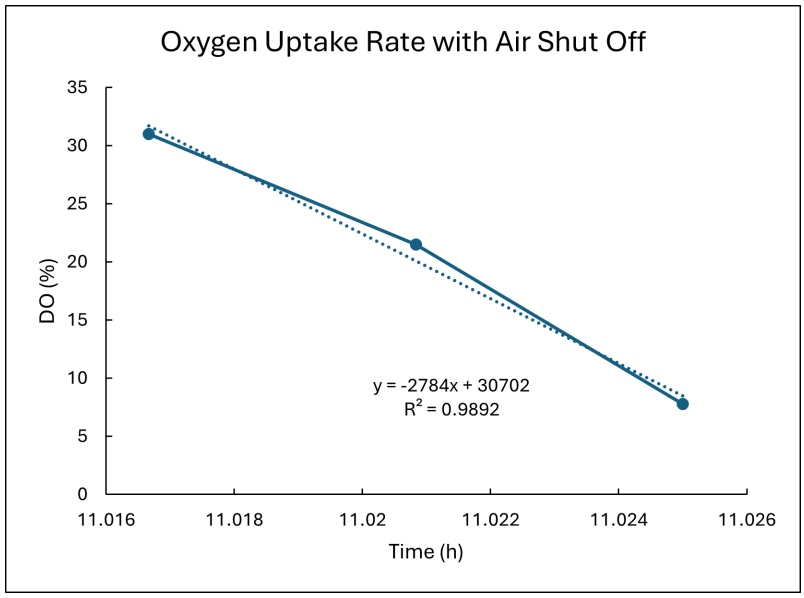


Figure B.10: Sample of oxygen uptake rate measurement taken from a nearly linear segment of the DO% profile when the air supply is shut off.

Table B.3: Conditions at which the k_La was measured for different DO% sensor heights for the 13.5 L fed-batch culture.

k_La Measurements at Different Heights for 13.5 L Fed-Batch Culture								
Change Number	Time (h)	Height (m)	Oxygen Uptake Rate (h^{-1})	k_La (h^{-1})	Agitation (rpm)	Cell Density (g/L)	pH	Air Flow Rate (SLPM)
1	9.090	0.140	21.48	33.0	349	1.296	6.98	8.6
1	9.230	0.305	32.95	48.0	351	1.345	6.98	8.7
1	9.320	0.470	24.48	39.8	360	1.377	6.99	9.3
2	10.810	0.140	25.80	41.0	371	1.877	7.00	9.8
2	10.950	0.470	37.92	56.5	372	1.919	6.97	9.9
2	11.030	0.305	27.84	40.1	371	1.942	6.99	9.8

B.2 Fed-Batch Experiment 2

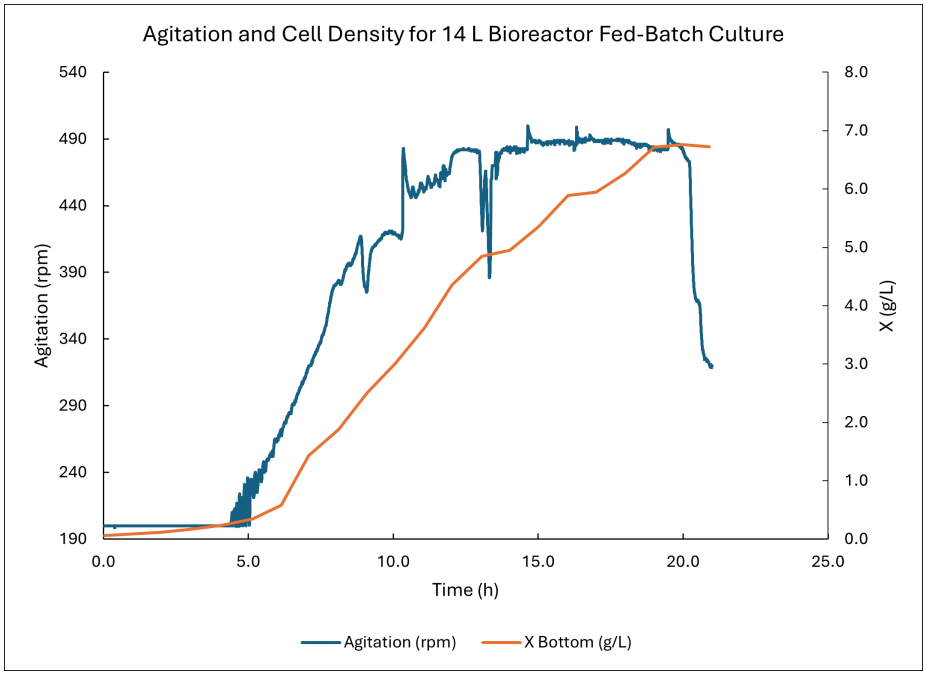


Figure B.11: Agitation rate in comparison to the bottom cell density over time for the 14 L fed-batch culture.

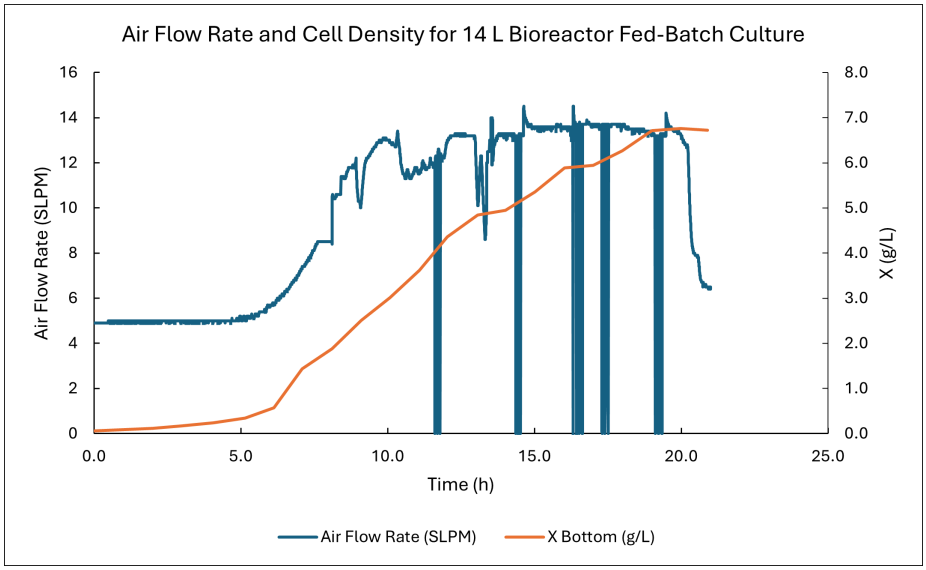


Figure B.12: Air flow rate in comparison to bottom cell density over time for the 14 L fed-batch culture.

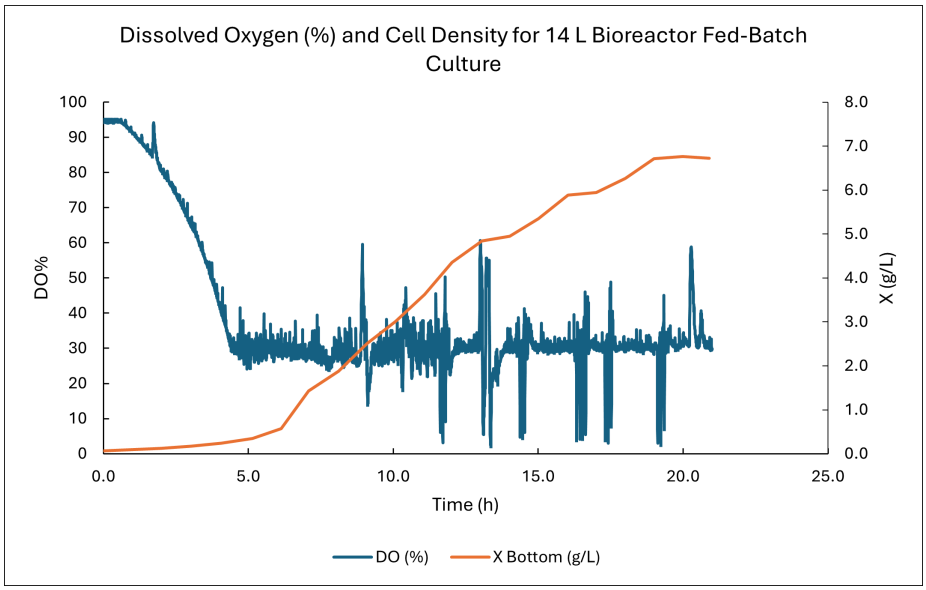


Figure B.13: DO% in comparison to bottom cell density over time for the 14 L fed-batch culture.

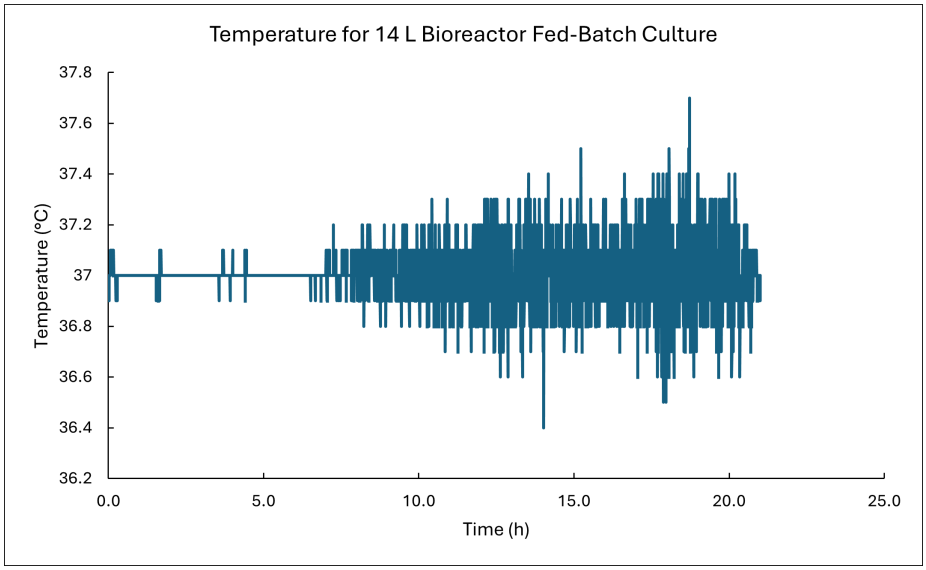


Figure B.14: Temperature of the 14 L fed-batch culture over time.

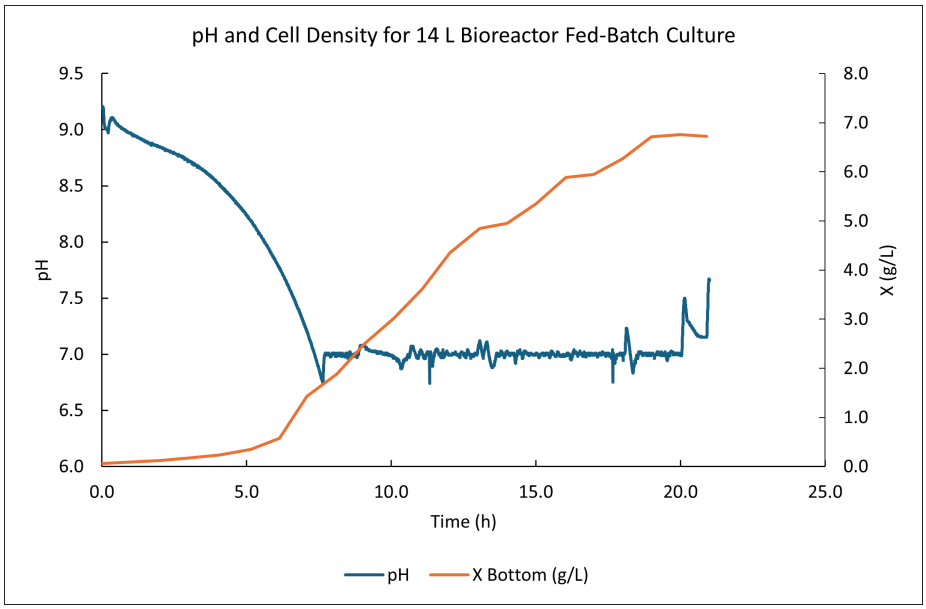


Figure B.15: pH in comparison to bottom cell density over time for the 14 L fed-batch culture.

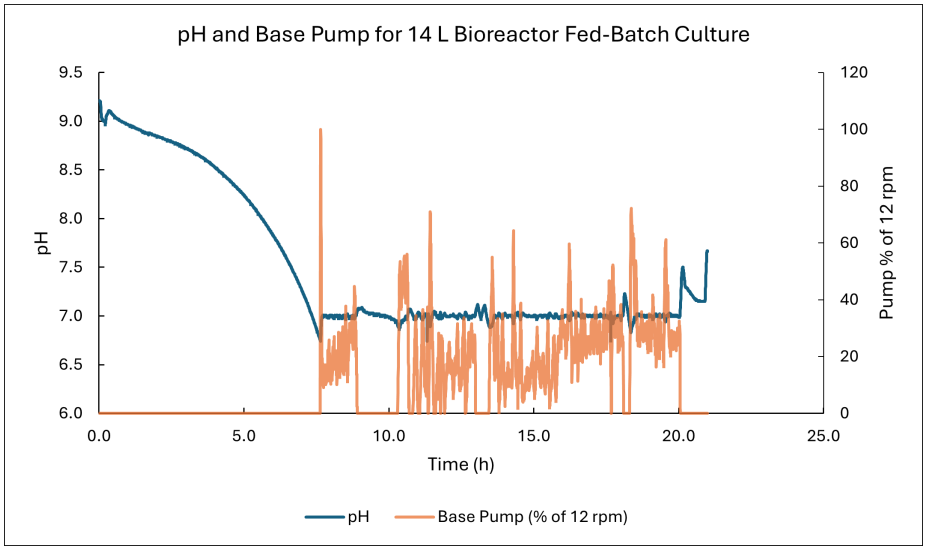


Figure B.16: pH in comparison to the base pump output over time for the 14 L fed-batch culture.

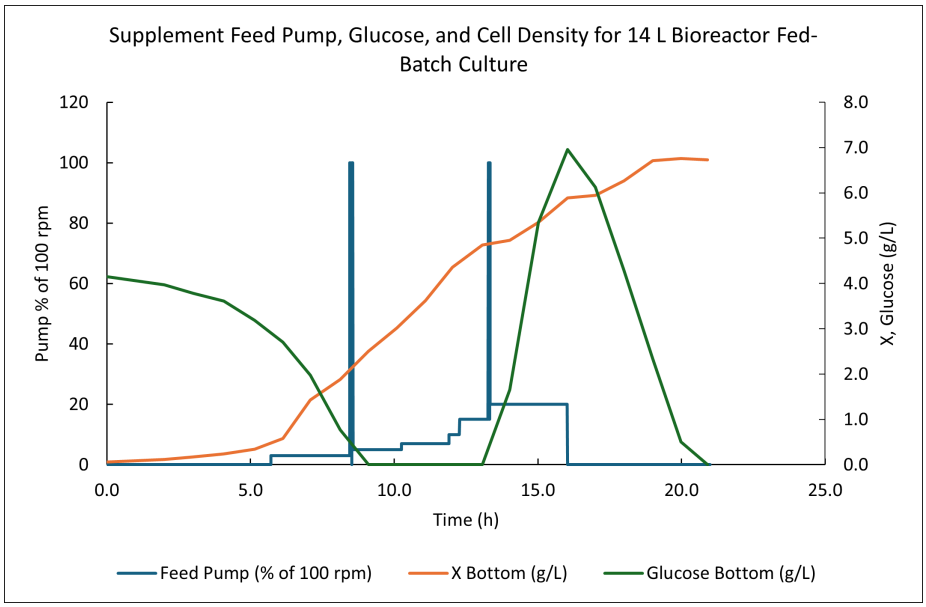


Figure B.17: Supplement feed pump output in comparison to the glucose concentration and bottom cell density over time for the 14 L fed-batch culture.

Table B.4: Conditions at which the DO% sensor height changes were made and measured in the 14 L fed-batch culture.

DO% Sensor Height Changes for 14 L Fed-Batch Culture							
Change Number	Time (h)	Height (m)	DO%	Agitation (rpm)	Cell Density (g/L)	pH	Air Flow Rate (SLPM)
1	11.517	0.140	29.7	459	4.036	7.02	12.0
1	11.538	0.305	32.1	459	4.049	7.04	11.9
1	11.554	0.470	34.5	458	4.058	7.04	11.9
2	11.575	0.305	35.1	456	4.071	7.05	11.8
2	11.596	0.140	27.0	456	4.083	7.03	11.8
3	11.833	0.470	37.7	463	4.222	6.98	12.2
3	11.846	0.305	28.6	463	4.229	6.98	12.1
3	11.863	0.140	24.3	463	4.238	6.99	12.2
4	14.304	0.140	29.6	482	5.176	6.94	13.3
4	14.317	0.305	31.4	483	5.306	6.95	13.2
4	14.321	0.470	38.7	482	5.433	6.97	13.2
5	14.333	0.305	32.0	482	5.312	6.98	13.2
5	14.354	0.140	28.7	482	5.194	7.00	13.2
6	14.583	0.470	33.3	482	5.535	7.01	13.2
6	14.604	0.305	29.5	482	5.412	7.03	13.2
6	14.621	0.140	27.1	482	5.286	7.03	13.2
7	16.221	0.140	31.3	486	5.798	6.95	13.5
7	16.229	0.305	32.9	485	5.943	6.96	13.4
7	16.238	0.470	39.6	482	6.087	6.96	13.2
8	16.246	0.305	32.1	484	5.948	6.98	13.4
8	16.271	0.140	26.4	486	5.814	6.99	13.5
9	16.708	0.470	37.2	489	6.220	7.00	13.7
9	16.721	0.305	32.0	489	6.088	6.99	13.7
9	16.742	0.140	28.5	489	5.958	6.99	13.7
10	17.567	0.470	37.6	489	6.439	7.00	13.6

Continued on next page

Table B.4 (continued)

DO% Sensor Height Changes for 14 L Fed-Batch Culture							
Change Number	Time (h)	Height (m)	DO%	Agitation (rpm)	Cell Density (g/L)	pH	Air Flow Rate (SLPM)
10	17.579	0.305	33.6	489	6.328	6.99	13.6
10	17.621	0.140	29.9	489	6.226	6.98	13.7
11	19.408	0.470	34.6	482	6.791	7.01	13.2
11	19.425	0.305	30.9	482	6.746	7.01	13.2
11	19.450	0.140	28.9	482	6.703	7.00	13.2

Table B.5: Conditions at which the pH sensor height changes were made and measured in the 14 L fed-batch culture.

pH Sensor Height Changes for 14 L Fed-Batch Culture							
Change Number	Time (h)	Height (m)	pH	Agitation (rpm)	Cell Density (g/L)	DO%	Air Flow Rate (SLPM)
1	11.333	0.140	6.98	455	3.859	25.8	11.7
1	11.350	0.305	7.00	456	3.902	27.9	11.8
1	11.367	0.470	7.02	456	3.946	28.6	11.8
2	11.379	0.305	6.99	456	3.919	27.2	11.8
2	11.392	0.140	6.96	456	3.891	30.6	11.8
3	14.242	0.470	7.01	483	5.401	30.1	13.3
3	14.267	0.305	6.98	481	5.287	29.3	13.1
3	14.296	0.140	6.92	483	5.173	29.3	13.3
4	16.167	0.470	7.00	488	6.066	29.9	13.6
4	16.196	0.305	6.98	487	5.933	30.5	13.5
4	16.221	0.140	6.95	486	5.798	31.3	13.5
5	17.633	0.140	6.99	489	6.230	30.2	13.7
5	17.642	0.305	7.02	489	6.345	29.6	13.7
5	17.654	0.470	7.04	489	6.460	33.2	13.7
6	17.679	0.305	7.00	489	6.355	29.3	13.7
6	17.700	0.140	6.94	489	6.250	29.4	13.7
7	19.454	0.140	6.99	482	6.704	29.0	13.3
7	19.463	0.305	7.00	482	6.752	29.9	13.2
7	19.471	0.470	7.02	482	6.799	29.2	13.2
8	19.500	0.305	6.98	495	6.757	35.2	14.0
8	19.517	0.140	6.96	493	6.715	34.9	13.9

Table B.6: Conditions at which the k_La was measured for different DO% sensor heights for the 14 L fed-batch culture.

k_La **Measurements at Different Heights for 14 L Fed-Batch Culture**								
Change Number	Time (h)	Height (m)	Oxygen Uptake Rate (h^{-1})	k_La (h^{-1})	Agitation (rpm)	Cell Density (g/L)	pH	Air Flow Rate (SLPM)
1	11.621	0.140	17.52	26.0	459	4.014	7.01	12.0
1	11.713	0.305	59.52	90.2	466	4.107	6.97	12.3
1	11.801	0.470	42.96	68.5	463	4.203	6.98	12.1
2	14.375	0.140	25.80	36.5	483	5.201	7.03	13.2
2	14.463	0.305	29.64	42.3	482	5.360	7.00	13.2
2	14.538	0.470	29.90	44.8	482	5.518	6.96	13.2
3	16.446	0.140	22.75	33.3	489	5.868	6.98	13.7
3	16.538	0.305	30.12	44.4	489	6.034	7.00	13.7
3	16.638	0.470	31.56	52.9	490	6.201	6.98	13.7
4	17.317	0.140	22.06	32.2	489	6.134	7.00	13.7
4	17.413	0.305	30.60	45.3	489	6.283	6.98	13.7
4	17.526	0.470	34.51	58.0	489	6.429	6.99	13.7
5	19.129	0.140	27.12	39.0	483	6.638	6.99	13.2
5	19.234	0.305	26.14	38.9	483	6.714	7.00	13.2
5	19.355	0.470	38.76	55.6	482	6.784	6.99	13.3

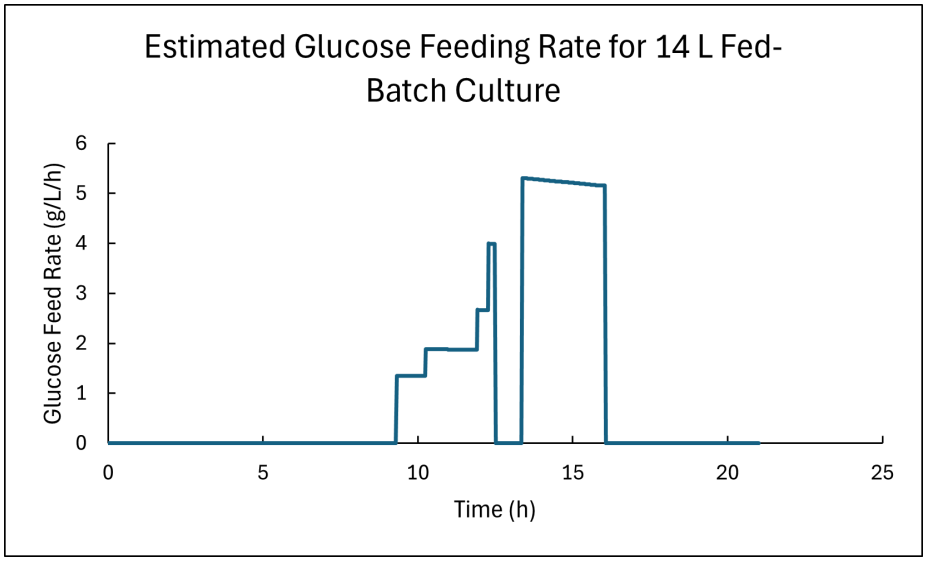


Figure B.18: Estimated glucose feeding rate for the 14 L fed-batch culture as there were uncertainties due to tubing occlusions.